The International Congress for global Science and Technology

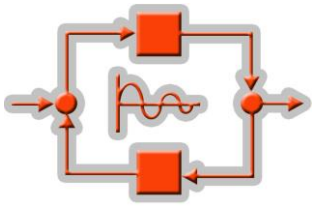

ICGST International Journal on Automatic Control & System Engineering (ACSE)

Volume (7), Issue (2)
November, 2007

wwww.icgst.com
www.icgst-amc.com
www.icgst-ees.com

ACSE Journal
ISSN: Print 1687-4811
ISSN Online 1687-482X
ISSN CD-ROM 1687-4838

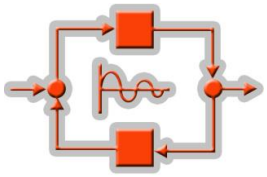

Table of Contents

Papers	Pages
P1110729003 A.Asokan and D.Sivakumar Fault Detection and Diagnosis for a Three-tank system using Structured Residual Approach	1--8
P1110708001 Tarek Aroui and Yassine Koubaa and Ahmed Toumi Modeling and Diagnostics of Inductions Machines under Rotor Failures	9--18
P1110624003 R. Ebrahimi and M. Samavat and M.A. Vali and A.A. Gharavisi APPLICATION OF FOURIER SERIES DIRECT METHOD TO THE OPTIMAL CONTROL OF SINGULAR SYSTEMS	19--24
P1110614002 C. Srinivasa Rao and S. Siva Nagaraju and P. Sangameswara Raju A MODIFIED GENETIC APPROACH TO HYDROTHERMAL SYSTEM WITH THYRISTOR CONTROLLED PHASE SHIFTER UNDER OPEN MARKET SYSTEM	25--31
P1110733001 Mourad KCHAOU and Mansour SOUISSI and Ahmed TOUMI Fuzzy Dynamic Output Feedback Control for Nonlinear Systems Integrated with H∞ and Quadratic D-Stability Strategies	33--41
P1110733002, K. Vaisakh and G. V.Siva Krishna Rao Line Flow Constrained Evaluation of Optimal Bilateral Real Power Contracts/Transactions	43--48
P1110549003 Mohammed El-Said El-Telbany Employing Particle Swarm Optimizer and Genetic Algorithms for Optimal Tuning of PID Controllers: A Comparative Study	49--54

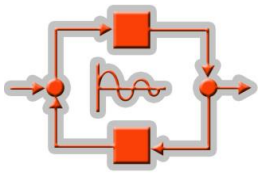

ICGST International Journal on Automatic Control & System Engineering - (ACSE)

A publication of the International Congress for global Science and Technology - (ICGST)

ICGST Editor in Chief: Dr. Ashraf Aboshosha

www.icgst.com, www.icgst-amc.com, www.icgst-ees.com

editor@icgst.com

Guest Editor: Prof. Dr. Z. Gao,

School of Electrical Engineering & Automation of Tianjin University, China

www.icgst.com

Fault Detection and Diagnosis for a Three-tank system using Structured Residual Approach

A.Asokan and D.Sivakumar
Department of Instrumentation Engineering, Faculty of Engineering & Technology
Annamalai University, *Annamalai Nagar-608 002, Tamilnadu, India*
E-mail:asokan_me@yahoo.co.in

Abstract
Fault detection and isolation (FDI) is a task to deduce from observed variable of the system if any component is faulty, to locate the faulty components and also to estimate the fault magnitude present in the system. This paper provides a systematic method of fault diagnosis to detect leak in the three-tank process. The proposed scheme makes use of structured residual approach for detection, isolation and estimation of faults acting on the process [1,2,3]. This technique includes residual generation and residual evaluation. A literature review showed that the conventional fault diagnosis methods like the ordinary Chi-square (Ψ2) test method, generalized likelihood ratio test have limitations such as the "false alarm" problem. From the results it is inferred that the proposed FDI scheme diagnoses better when compared to other conventional methods.

Keywords: *Fault detection and Diagnosis, Residual Generation, Structured Residual Approach*

1. Introduction
A fault is any kind of malfunction in a system that is a deviation from the normal behavior in the plant or its instrumentation [4]. Fault detection is the indication that something is going wrong in the monitored system. Fault isolation is the determination of the exact location of the fault (the component which is faulty) [5,6]. Detection and isolation of faults are very important tasks in intelligent control systems because a fault can lead to a reduction in performance or even to breakdowns or catastrophes. Many different approaches to Fault Detection and Isolation (FDI) have been proposed over the years. They are based either on the model of the system (analytical methods) [6, 7, 8, 9] or on the knowledge about the system (heuristic methods) [10,11,12, 13, 14].One way to detect faults in a system is by means of analytical redundancy [5, 9].This consists of comparing the behaviour of the real system and the behaviour of a model of the system. In an ideal case, the system and the model behave exactly the same and a fault is detected when the behaviours are different, but usually there are differences between the behaviours of the system and the model.

Among the various FDI schemes, the structured residual approach (SRA) proposed by Gertler, J., Staroswiecki, M. and Shen, M [3] is powerful in isolating faults. In this paper the structured residual approach is applied to obtain estimates of the envelopes for detecting faults in a Three-Tank System [6] system which is formed by a sequence of three interconnected tanks and has been declared as a benchmark. This system has the typical characteristics of tanks, pipelines and pumps used in many industries. In this case, the faults are clogging and leakages. The SRA proposed by Gertler is further simplified and applied to Three-Tank System. The SRA involves two steps i) generation of Primary Residual Vector (PRV) for fault detection and ii) transformation of PRV into structured residual vector (SRV) for fault isolation.
The implementation procedure of the proposed FDI scheme is illustrated in Figure 1. The controller in the system is used to maintain the process variable at its set point. When there is a fault in the process, its output differs with model output. This difference is termed as residual. By simply monitoring the residuals one can say that something is going wrong. But it is not possible to identify the location of the fault. So the residual has to be processed to enhance isolation. In this paper the structured residual approach is applied to a MIMO system to enhance fault isolation. This paper also considers the isolation of multiple faults that may occur at the same time. Theoretically, any faulty scenarios, e.g. one, two, or multiple simultaneous faults can occur. However, the probability of such scenarios can vary from high to low.

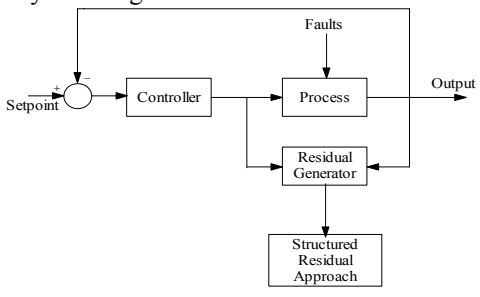

Figure 1. Block diagram representation of proposed FDI scheme

This paper is organized as follows. In section 2 the system under study which is the three-tank system is described. In section 3, the identification of un-measured disturbance variables (faults) using residual approach as reported in literature is explained. The proposed scheme to identify and estimate the unmeasured disturbance acting on the process is presented in section 4. In section 5 the simulation results are discussed. Finally the conclusions are drawn and scope of further work is provided in section 6.

2. System descriptions

The three-tank system considered for study [6] is shown in Figure2. The controlled variables are the level of the tank1 (h1) and level of the tank3 (h3). In flow of tank1 (fin_1) and in flow of tank3 (fin_3) are chosen as manipulated variables to control the level of the tank1 and tank3. The unmeasured outflow of that is leak of tank1, tank2 and tank3 have been considered as fault variables (L_1 ,L_2 and L_3).In this paper it is assumed that the leaks are independent of level of the tank.

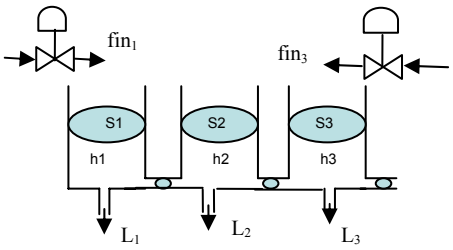

Figure .2. Three Tank System

The material balance equation for the above three-tank system is given by

$$\frac{dh1}{dt} = \frac{fin_1}{S1} - \frac{Az1}{S1}\sqrt{2g(h1-h2)} \quad - L_1 \qquad (1)$$

$$\frac{dh2}{dt} = \frac{Az1}{S2}\sqrt{2g(h1-h2)} - \frac{Az3}{S2}\sqrt{2g(h1-h3)} \quad - L_2 \qquad (2)$$

$$\frac{dh3}{dt} = \frac{fin_3}{S3} + \frac{Az3}{S3}\sqrt{2g(h2-h3)} - \frac{Az2}{S3}\sqrt{2gh3} \quad - L_3 \qquad (3)$$

The steady state operating data of the Three-tank system is given in Table1.The state space model of the three tank system around the operating point which are given in the table is

$$\dot{x} = Ax + Bu$$

$$y = Cx + Du$$

Where

$$A = \begin{bmatrix} -0.00723996 & 0.00723996 & 0 \\ 0.00723996 & -0.01707086 & 0.0098303 \\ 0 & 0.0098309 & -0.012540553 \end{bmatrix}$$

$$B = \begin{bmatrix} 64.935 & 0 & 0 \\ 0 & 64.935 & 0 \\ 0 & 0 & 64.935 \end{bmatrix}$$

$$C = \begin{bmatrix} 1 & 0 & 0 \\ 0 & 1 & 0 \\ 0 & 0 & 1 \end{bmatrix}$$

$$D = \begin{bmatrix} 0 & 0 & 0 \\ 0 & 0 & 0 \\ 0 & 0 & 0 \end{bmatrix}$$

When fault (leak) occurs the state space model is given by

$$\dot{x} = Ax + Bu + B_f f$$

$$y = Cx + Du$$

$$B_f = \begin{bmatrix} 64.935 & 0 & 0 \\ 0 & 64.935 & 0 \\ 0 & 0 & 64.935 \end{bmatrix}$$

3. Fault [leak] detection using residual generator

Residuals are generated from the observable variable of the monitored plant, that is, from the command values of the controlled inputs and the outputs [6].

Table.1 Steady state operating data

h1, h2,h3 in m	0.7,0.5,0.3
fin_1 and fin_3 in ml/sec	100
Outflow coefficient (Az1, Az2, Az3)	2.251e-5,3.057e-5,2.307e-5
Area of tank (S1-S3)in m^2	0.0154
L_1,L_2,L_3 in ml/sec	0
Acceleration due to gravity in m/sec^2	9.81

Ideally, the residuals should only be affected by the faults. However, the presence of disturbances, noise and modeling errors also causes the residuals to become nonzero and thus interferes with the detection of faults. Therefore the residual generator needs to be designed so that it is maximally unaffected by these nuisance inputs, which means that it is robust in the face of disturbance, noise and model errors.

Structured residual are so designed that each residual responds to a different subset of faults and insensitive to the others. When a particular fault occurs, some of the residuals do respond and others do not. Then the pattern of the response set, the fault signature or fault code, is characteristic of the particular fault.

Example for fault code;-

	R_1	R_2	R_3
L_1	1	0	0
L_2	0	1	0
L_3	0	0	1

The above fault code implies that fault L1 affects only residual R1 like L2 affects R2 and L3 affects R3.In order to perform detection and isolation of set of faults, structured residuals can be used. The so called signature code describes the subset of residuals which react to each fault. Since the levels of all three-tank are assumed


to be measurable, there will be three residuals corresponding to each of the three tanks When there is a fault, all the three residuals get affected. By simply monitoring the residuals it is possible to predict the change in behavior of the system from normal. But it is not possible to identify the location of the fault. So the residual has to be transformed to enhance isolation.

Let the plant output is given by

$$Y_P(s) = G(s)U(s) + G_F(s)L(s) \quad (4)$$

Where

G(s) =Transfer function under normal conditions

$G_F(s)$ = Fault Transfer function

U(s) =input to the system

L(s) =fault input (leak) in the system

Let the output of the model be given by

$$Y_M(s) = G(s)U(s) \quad (5)$$

Where

$$U(s) = \begin{bmatrix} fin_1(s) \\ 0 \\ fin_3(s) \end{bmatrix}$$

$$L(s) = \begin{bmatrix} L_1(s) \\ L_2(s) \\ L_3(s) \end{bmatrix}$$

Residual R(s) is defined as difference between process output and model output.

$$R(s) = Y_P(s) - Y_M(s) \quad (6)$$

Substituting the expressions for Y_p(s) and Y_m(s) in equation (6)

$$R(s) = G_F(s)\, L(s)$$

$$\begin{bmatrix} R_1(s) \\ R_2(s) \\ R_3(s) \end{bmatrix} = \begin{bmatrix} G_{F11} & G_{F12} & G_{F13} \\ G_{F21} & G_{F22} & G_{F23} \\ G_{F31} & G_{F32} & G_{F33} \end{bmatrix} \begin{bmatrix} L_1(s) \\ L_2(s) \\ L_3(s) \end{bmatrix} \quad (7)$$

$$R_1(s) = G_{F11}(s)L_1(s) + G_{F12}(s)L_2(s) + G_{F13}(s)L_3(s) \quad (8)$$

$$R_2(s) = G_{F21}(s)L_1(s) + G_{F22}(s)L_2(s) + G_{F23}(s)L_3(s) \quad (9)$$

$$R_3(s) = G_{F31}(s)L_1(s) + G_{F32}(s)L_2(s) + G_{F33}(s)L_3(s) \quad (10)$$

The above equation is valid only in the absence of plant model mismatch and in the absence of state and measurement noise. From the above equations, it is evident that the presence of fault will affect all the three residuals. It is difficult to identify the location of fault by monitoring the residuals. Therefore in order to enhance the fault isolation it is required to transform the residuals. The design of transformation matrix is discussed in the subsequent section.

4. Design of transformation matrix

To transform raw residual R(s) into structured form R_t(s), multiply R(s) with weighting matrix W(s)

$$R_t(s) = W(s)R(s) \quad (11)$$

Weighting matrix is chosen as to contain inverse of Identified fault model to cancel the effects of fault transfer function present in residual.

$$W(s) = Z(s)G_F^{-1}(s) \quad (12)$$

Where Z(s) is user defined matrix

Substituting W(s) in expression (11)

$$R_t(s) = [Z(s)G_F^{-1}(s)][R(s)]$$

Substituting R(s) in the above expression

$$R_t(s) = [Z(s)G_F^{-1}(s)][G_F(s)L(s)]$$

$$R_t(s) = Z(s)IL(s)$$

(13)

Where I is the identity matrix.

$$R_t(s) = Z(s)L(s) \quad (14)$$

If Z(s) is the diagonal matrix then

$$R_{1t}(s) = Z_{11}(s)L_1(s) \quad (15)$$

$$R_{2t}(s) = Z_{22}(s)L_2(s) \quad (16)$$

$$R_{3t}(s) = Z_{33}(s)L_3(s) \quad (17)$$

It is inferred that the first element of $R_t(s)$ that is $R_{1t}(s)$ affected only if there is a leak in the first tank. The second element of $R_t(s)$ that is $R_{2t}(s)$ affected only if there is a leak in the second tank. Like that the third element of $R_t(s)$ that is $R_3(s)$ affected only if there is a leak in the third tank.

The transformation matrix $W(s)$ is

$$W(s) = \begin{bmatrix} W_{11} & W_{12} & W_{13} \\ W_{21} & W_{22} & W_{23} \\ W_{31} & W_{32} & W_{33} \end{bmatrix} \quad (18)$$

Where W_{11}=1

$$W_{12} = \frac{-0.0011}{0.0154s + 0.00011}$$

W_{13}=0

$$W_{21} = \frac{-0.0011}{0.0154s + 0.00011}$$

W_{22}=1

$$W_{23} = \frac{-0.0015}{0.0154s + 0.00011}$$

W_{31}=0

$$W_{32} = \frac{-0.0015}{0.0154s + 0.00011}$$

W_{33}=1

The user specified residual specification matrix Z(s) is chosen in the way not disturbing fault matrix even it can be identity matrix and it is given by

$$Z(s) = \begin{bmatrix} Z_{11} & 0 & 0 \\ 0 & Z_{22} & 0 \\ 0 & 0 & Z_{33} \end{bmatrix} \quad (19)$$

Where $Z_{11} = \frac{1}{0.0154s + 0.000112}$

$$Z_{22} = \frac{1}{0.0154s + 0.00026}$$

$$Z_{33} = \frac{1}{0.0154s + 0.000193}$$

5. Simulation results

The proposed FDI scheme has been implemented on a three-tank system and its performance is observed. The controlled variables are the level of tank1 (h1) and tank3 (h3). Inflow of tank1 (fin_1) and tank3 (fin_3) are chosen as manipulated inputs. Outflow of tank1 (L_1),

tank2 (L_2) and tank3 (L_3) are considered as leak variables. The synthesis method [15,16] is used for the design of PI controller. The PI controllers are designed so that the closed loop process behaves like a first order system with unity gain and time constant same as the open loop time constant. The resulting parameter for controlling the height of tank1 using the inflow of tank1 is given by Kc = 2.54e-04 (ml/sec/m) and Ti=222 seconds and that of tank3 using the inflow of tank3 is given by Kc=7.69e-4 (ml/sec/m) and Ti=200 seconds. The process is simulated using the non-linear first principles model, whereas the FDI is based on the time invariant linearized model (Transfer function model).

The closed loop behavior of the process when a leak of magnitude 50ml/sec introduced at time t= 3000 seconds in tank1 is shown in Figure3. The behavior of the residuals is shown in Figure4. From the Figure4 one can infer the presence of leak in tank1 affect all the three residuals. By simply monitoring either the Process output or the residual it is not possible to identify the location of the fault. The Structured residual output is shown in Figure 5, 6&7. From these figures one can conclude that there is leak only in the first tank.

Closed loop response of the System when leak occurs in all the three-tanks is shown in the Figure 8 that is, a leak of magnitude 50ml/sec given in tank1 at t=2750sec, leak of magnitude 50ml/sec given in tank2 at t=4000sec and leak of magnitude 100ml/sec given in tank3 at t=6000sec. It is observed that the levels of the tank are maintained even though the fault occurs in the process. So simply monitoring the process output it is not possible to detect the fault. The behavior of the residuals is shown in Figure9.With the residual one cannot find the location of fault. The Structured residual outputs are shown in Figure 10, Figure 11, and Figure 12. From these figures one can conclude that there is leak in the all the three tanks.

The structured residual approach is tested for modeling errors that is 10% deviation in time constant is considered. The closed loop behavior of the process when a leak of magnitude 50ml/sec introduced at time t= 6000 seconds in tank3 is shown in Figure 13. The behavior of the residuals is shown in Figure14. The Structured residual outputs are shown in Figure 15, Figure 16, and Figure 17. From these figures one can conclude that there is leak in the third tank only.

Structured residual approach is also tested for another set of controller parameters. The PI controller settings are obtained so that the closed loop process behaves like a first order system with unity gain and time constant 10%less than the open loop time constant. The closed loop behavior of the process when a leak of magnitude 100ml/sec introduced at time t= 6000 seconds in tank3 under the new settings is shown in Figure 18. The behavior of the residuals is shown in Figure19. The Structured residual outputs are shown in Figure20, 21&22. From these figures one can conclude that there is leak in the third tank only.

The structured residual approach is tested for slope fault. Leak is introduced as a ramp starting with zero value at t= 4000 seconds and reaching a maximum value of 100 ml/sec at t=5000 seconds, at which it remains constant up to time t<=6000 seconds after that a negative ramp starts and it's reaching zero at t=8000 seconds. Closed loop response of the System when ramp leak introduced is shown in the Figure23. It is observed that the levels of the tank are maintained even though the fault occurs in the process. The behavior of the residuals is shown in Figure24. The Structured residual outputs are shown in Figure25, 26&27.From these figures it is inferred that the proposed scheme can identify slope fault.

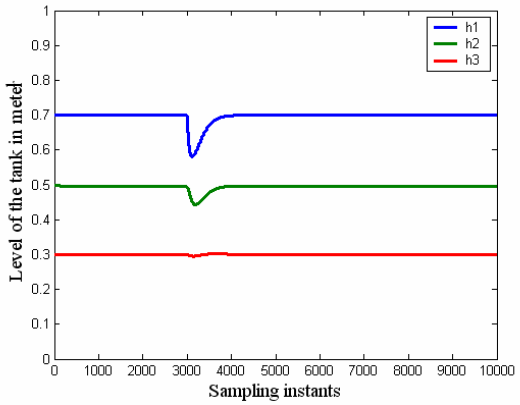

Figure.3 Closed loop response of the System when a leak of magnitude 50ml/sec occurs in tank1 at t=3000sec

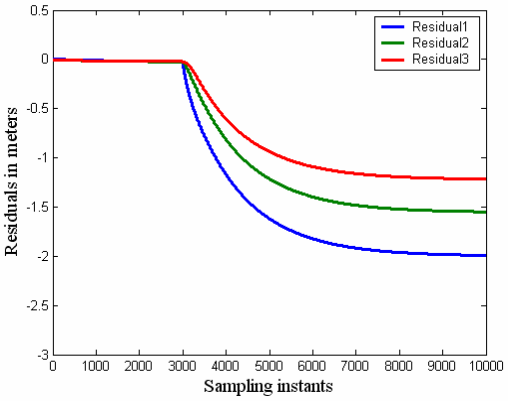

Figure 4. Evolution of residuals when step change in leak of tank1 of magnitude 50ml/sec introduced at t=3000 seconds

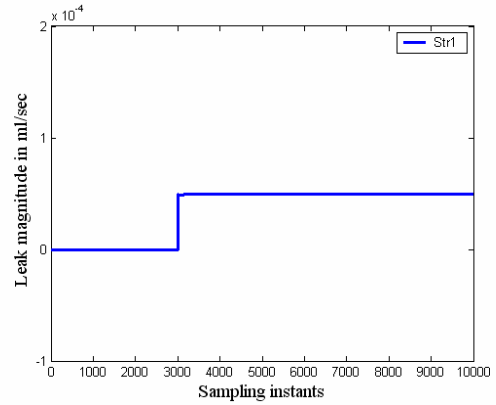

Figure 5. Structured residual1 of the system when leak of magnitude 50ml/sec is given in Tank1 at t=3000 seconds

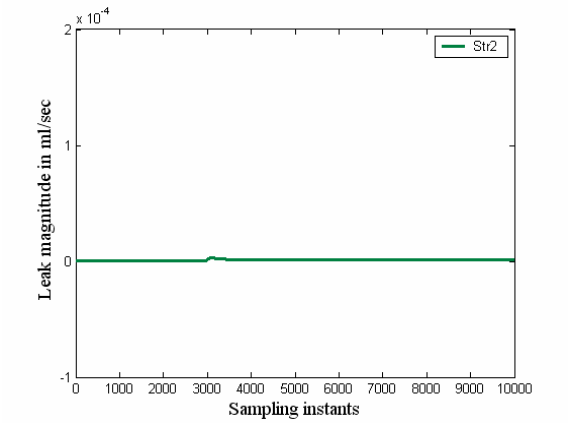

Figure 6. Structured residual2 of the system when leak of magnitude 50ml/sec is given in Tank1 at t=3000 seconds

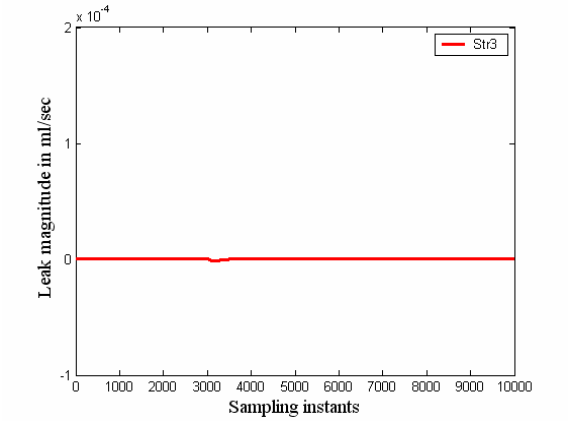

Figure 7. Structured residual3 of the system when leak of magnitude 50ml/sec is given in Tank1 at t=3000 seconds

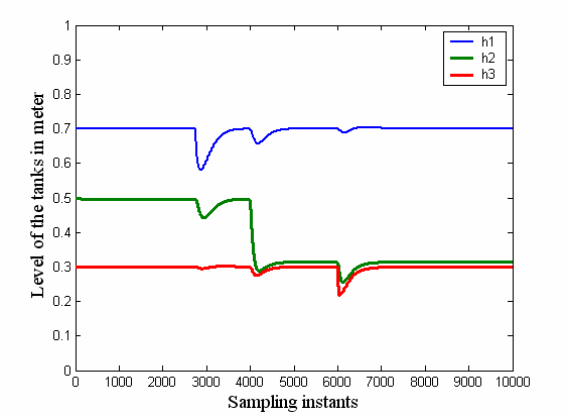

Figure 8. Closed loop response of the System when a leak of magnitude 50ml/sec given in tank1 at t=2750sec, leak of magnitude 50ml/sec given in tank2 at t=4000sec and leak of magnitude 100ml/sec given in tank3 at t=6000sec

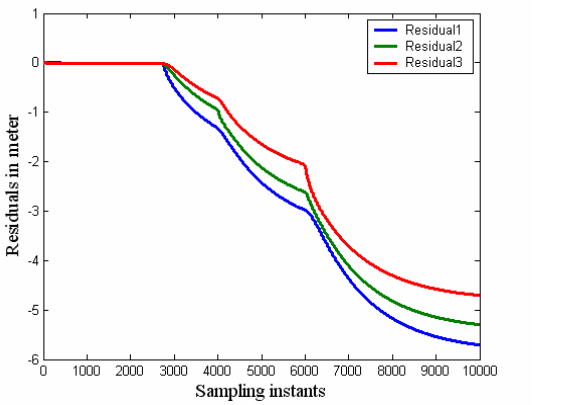

Figure 9. Evolution of residuals when a leak of magnitude 50ml/sec given in tank1 at t=2750sec, leak of magnitude 50ml/sec given in tank2 at t=4000sec and leak of magnitude 100ml/sec given in tank3 at t=6000sec

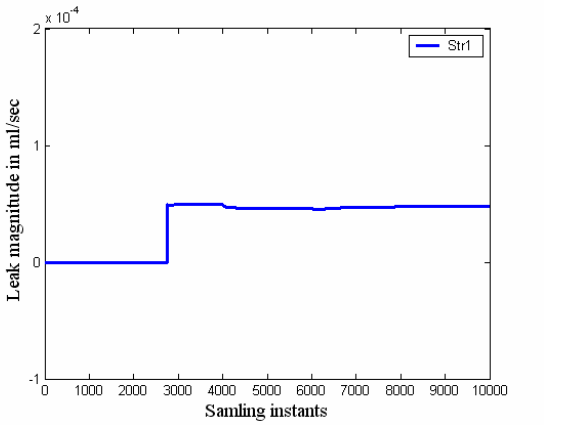

Figure 10. Structured residual1 of the system when a leak of magnitude 50ml/sec given in tank1 at t=2750sec, leak of magnitude 50ml/sec given in tank2 at t=4000sec and leak of magnitude 100ml/sec given in tank3 at t=6000sec

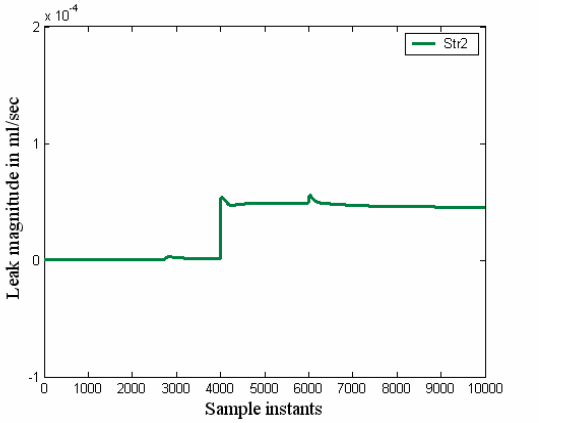

Figure 11. Structured residual2 of the system when a leak of magnitude 50ml/sec given in tank1 at t=2750sec, leak of magnitude 50ml/sec given in tank2 at t=4000sec and leak of magnitude 100ml/sec given in tank3 at t=6000sec

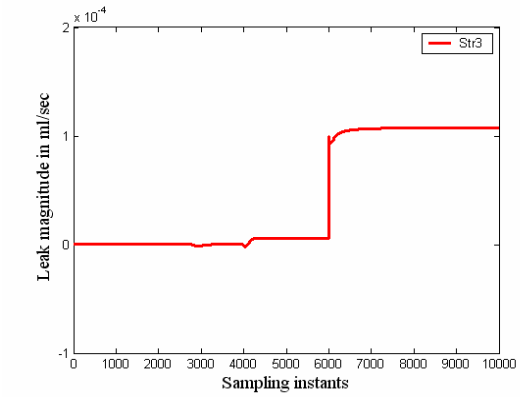

Figure 12 Structured residual3 of the system when a leak of magnitude 50ml/sec given in tank1 at t=2750sec, leak of magnitude 50ml/sec given in tank2 at t=4000sec and leak of magnitude 100ml/sec given in tank3 at t=6000sec

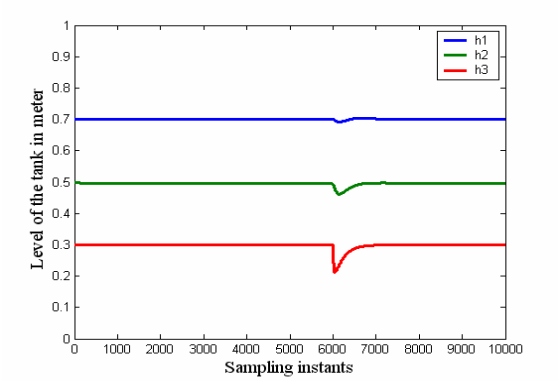

Figure.13 Closed loop response of the System when a leak of magnitude 100ml/sec occurs in tank3 at t=6000sec

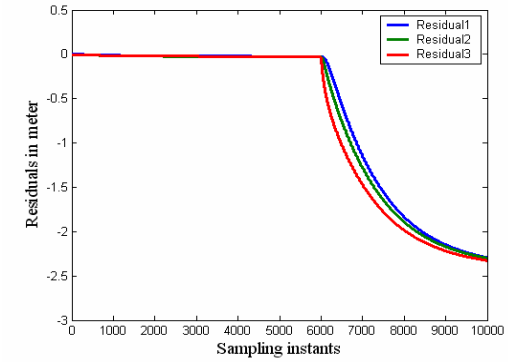

Figure14. Evolution of residuals when step change in leak of tank3 of magnitude 100ml/sec introduced at t=6000 seconds

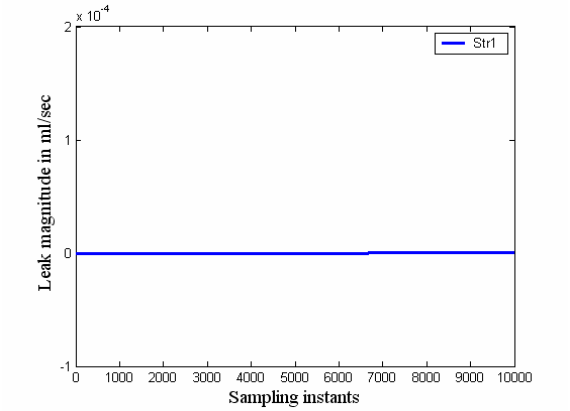

Figure 15.Structured residual1 of the system when leak of magnitude 100ml/sec is given in Tank3 at t=6000 seconds

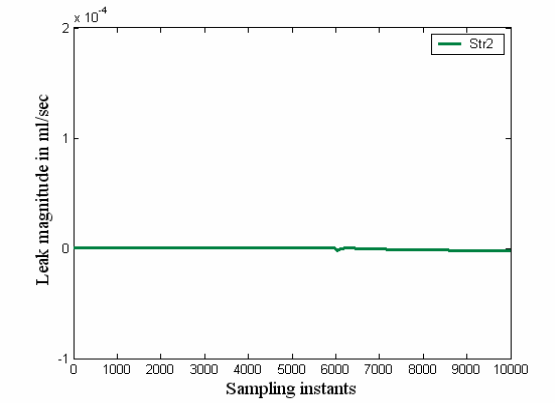

Figure 16.Structured residual2 of the system when leak of magnitude 100ml/sec is given in Tank3 at t=6000 seconds

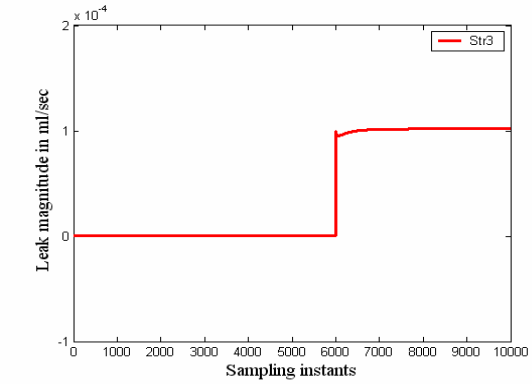

Figure17. Structured residual3 of the system when leak of magnitude 100ml/sec is given in Tank3 at t=6000 seconds

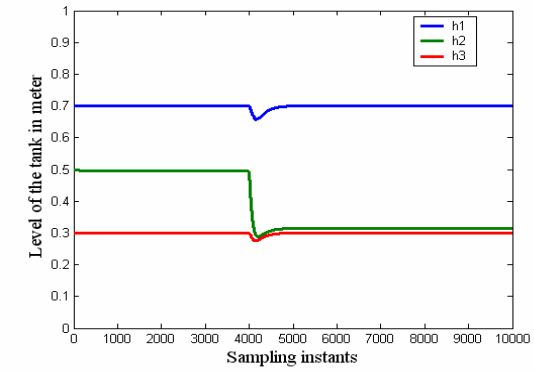

Figure.18 Closed loop response of the System when a leak of magnitude 100ml/sec occurs in tank2 at t=4000sec

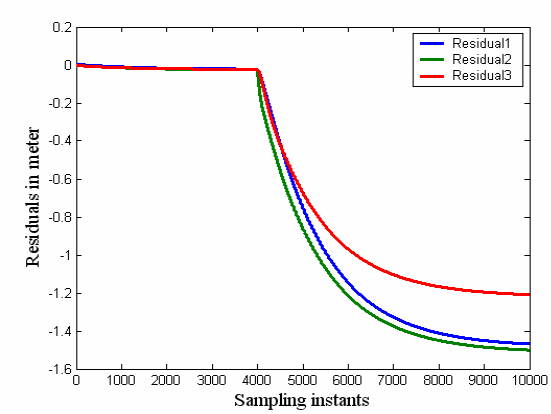

Figure19. Evolution of residuals when step change in leak of tank2 of magnitude 100ml/sec introduced at t=4000 seconds

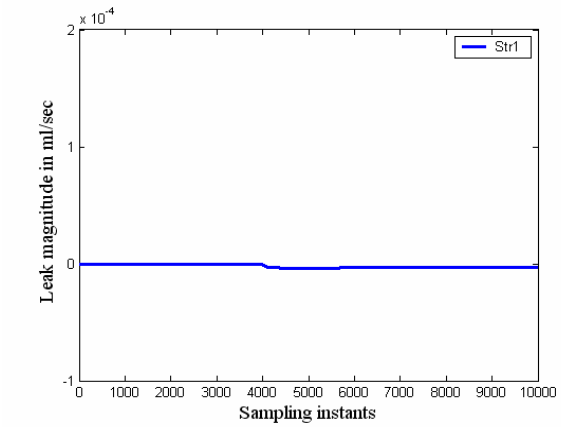

Figure 20.Structured residual1 of the system when leak of magnitude 100ml/sec is given in Tank2 at t=4000 seconds

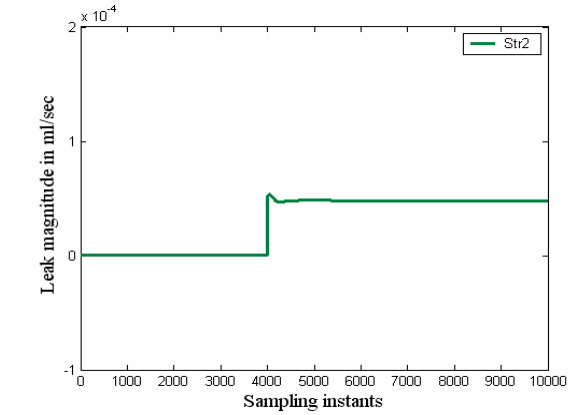

Figure 21.Structured residual2 of the system when leak of magnitude 100ml/sec is given in Tank2 at t=4000 seconds

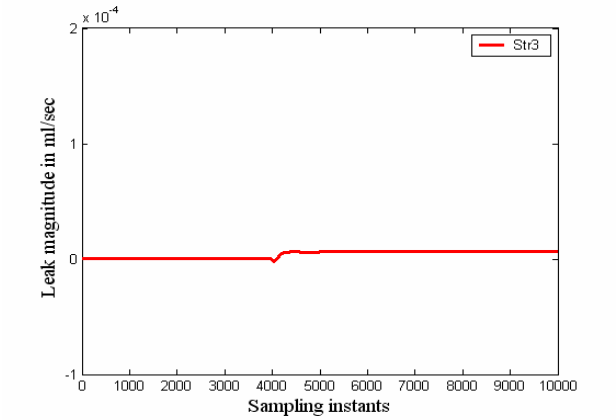

Figure22. Structured residual3 of the system when leak of magnitude 100ml/sec is given in Tank2 at t=4000 seconds

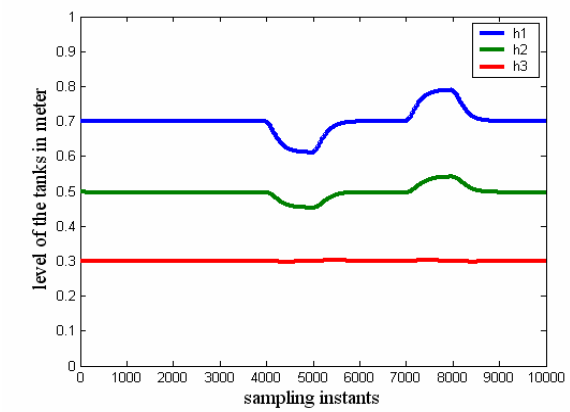

Figure.23 Closed loop response of the System when a leak of varying magnitude (ramp) 100ml/sec occurs in tank1 at t=4000sec to t=8000 sec

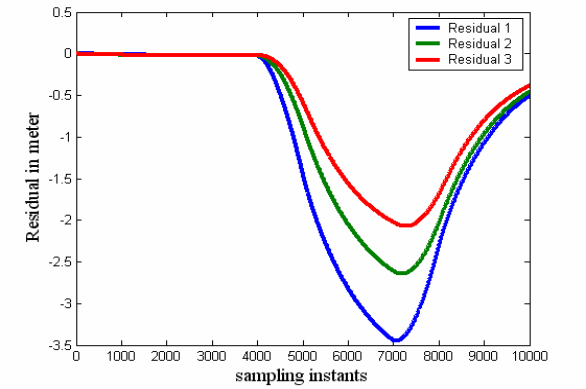

Figure24. Evolution of residuals when a leak of varying magnitude (ramp) 100ml/sec occurs in tank1 at t=4000sec to t=8000 sec

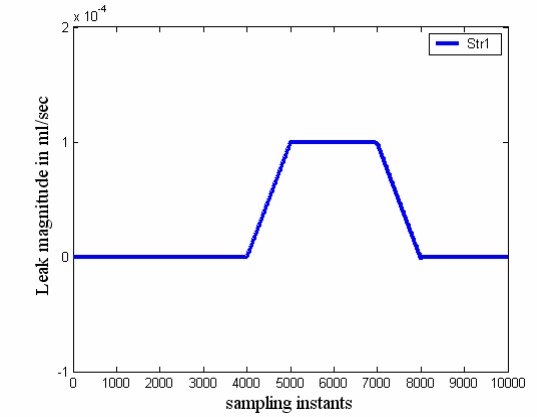

Figure 25.Structured residual1 of the system when leak of varying magnitude (ramp) 100ml/sec occurs in tank1 at t=4000sec to t=8000 sec

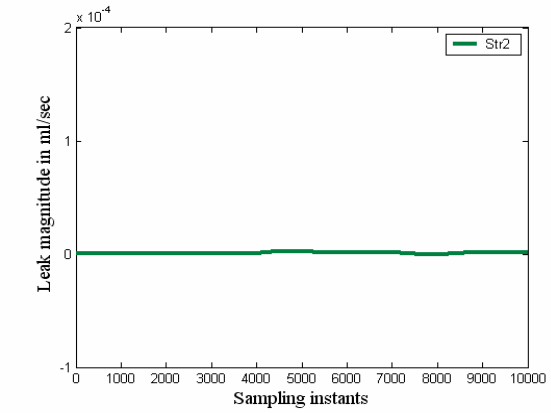

Figure 26.Structured residual1 of the system when leak of varying magnitude (ramp) 100ml/sec occurs in tank1 at t=4000sec to t=8000 sec

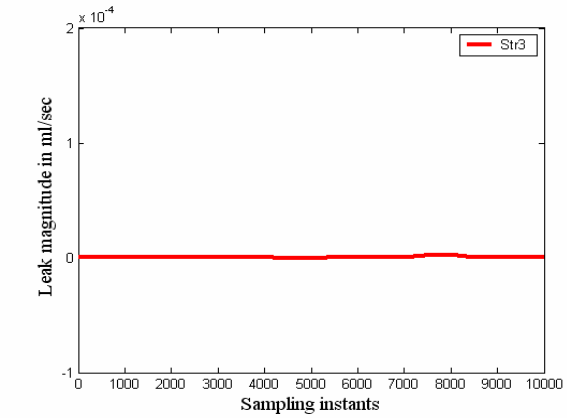

Figure 27.Structured residual1 of the system when leak of varying magnitude (ramp) 100ml/sec occurs in tank1 at t=4000sec to t=8000 sec

6. Conclusions

The performance of the proposed scheme has been evaluated on a three- tank process for leak in the tanks. The proposed FDI scheme can provide fault information even when there is simultaneous change in more than one leak. It should be noted that the proposed method is independent of the controller design. From the structured residuals, the magnitude of leak and time of occurrence of leak are also found. And one can conclude that the estimated magnitude and time of occurrence of the leak variable (fault) are close to the true value. So from the proposed method one can identify the fault as soon as it occurs in the process. The proposed method is found to be robust to plant model mismatch.

7. Acknowledgements

The authors would like to acknowledge Dr.S.P.Natarajan, Department of Electronics and Instrumentation Engineering, Annamalai University, Annamalai Nagar for granted permission to use the computer control of process laboratory.

8. References

[1] Gertler, J *Fault Detection of Dynamical Systems*, Marcel Dekker, Inc. USA(1998).

[2] Gertler, J. and Staroswiecki, M. *Structured fault diagnosisin mildly nonlinear systems: Parity space and input-output formulation*. FAC 15th World Congress, Barcelona, Spain, July 2002.

[3] Gertler, J., Staroswiecki, M. and Shen, M.:*Direct design of structured residuals for fault diagnosis in linear systems.* American Control Conference,Anchorage, Alaska, May 2002.

[4] Gertler, J. *Residual Generation in Model Based Fault Diagnosis*. Control- Theory and Advanced Technology, Vol. 9, pp. 259-285 (March 1993).

[5] Gertler, J. *A Survey of Model Based Failure Detection and Isolation in Complex Plants*. IEEE Control Systems Magazine, Vol. 8, No.6, pp. 3-11 (1988).

[6] J. Wu, G. Biswas, S. Abdelwahed, and E Manders. *A hybrid control system design and implementation for a three tank testbed*.In Proceedings of the 2005 IEEE Conference on Control Applications,pages 645–650, August 2005.

[7] Gao, Z. W., Ding, S. X. and Ma, Y. (2007): Robust fault estimation approach and its application in vehicle lateral dynamical systems, Optimal Control Applications and Methods, vol.28, no.3, pp. 143-156.

[8] Gertler, J. A Survey of Model Based Failure Detection and Isolation in Complex Plants. *IEEE Control Systems Magazine,* Vol. 8, No.6, pp. 3-11 (1988).

[9] Gertler, J. Residual Generation in Model Based Fault Diagnosis. *Control- Theory and Advanced Technology, Vol.* 9, pp. 259-285 (March 1993).

[10] Gao, Z. W., Breikin, T and Wang, H. (2007): High-gain estimator and fault-tolerant design with application to a gas turbine dynamic system, IEEE Transactions on Control Systems Technology, vol.15, no.4, pp.740-753.

[11] Gao, Z. W. and Wang, H. (2006): Descriptor observer approaches for multivariable systems with measurement noises and application in fault detection and diagnosis, Systems and Control Letters, vol.55, no.4, pp.305-313

[12] KÄoppen-Seliger, B., Alcorta-Garca, E., Frank P.M., *Fault Detection: Different strategies for Modelling Applied to the Three tank Benchmark - A Case Study*, European Control Conference, Karlsruhe, Germany, (1999).

[13] S.AbrahamLincon., D.Sivakumar., J.Prakash., *State and Fault Parameter Estimation Applied To Three-Tank Bench Mark Relying On Augmented State Kalman Filter.,* ICGST-ACSE Journal, Volume 7, Issue 1, May 2007.

[14] Frank, P. M. and Ding, X., *Survey of robust residual generation and evaluation methods in observer-based fault detection systems*, Journal of Process Control, 7(6), pp. 403-424, (1997)

[15] Marlin, E *Process Control: Designing Processes and Control Systems for Dynamic Performance,* McGraw-Hill International Editions (1995).

[16] George Stephanopoulos *Chemical process control ,An introduction to theory and practice* ,Prentice-hall India publications (2000)

A.Asokan obtained his B.E degree in Instrumentation and control Engineering in the year 1997 and received M.E. degree in Process Control and Instrumentation Engineering in 2001from the Annamalai university, Chidambaram. Presently he is working as a Lecturer of the Department of Instrumentation Engineering in Annamalai University. His areas of research are Process Control, Fault Detection and Diagnosis and Multivariable Control

Dr. D. Sivakumar obtained his B.E degree in Electronics and Instrumentation Engineering in the year 1984 and further the M.E. degree in Power Systems in the year 1990 from the Annamalai University, Chidambaram. Presently he is working as a Professor in the Department of Instrumentation Engineering in Annamalai University. He is presently guiding many Ph.D research scholars in areas like Fault Detection and Diagnosis, Neural Networks and Fuzzy Logic applied to Process Control, Signal and Image Processing.

www.icgst.com

Modeling and Diagnostics of Inductions Machines Under Rotor Failures

Tarek Aroui , Yassine Koubaa, Ahmed Toumi
Research Unity of Industrial Process Control (UCPI)
National Engineering School of Sfax (ENIS)
B.P. : W 3038 Sfax-Tunisia
Tarek.Aroui@ eniso.rnu.tn ,Yassine.koubaa@enis.rnu.tn, ahmad.tomi@enis.rnu.tn

Abstract
In this paper, a transient model of the faulty machine is developed. The model is referred to a three phase stator winding, while the rotor has been represented by all the meshes allowing for the representation of various faults. The model is based on coupled magnetic circuit theory and incorporates non sinusoidal air-gap magneto motive force (MMF) produced by both stator and rotor, therefore it will include all the space harmonics in the machine. Simulation and experimental results were first used to identify low and high frequency spectral components created by rotor anomalies in the stator current spectrum. This paper then presents an approach for motor rotor fault diagnosis using neural networks. The proposed methodology has been experimentally tested on a 5.5Kw/3000rpm induction motor. The obtained results provide a satisfactory level of accuracy.

Keywords **:** *Induction machines, coupled magnetic circuit, rotor failures, Neural networks, diagnostic.*

1. Introduction
The use of induction motors in today's industry is extensive, and the motor can be exposed to different hostile environments, misoperations, and manufacturing defects. Internal motor faults (e.g., short circuit of motor leads, interturn short circuits, ground faults, bearing and gearbox failures, broken rotor bar and cracked rotor end-rings, as well as external motor faults (e.g., phase failure, asymmetry of main supply and mechanical overload), are expected to happen sooner or later [1]. Furthermore, the wide variety of environments and conditions that the motors are exposed to can age the motor and make it subject to incipient faults. These incipient faults can lead to motor failure if left undetected.
With proper system monitoring and fault detection schemes, the costs of maintaining the motors can be greatly reduced and the availability of these machines can be significantly improved.
Many researchers have focused their attention on incipient fault detection and preventive maintenance in recent years. There are invasive and noninvasive methods for machine fault detection, the noninvasive methods are more preferable than the invasive methods because they are based on easily accessible and inexpensive measurements to diagnose the machine conditions without disintegrating the machine structure.
Recently, artificial intelligence (AI) techniques have been proposed for the noninvasive machine fault detection [2,3]. These AI-based techniques include expert systems, neural network, fuzzy logic and combined techniques.
These AI-based techniques have numerous advantages over conventional diagnostic approaches. In general, they can lead to improved performance when properly tuned, they are easy to extend and modify, and they can be easily made adaptive by the incorporation of new data or information, as they become available.
In the AI-based systems, several quantities are utilized as input signals: stator currents and voltages, magnetic fields and frame vibrations, etc. In general, stator currents and voltages are preferred because they allow for the realization of non-invasive diagnostic systems
The diagnostic procedure, based on the current signal, can be organized in the following steps [2]:

- Choice of the failure to be considered,
- Definition of cause-effect relationships,
- Computation of the diagnostic indexes linked to the fault extent.

Filippetti[4] note that the AI techniques to induction machines diagnostics should correspond to wide industrial applications, but plant operators look at these tools with a certain degree of suspicion, due to their complexity and their cost. To implement a complete diagnostic system for industrial applications, it is fundamental to:

- Employ a minimum configuration intelligence,
- Develop a knowledge base transferable from machine to machine.

With regard to the first point, in connection to the structure of a diagnostic system, the best idea appears to be a global neural solution.
In order to develop technologies for motor fault detection and diagnosis, it is important to show the proposed theory, schemes, feasibility, and limitations. In the research stage, we require a controllable environment so

that we know what types of faults are induced and what types of motor performance are resulted.
The objective of this paper is to develop a model which is capable to predict the performance of induction machines under broken rotor bars and end-ring faults then a supervised neural network is applied to motor rotor faults detection and severity evaluation. Neural network is trained and tested using measurement data of stator current spectra.
The remainder of the paper is organized as follows: Section (2) focuses on the complete model of a squirrel cage induction machine. In section (3) we discuss the modeling of rotor failures. In Section (4) simulation results are present. In Section (5) we describe the experimental setup and results. In section (6) the neural networks-based detection system is implemented. We present in section (7) results using neural network. Section (8) concludes this paper.

2. Induction machine modeling

This model follows the coupled magnetic approach by treating the current in each rotor bar as an independent variable. The effect of non-sinusoidal air-gap MMF produced by both the stator and the rotor currents have been incorporated into the model. This is done by use of the winding function approach.
Our analysis is based on the following assumptions [5]: Symmetric machine, uniform air-gap, negligible saturation and insulated rotor bar.
The stator comprises of three phase concentric winding. Each of these windings is treated as a separate coils. The cage rotor consists of n bars can be described as n identical and equally spaced rotor loop [6,7]. Each loop is formed by two adjacent rotor bars and the connecting portions of the end-rings between them. Hence, the rotor circuit has $n+1$ independent currents as variables. The n rotor loop currents are coupled to each other and to the stator windings through mutual inductances. The end-ring loop does not couple with the stator windings [7], it however couples the rotor currents only through the end leakage inductance and the end-ring resistance.

2.1. Stator voltage equations

The stator equations for the induction machine can be written in vector matrix form as:

$$\left[V_s\right]=\left[R_s\right]\left[I_s\right]+\frac{d}{dt}\left[\Phi_s\right] \tag{1}$$

where

$$\left[\Phi_s\right]=\left[L_{ss}\right]\left[I_s\right]+\left[L_{sr}\right]\left[I_r\right] \tag{2}$$

and

$$\left[I_s\right]=\left[I_{s1}\ I_{s2}\ I_{s3}\right]^T \tag{3}$$

$$\left[I_r\right]=\left[I_{r1}\ I_{r2}\cdots I_{rn}\ I_e\right]^T \tag{4}$$

$$\left[V_s\right]=\left[V_{s1}\ V_{s2}\ V_{s3}\right]^T \tag{5}$$

The matrix $[R_s]$ is a diagonal 3 by 3 matrix which consists of resistances of each coil.
Due to conservation of energy, the matrix $[L_{ss}]$ is a symmetric 3 by 3 matrix. The mutual inductance $[L_{sr}]$ matrix is an 3 by n matrix comprised of the mutual inductances between the stator coils and the rotor loops.

$$\left[L_{sr}\right]=\begin{bmatrix} L_{sr11} & L_{sr12} & \cdots & L_{sr1n} & L_{sr1e} \\ L_{sr21} & L_{sr22} & \cdots & L_{sr2n} & L_{sr2e} \\ L_{sr31} & L_{sr32} & \cdots & L_{sr3n} & L_{sr3e} \end{bmatrix} \tag{6}$$

Where L_{srij} is the mutual inductance between the stator phase i (i=1,2 or 3) and the rotor loop j (j=1,2 … n) and L_{srie} the mutual inductance between the stator phase i (i=1,2 or 3) and the end-ring.

2.2. Rotor voltage equations

Given the structural symmetry of the rotor, it is convenient to model the cage as identical magnetically coupled circuits. For simplicity, we assume that each loop is defined by two adjacent rotor bars and the connecting portions of the end-rings between them [7].
For the purpose of analysis, each rotor bar and segment of end-ring is substituted by an equivalent circuit representing the resistive and inductive nature of the cage. Such an equivalent circuit is shown in Figure 1.

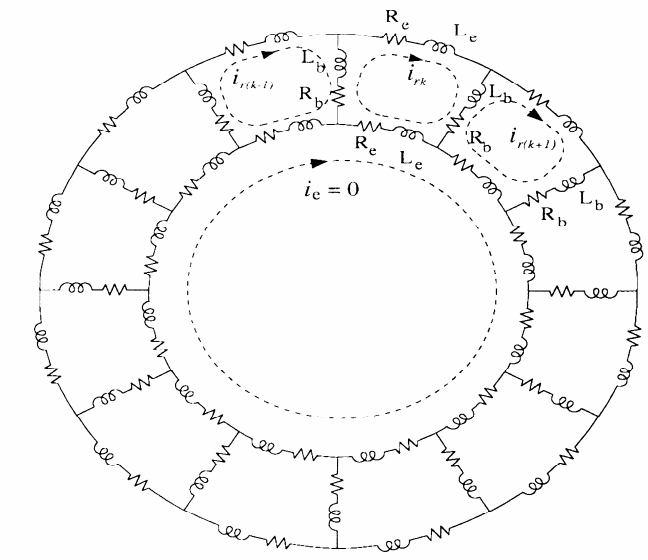

Figure 1. Rotor cage equivalent circuit showing rotor loop currents and circulating end ring current.

From Figure 1, the voltage equations for the rotor loops can be written in vector matrix form as:

$$\left[V_r\right]=\left[R_r\right]\left[I_r\right]+\frac{d}{dt}\left[\Phi_r\right] \tag{7}$$

where

$$\left[V_r\right]=\left[V_{r1}\ V_{r2}\ \cdots V_{rn}\ V_{re}\right]^T \tag{8}$$

and

$$\left[\Phi_r\right]=\left[L_{rs}\right]\left[I_s\right]+\left[L_{rr}\right]\left[I_r\right] \tag{9}$$

In case of a cage rotor, the rotor end ring voltage is V_{re}=0, and the rotor loop voltages are V_{rk}=0, k = 1,2…n.

The loop equation for *k*th rotor circuit is:

$$V_{rk}=0=2(R_b+R_e)I_{rk}-R_bI_{r(k-1)}-R_bI_{r(k+1)}-R_eI_e+\frac{d\Phi_{rk}}{dt} \tag{10}$$

The voltage equation for the end-ring is:

$$V_{re}=0=-R_eI_{r1}-R_eI_{r2}-\cdots-R_eI_{rn}+nR_eI_{re}+\frac{d\Phi_{rk}}{dt} \tag{11}$$

Where R_b is the rotor bar resistance, R_e is the end-ring segment resistance and Φ_{rk} is the total flux linked by the *k*th loop.
Since each loop is assumed to be identical, the equation (10) is valid for every loop. Therefore the resistance matrix $[R_r]$ is a symmetric (n+1) by (n+1) matrix given by:

$$\left[R_r\right]=\begin{bmatrix} 2(R_b+R_e) & -R_b & 0 & \vdots & 0 & -R_b & -R_e \\ -R_b & 2(R_b+R_e) & -R_b & \vdots & 0 & 0 & -R_e \\ \vdots & \vdots & \vdots & \vdots & \vdots & \vdots & \vdots \\ \vdots & \vdots & \vdots & \vdots & \vdots & \vdots & \vdots \\ 0 & 0 & 0 & \vdots & 2(R_b+R_e) & -R_b & -R_e \\ -R_b & 0 & 0 & \vdots & -R_b & 2(R_b+R_e) & -R_e \\ -R_e & -R_e & -R_e & \vdots & -R_e & -R_e & nR_e \end{bmatrix} \tag{12}$$

Due to the structural symmetry of the rotor, $[L_{rr}]$ can be written in matrix form (13).

$$\left[L_{rr}\right]=\begin{bmatrix} L_{11}+2(L_b+L_e) & L_{12}-L_b & L_{13} & \cdots & L_{1(n-1)} & L_{1n}-L_b & -L_e \\ L_{21}-L_b & L_{22}+2(L_b+L_e) & L_{23}-L_b & \cdots & L_{2(n-1)} & L_{2(n-1)} & -L_e \\ \vdots & \vdots & \vdots & \cdots & \vdots & \vdots & \vdots \\ \vdots & \vdots & \vdots & \cdots & \vdots & \vdots & \vdots \\ L_{(n-1)1} & L_{(n-1)2} & L_{(n-1)3} & \cdots & L_{(n-1)(n-1)}+2(L_b+L_e) & L_{(n-1)n}-L_b & -L_e \\ L_{n1}-L_b & L_{n2} & L_{n3} & \cdots & L_{n(n-1)}-L_b & L_{nn}+2(L_b+L_e)-L_e & \\ -L_e & -L_e & -L_e & \cdots & -L_e & -L_e & nL_e \end{bmatrix} \tag{13}$$

where L_{kk} is the self inductance of the *k*th rotor loop, L_b is the rotor bar leakage inductance, L_e is the rotor end-ring leakage inductance and L_{ki} is the mutual inductance between two rotor loop.

2.3. Calculation of torque

The mechanical equation of the machine is [5]:

$$C_{em}-C_r=J\frac{d\Omega_m}{dt} \tag{14}$$

Where C_{em} is the electromagnetic torque, C_r is the load torque , J is the inertia of the rotor and Ω_m is the mechanical speed.

$$\Omega_m=\frac{1}{P}\frac{d\theta}{dt} \tag{15}$$

where θ is the angular position of the rotor and p denotes the number of motor pole pairs.
The electromagnetic torque is given by the following equation [8]:

$$C_{em}=PI_s^t\left\{\frac{d}{d\theta}\left[L_{sr}\right]\right\}I_r \tag{16}$$

2.4. Calculation of inductances

It is apparent that the calculation of all the machine inductances as defined by the inductances matrices in the previous section is the key to the successful simulation of an induction machine.
The model must take into account the geometric construction of the machine and then will include all the space harmonic.
These machine inductances are conveniently calculated by means of winding functions. This method assumes no symmetry in the placement of any motor coil in the slots. According to winding function theory, the mutual inductance between two windings *i* and *j* in any electric machine can be computed by the following equation [8,9,10]:

$$L_{ij}(\theta) = \frac{\mu_0 l r}{g}\int_0^{2\pi}\varepsilon_i(\theta,\varphi)\,\varepsilon_j(\theta,\varphi)\,d\varphi \tag{17}$$

where $\mu_0 = 4\pi.10^{-7}$ H/m, g is the air gap, θ is the angular rotor position, r is the average radius of the air gap, l is the active length of the motor, φ is a particular point along the air gap and $\varepsilon_i(\theta,\varphi)$ is called the winding function and represents the magneto motive force (MMF) distribution along the air gap for a unit current flowing in winding *i*.
For simulation purposes a three phase, 4Kw, 50hz, 4 pole, 380/220V squirrel-cage induction motor will be treated in this paper. The machine has a stator comprises of three phase concentric winding with 36 slots, 28 rotor bars and two coils per phase. Each coils is constituted of three sections having N_S turns in series (N_S=26 for the machine under test). Figure 2 shows the MMF distribution produced by 1A of current through the stator phase ″1″ obtained by summing all the winding function of the stator phase coils [10]. Note that the both stator

phases ″2″ and ″3″ produce a similar MMF distribution but shifted by $\frac{\pi}{3}$ and $\frac{2\pi}{3}$.

The MMF distribution produced by 1A of current through a rotor loop can only take two values depending on whether we are inside or outside the loop. The angle between two adjacent rotor bars is $\alpha=\frac{\pi}{14}$, the MMF distribution produced by 1A of current through the first rotor loop, is shown in Figure 3.

The mutual inductance between stator and rotor branches will be a function of the rotor position angle, θ. Figure 4 gives the mutual inductance $(L_{sr11}(\theta))$ between the stator phase ″1″ and the rotor loop ″1″. Note that the mutual inductance between the phase ″2″ and the rotor loop ″1″ is $L_{sr11}(\theta)$ but shifted to the right by 6γ, where γ is the angle between two stator slots. Mutual inductance between the phase ″1″ and the rotor loop ″2″ is $L_{sr11}(\theta)$ but shifted to the left by α, where α is the angle between two rotor bars.

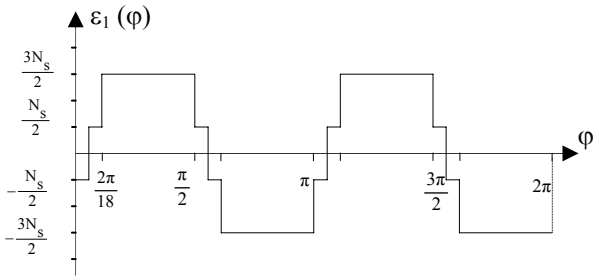

Figure 2. MMF distribution of the stator phase ″1″

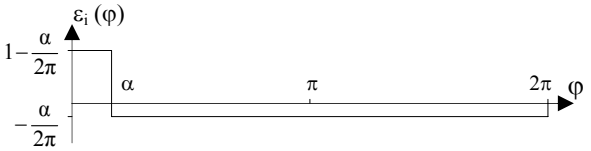

Figure 3. MMF distribution of the rotor loop ″1″

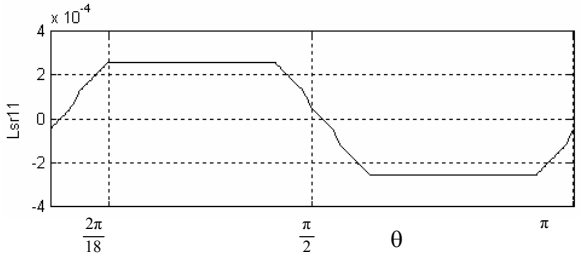

Figure 4. Mutual inductance between the stator phase ″1″ and rotor loop ″1″

3. Modeling rotor bars faults

Broken bar faults can be incorporated in the healthy machine model by assuming that bars or end-ring segments are fully broken [6]. Thus, one can remove the loop equations corresponding to the broken bars or the end-ring segments from (7) in order to model the broken-bar or end-ring faults. In the case of *m* fully broken bars or end-ring segments, *m* loop equations are removed.

4. Simulation results

To validate the proposed model, a functional schema of the induction machine was developed on the MATLAB-SIMULINK platform.

The machine is first simulated under healthy condition. Figure 5 shows the instantaneous electromagnetic torque, speed and the phase current of the machine during a start up with a balanced sinusoidal voltage supply followed by the application of a load (C_r = 11Nm) at instant t=0.8s.

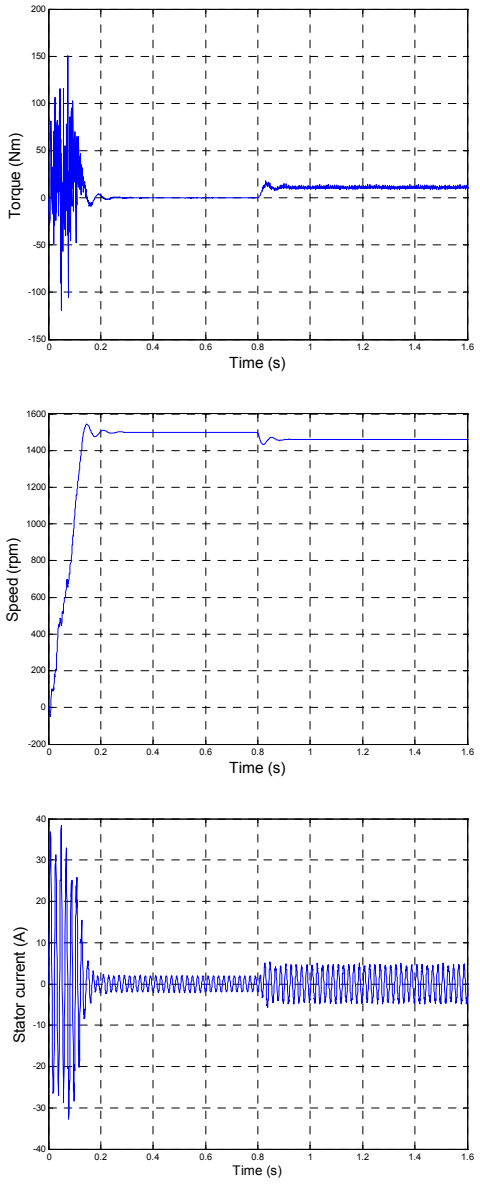

Figure 5. Torque, Speed and stator current in phase ″1″(top to bottom). Normal machine

Next the rotor failures were simulated. Figure 6 Shows the instantaneous electromagnetic torque, speed and the phase current of the machine with four broken rotor bars and one end-ring, during a start up with a balanced sinusoidal voltage supply followed by the application of a load (C_r = 11Nm) at instant t=0.8s. We can easly see that

the effect of four broken rotor bars and one end-ring is very important. (e.g., the acceleration time under rotor asymmetry is larger than under healthy machine).

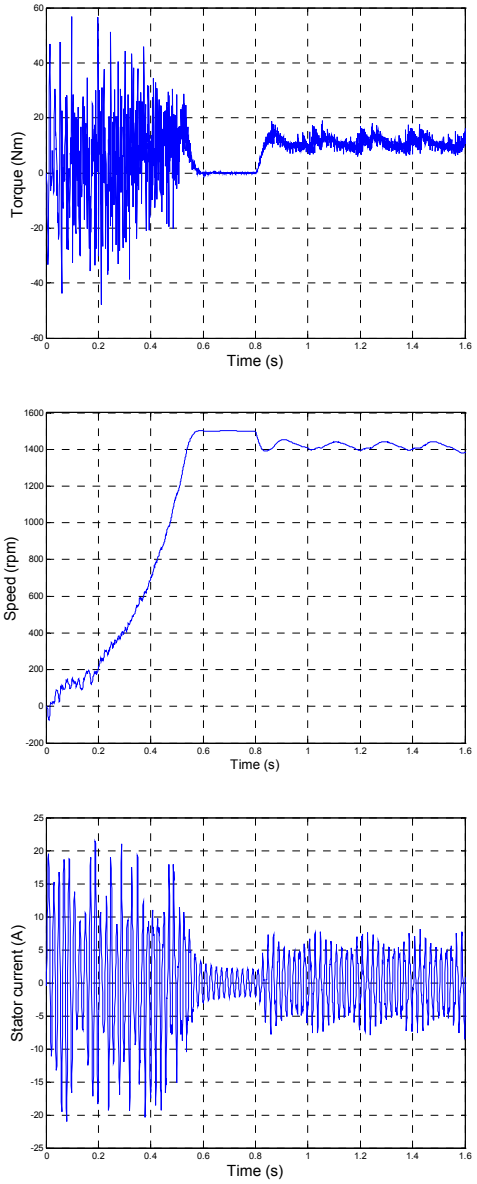

Figure 6. Torque, speed and stator current in phase"1"(top to bottom). Machine with four broken rotor bars and one end-ring

4.1. Analysis of steady state operation

The stator current signal at steady state for the loaded machine is transformed by the Fast Fourier Transform (FFT) into signal in the frequency domain to generate the power spectral density (PSD). The spectrum generated by this transformation includes only the magnitude information about each frequency component, which can be analyzed and processed easier than signal in the time domain.

4.1.1. Spectrum analysis in the bandwidth [25Hz-75Hz]

Figure 7 reports stator current spectrum around fundamental for a normal machine and a machine with four broken bars and one broken end-ring. We can see that rotor anomalies induce some harmonic components, given by [4,11]:

$$f_{bc} = (1 \pm 2ks)\, f_s \quad ,k = 1, 2, 3, \ldots\ldots \tag{18}$$

where f_{bc} are frequencies associated with the broken bar, s is the slip and f_s is the supply frequency.

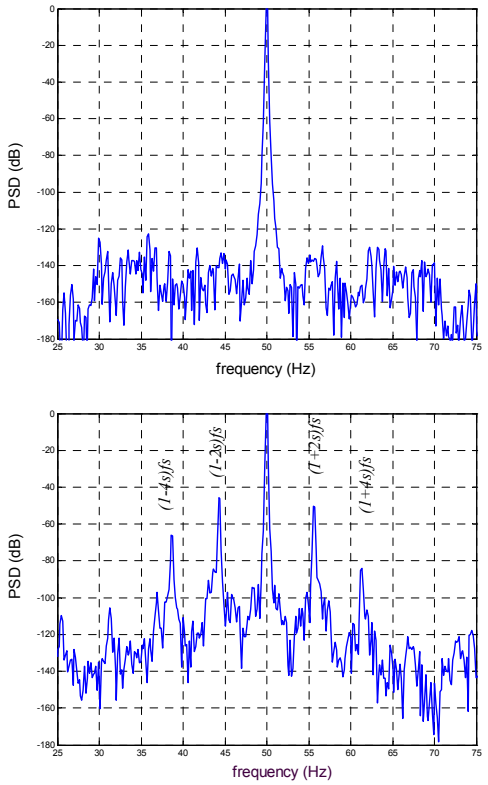

Figure 7. Simulated stator current spectrum for healthy machine and for the case of four broken rotor bars and one end-ring (top to bottom)

4.1.2. Spectrum analysis in the bandwidth [100Hz-1000Hz]

There are other spectral components that can be observed in the stator line current due to broken rotor bar fault. The equation describing these frequency components is given by Nandy [11]

$$f_{hbc}^{\pm} = \left[\left(\frac{k}{p}\right)(1-s) \pm s\right] f_s \tag{19}$$

where, $f_{hbc}^{\pm}$ are detectable broken bar frequencies; $\frac{k}{p}$=3, 5,7,9,11,13,……..

Figure 8 shows the simulated plot of the stator currents spectrum around 5th time harmonic with rotor failures, we can visualize the presence of the principal components $f_{hbc}^{\pm}$. We notice the presence of additional frequency components which are spaced by $2sf_s$. This can be verified on space harmonic 7, 11, 13 …

Then, it is necessary to complete equation (19) to take into consideration these harmonics because they are indicative of failure presence in the rotor cage. The new equation will be:

$$f_{hbc}=\left[\left(\frac{k}{p}\right)(1-s)\pm(1+2\beta)s\right]f_s \qquad (20)$$

where, f_{hbc} is detectable broken bar frequencies; $\frac{k}{p}$=3,5,7,9,11,13,…….. And β= 0,1,2,3,……

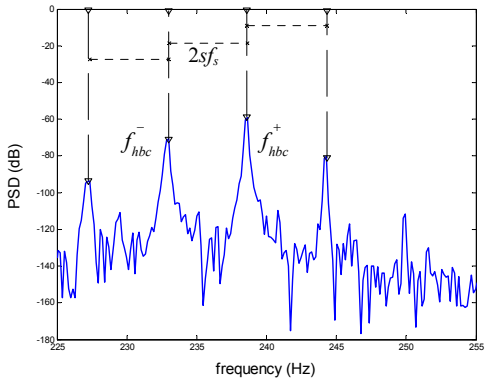

Figure 8. Simulated stator current spectrum for faulty machine around the 5th time harmonic

5. Experimental setup and results

The characteristics of the 3-phase induction motor used in our experiment are listed in Table1. The needed load of the induction motor was established by connecting the test motor to an eddy current brake via a flexible coupling (Figure 9). In order to allow tests to be performed at different load levels, the brake DC supply current is controllable.

Figure 9. View of the experimental setup

A current Hall effect sensor (Honeywell type CSNA111) was placed in one of the line current cables. The stator current was sampled with a 4 KHz rate and interfaced to a pentium PC by an ARCOM(APCI-ADADIO) acquisition board. The APCI-ADADIO is a 32-bit PCI local bus board, which provides 8 differential or 16 single-ended multiplexed 12-bit ADC channels.

A MATLAB Application Program Interface (API) is built to allow The ARCOM A/D PC card to communicate directly with MATLAB.

The motor was tested with the healthy rotor and a faulty rotor with two broken bars. The bars were broken by drilling holes through them.

Description	*Value*
Power	5.5 kW
Input Voltage	220/380 V
Full load current	20.6/11.9A
Supply frequency	50 Hz
Number of poles	2
Number of rotor slots	28
Number of stator slots	36
Full load speed	2875 rpm

Table 1. Induction motor Characteristics used in the experiment

As predicted by simulation, Figures 10, 11 and 12 show the experimental results with healthy and faulty machine around fundamental. We can see the amplitude of the sidebands components f_{bc} according to equation (18) in the faulty machine current increase over their counterpart in the case of the healthy machine.

Experimental results show significant changes around the 5th time harmonic (Figure 13). According to equation (20), space harmonic spaced by $2sf_s$ can be clearly seen.

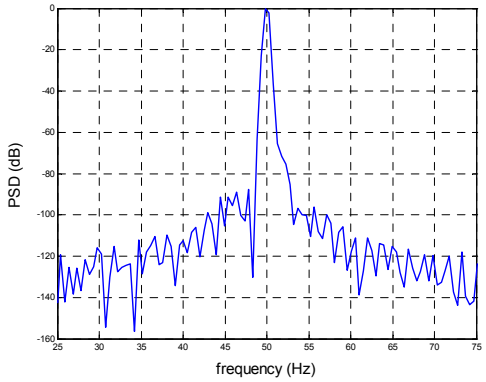

Figure 10. Experimental stator current spectrum around fundamental of the healthy machine

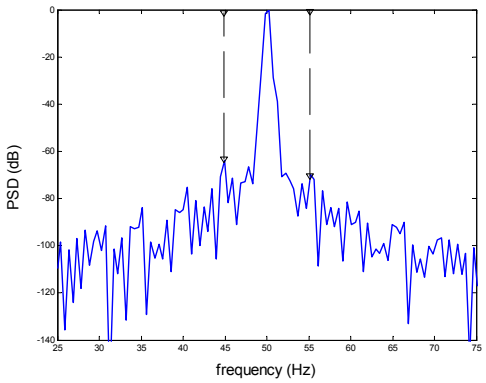

Figure 11. Experimental stator current spectrum around fundamental of the faulty machine with one broken bars

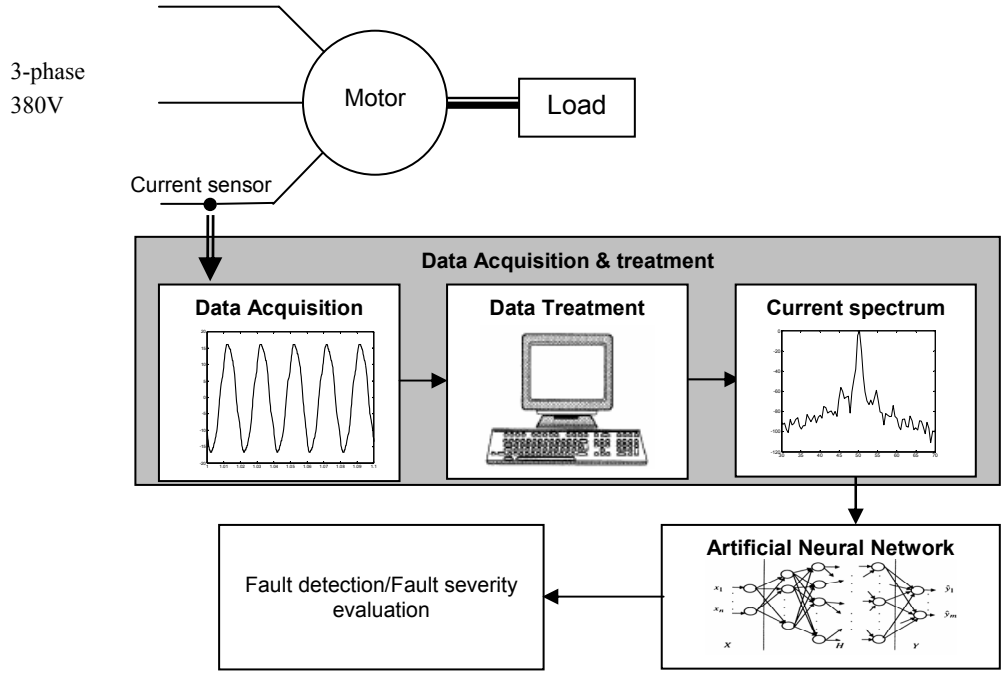

Figure 14. : Block diagram of the experimental NN-based detection system

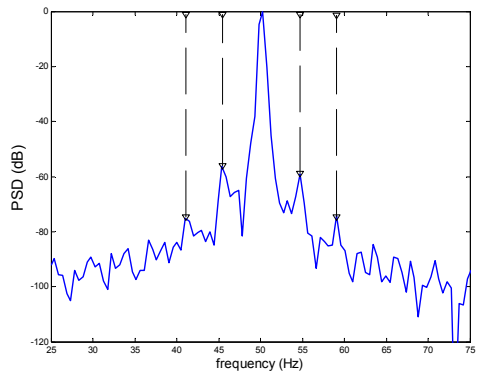

Figure 12 Experimental stator current spectrum around fundamental of the faulty machine with two broken bars

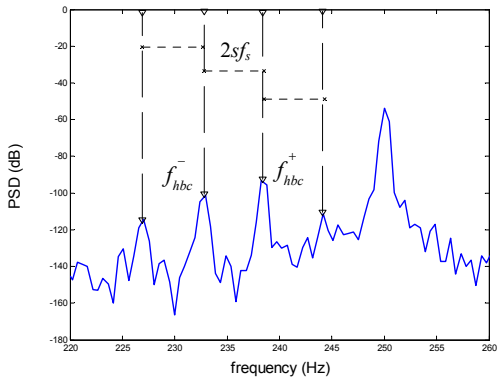

Figure 13. Experimental stator current spectrum around 5th time harmonic of the faulty machine with two broken bars

6. Description of the experimental Neural Networks-based detection system

Stator current analysis is based on the principle, as the fault progresses, its characteristic spectral components continue to increase over time. Therefore, the correlation between the amplitude of these components and the fault extent is the issue of the diagnostic system.

In this section, real motor stator current data were collected to verify the feasibility of applying a neural network to diagnose rotor fault.

Figure 14 describes the basic fault detection system in the frequency domain. First stator current signal are collected from Hall effect sensor at an equal sampling time. Then the signals are transformed by the Fast Fourier transform (FFT) into signals in the frequency domain, which can provide salient features for the diagnosis of rotor condition. The spectrum generated by this transformation includes the magnitude information about each frequency component. Signal noise that exists in the spectrum is reduced by averaging and windowing.

The ability to average a series of measurements is useful to discriminate between noise and components that are actually part of the signal. This ensemble-averaging technique is very effective for determining the frequency content of a signal buried in a random noise.

Finally, the rotor faults frequency signature is extracted as inputs of neural networks. Through supervised training with inputs and outputs, the learned neural networks can detect rotor faults and also the extent of the faults.

6.1. Artificial Neural Networks (ANN)

Artificial neural networks (ANN) are used to recognize and classify complex fault patterns without much knowledge about the system they deal with. They are designed to mimic the human nervous system using massively parallel nets composed of many computational elements connected by links with variable weights. Of all

the ANNs, the multi-layer feedforward artificial neural network, trained using the back-propagation algorithm, is the most commonly and flexibly used [12]. Its typical architecture, which contains the input layer, a number of hidden layers and the output layer, is shown in Figure 15. Initially, an input pattern is applied to the input layer, then signals propagate forward, level by level, through the hidden layers and the output layer produces the network output. Each neuron in a layer (except the ones in the input layer) sums up their input value (x) with interconnection to its associated weight (w) and corresponding bias (b) to form its own scalar output (Net). The bias is added to shift the sum relative to the origin. The Net passes through a non-linear activation function (f), providing an output value (Y).
The activity level of the jth neuron in layer l is obtained as [13]:

$$o_j = f_j(Net_j) = f_j\left[\sum_i (w_{ji} v_i) + b_j\right] \tag{21}$$

where o_j is the activity level (output) of the jth neuron, Net_j is the input of the jth neuron, f_j is the activation function of the jth neuron, w_{ji} is the connection weight from the ith neuron to the jth neuron, v_j is the activity level of the ith neuron in the prior layer and b_j is the bias term of the jth neuron.

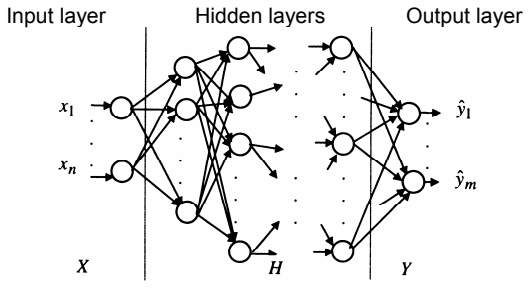

Figure 15 . Basic structure of a multi-layer feedforward artificial neural network

The active function defines the output of a neuron in terms of the activity level at its level. There are three basic types of activation functions: threshold, piece-linear and sigmoid [3]. The sigmoid function is by far the most common activation function. In this paper the tan-sigmoid transfer function is used, which generates outputs between -1 and +1. Its definition is expressed in equation (22):

$$f(Net) = \frac{1}{1+e^{-2Net}} - \frac{1}{1+e^{2Net}} \tag{22}$$

The backpropagation algorithm is used to train the network [1]. The connection weights are iteratively adjusted so that the error between the network output and the desired output (target) for a given reference input is minimized. The error goal is expressed as the sum of the squared error (SSE), calculated as follows:

$$SSE = \sum_{k=1}^{m}\left(t_k - y_k\right)^2 \tag{23}$$

Where t_k represents the desired output of the kth neuron in the output layer.
The incremental change of weight from the ith neuron to the jth is computed by [14]:

$$\Delta w_{ji}(t+1) = \eta \delta_j o_i + \alpha \Delta w_{ji}(t) \tag{24}$$

$$\delta_k = (t_k - o_k) f_k^{'}(Net_k) \tag{25}$$

$$\delta_m = f_m^{'}(Net_m)\left(\sum_k \delta_k w_{kj}\right) \tag{26}$$

where $\Delta w_{ji}(t)$ is the incremental change in the weight w_{ij} at time t, t_k is the desired output of the kth neuron in the output layer, η is the learning rate and α is the momentum.
The momentum term ($\alpha \Delta w_{ji}(t)$), included in the weight update equation to try to avoid a local minimum [1].
Equation (25) holds for the kth neuron in the output layer, and (26) holds for the mth neuron in the hidden layer.

6.2. Data normalization

In order to improve the neural network performance, the data must be well-processed and properly-scaled before inputting them to ANN[13]. The normalization process was required to restrict the range of the patterns for input into the neural networks. In this study, the inputs to the neural network are normalized between [-1,+1] by equation (27):

$$x_n = \left(\frac{x - x_{\min}}{x - x_{\max}}\right) \times 1{,}8 - 0{,}9 \tag{27}$$

Where $x_{\max}$ is the maximum magnitude of the input vector and $x_{\min}$ is the minimum magnitude of the input vector

6.3. Machine slip computation

The current spectrum components depend on the machine speed or slip. Therefore to avoid the need to measure the machine speed using conventional transducers, we choose to calculate the rotor slot harmonics given by the following equation [4]:

$$f_r^{\pm} = \left[\left(\frac{N_r}{p}\right)(1-s) \pm 1\right] f_s \tag{28}$$

where P is the pole pair number, f_s is the supply frequency and N_r is the rotor slot number.
These components are always present in the stator current spectrum with healthy and faulty rotor. Figure 16 shows these components for full load condition of the motor with two broken rotor bar fault. However, the analyze of this spectrum reports that the detection of the first slot


harmonic line at frequency f_r^+ is easy and represents the component with the maximum amplitude in this bandwidth.

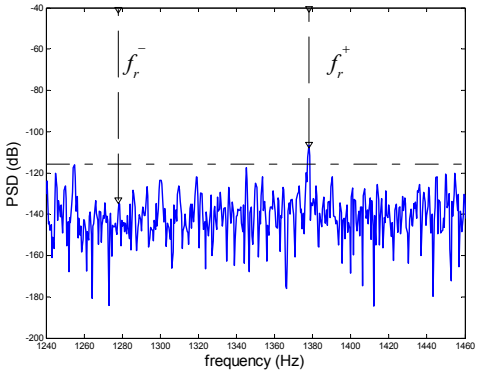

Figure 16. Experimental stator current spectrum in the frequency bandwidth [1200 Hz – 1450 Hz]

7. Results using the neural network

Experimental data were collected for each operating condition of the motor (healthy, rotor with one and two broken bar) under four different load conditions. The load conditions of the motor are 25%, 50%, 75% and full load respectively. These load condition percentages are determined according to the motor nameplate information given in Table1. A total set of 180 sets of current was collected, and two thirds of them were used to train the neural networks. The rest of the data set was used to test the network's performance.

The Neural Network Toolbox used of MATLAB was employed to train the artificial neural networks for this investigation. A three layered feed-forward neural network with backpropagation algorithm was used to perform the desired analysis. The network topology is as follows:

- The NN input layer is constituted by a set of 14 neurons in order to consider 10 spectrum components centred around the fundamental, 2 spectrum components around 5th harmonic and 2 spectrum components around 7th harmonic. We have considered the fundamental harmonic given by equation (20) when η=0 and $\frac{k}{p}$ respectively equal to 5 and 7.
- A proper selection on the number of hidden neurons has significant effect on the network performance. In order to demonstrate the performance of the FFNN, the number of hidden neurons is varied to find the optimal design. The different numbers of hidden neurons applied in the verification are 5, 6, 7, 8, 9, 10,11 and 12.
- The output layer of the neural network has three neurons representing different states of the machine. Since the FFNN type neural network belongs to supervised learning, it needs a teacher to lead it in order to achieve the determined goal. The expect target vectors were defined as three different pattern: $T1=[1\ -1\ -1]^T$, $T_2=[-1\ 1\ -1]^T$, $T_3=[-1\ -1\ 1]^T$ for healthy, faulty with one n be extended broken bar and faulty with two broken bar respectively. 1 is set as the correct class and -1 for all the other classes.

After successful training, the network was used to distinguish between the rotor states. The test data was unseen by the neural network. A learning rate of 0.01 and momentum of 0.95 was selected for all cases based on the experience. Optimum results were obtained with 11 hidden neurons. The accuracy is 100% for the training data, and 96.66% for the testing data, the performance of the FFNN is summarized in Figure 17.

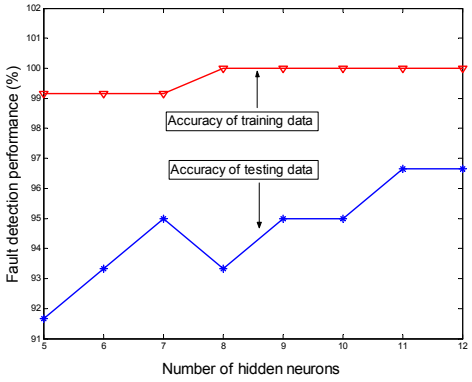

Figure 17. Accuracy of training and testing data at different number of hidden neurons

8. Conclusion

A detailed model of a squirrel-cage induction machine has been developed. In order to simulate cage defects, the machine was modelled as a group of coupled magnetic circuits by considering the current in each rotor bar as an independent variable. The model can simulate the performance of induction machines during transient as well as at steady state, including the effect of rotor faults. Simulated and experimental data were first used to study rotor faults cause-effect relationships in the stator current and the current spectrum signature. Experimental stator current data were then applied to verify the feasibility of applying a feed-forward neural network with backpropagation algorithm to diagnosis rotor faults. The results show that FFNN is not only able to automatically identify rotor status, the neural network is also designed to determine the extent of faults. This is very useful for early fault detection and preventive maintenance. The proposed methodology has been tested on a 5.5Kw/3000rpm squirrel-cage induction motor. Experimental tests have led to results with a satisfactory level of accuracy greater than 96%.

Future work consists to test this AI-diagnosis rotor faults when the motor is connected to a motor speed drive. A Self-Organizing Map (SOM) could be used for initial classification of motor faults, as an introductory step. Then, the diagnosis problems of induction motors will be extended in the case of rotor and rolling bearing faults.

9. Acknowledgements

The authors would like to thank SITEX Company who finances this work. They also wish to express their deep appreciation for the support rendered by the electrical department members

10. References

[1] M. Y. Chow, Methodologies of using neural network and fuzzy logic technologies for motor incipient fault detection, World Scientific Publishing Co. Pte. Ltd, Singapore, 1997.

[2] F.Filippetti, G. Franceschini, C. Tassoni and P. Vas. Recent developments of induction motor drives fault diagnosis using AI techniques. IEEE Transactions on Industrial ELECTRONICS. Vol.47, n°5, pp.994-1004, 2000.

[3]R. R. Schoen, T. G. Habetler, F .Kamran and R.G. Bartheld. Motor Bearing Damage Detection Using Stator Current Monitoring. IEEE Transaction on Industry Applications vol.31, N°6, pp.1274-1279, November/December 1995.

[4] F.Filippetti, G. Franceschini, C. Tassoni and P. Vas. AI techniques in induction machines diagnosis including the speed ripple effect. *IEEE Trans*. Indus. Appli. Vol.34, n°1, pp.98-108, 1998.

[5] H.A . Toliyat, T.A. Lipo, and J.C. White. Analysis of a concentrated winding induction machine for djustable speed drive application part 1 (Motor analysis). IEEE Transaction on Energy Conversion, vol. 6, N° 4, pp 679-684, Dec 1991.

[6] A. Ah-jaco. Modélisation des moteurs asynchrones triphasés en régime Transitoire avec saturation et harmoniques d'espace. Application au diagnostic. PhD thesis, Université de Lyon, juillet 1997.

[7] A.R. Munoz and T.A. Lipo. Complex vector model of the squirrel-cage induction machine including instantaneous rotor bar currents. IEEE-IAP, vol. 35, N°6, 1999

[8] X. Luo, Y. Liao, H.A. Toliyat, A. El-Antably and T.A. lipo. Multiple coupled circuit modeling of induction machines. IEEE Transaction on Industry apllications, vol. 31, N° 2, pp 311-318, March/April 1995.

[9] N.A. Al-Nuaim and H.A. Toliyat. A novel method for modeling dynamic air-gap eccentricity in synchronous machines based on modified winding function theory. IEEE Transaction on Energy Conversion, vol. 13, N° 2, pp 156-162, June 1998.

[10] G.Houdouin, G. Baraket, B. Dakyo, H. Henao and G.A. Capolino. Coupled Magnetic Circuit Modeling of the Stator Windings Faults of Induction Machines Including Saturation Effect. In proceedings of the IEEE International Conference on industrial Technology(ICIT), pp 148-153, 2004.

[11] S. Nandi and H.A . Toliyat. Condition monitoring and fault diagnosis of electrical machines—A review. in Conf. Rec. 1999 IEEE-IAS Annu. Meeting, vol. 1, Phoenix, AZ, pp. 197–204.

[12] X. Z. Gao , S. J. Ovaska and X. Wang, Neural Networks-based Fault Detection with Application in Ink Jet Printer. ICGST, ACSE journal Vol.05, ISSUE I, pp.9-15, Dec 2004.

[13] Da-Ming Yang and J. Penman. Intelligent detection of induction motor bearing faults using current and vibration monitoring. In proceedings of the COMADEM 2000, 3-8 December, 2000.

[14] H. Nejjari and M.E.H. Benbouzid. Monitoring and Diagnosis of Induction Motors Electrical Faults Using a Current Park's Vector Pattern Learning Approach. *IEEE* Transactions on Industry Application. Vol.36, n°3, pp.730-735, MAY/JUNE 2000.

Tarek Aroui was born in Mahdia, Tunisia in 1969. He received the Electrical Engineering Diploma from National Engineering school of Monastir (ENIM) in 1994. He received DEA(Master) degrees in 2001 and he is currently working toward the Doctoral thesis in the National Engineering school of Sfax (ENIS). He was an Electrical Engineer with the SITEX Company for several years. He is currently an Assistant professor at the National Engineering school of Sousse(ENISo).

Yassine Koubaa was born in Sfax, Tunisia in 1961. He received the B.S. and DEA degrees in 84 and 86, respectively, the Doctoral thesis in 1996, the ''Habilitation Universitaire'' (HDR) from the National Engineering school of Sfax (ENIS) all in electrical engineering. From 1989 to 1996, he was an Assistant professor in the Electrical Engineering Department of ENIS. In september 1997, he has been an Associate Professor. Since September 2005, he becomes a full Professor at the same university.

His main research interests cover several aspects related to electrical machines, including systems identification, advanced motion control and diagnostics. He has authored more than 60 papers in international conferences and technical journals in the area as well as many patents. He serves as a member of the Scientific and the Technical Program Committees of several international conferences and technical journals in the motor drives fields.

Ahmed Toumi (born on 1952), Professor in the Sfax Engineering National School (ENIS), received the Electrical Engineering Diploma from (ENIS/Tunisia), the DEA (Master) in Instrumentation and Measurement from University of Bordeaux-1/France in 1981 and the Doctoral Thesis from the University of Tunis in 1985. He joined the Sfax Engineering National School (ENIS), as an Associate Professor of Electric Engineering, since October 1981. In 2000, he obtained the University Habilitation (HDR) from the Sfax Engineering School (ENIS). He is at present the Director of the Electrical Engineering Department in ENIS. The main research area concerns the modelling, the stability of the electric machines, the electrical networks, the fuzzy logic control. He is the Head of the Research Unit of Industrial Processes Control (UCPI) of the Sfax University. Since 2002, he is the President of the international conference on Sciences and Techniques of Automatic control (STA) which have taken place in a number of tourist cities of Tunisia.

www.icgst.com

APPLICATION OF FOURIER SERIES DIRECT METHOD TO THE OPTIMAL CONTROL OF SINGULAR SYSTEMS

R. Ebrahimi[1], M. Samavat[1], M.A. Vali[2], A.A. Gharavisi[1]
1. Department of Electrical Engineering, Shahid Bahonar University
2 .Department of mathematics, Shahid Bahonar University, Kerman, IRAN
Ebrahimi_123ali@yahoo.com, msamavat@mail.uk.ac.ir, mvali@mail.uk.ac.ir, a _gharaveisi@yahoo.com

Abstract
By the use of elegant operational properties of Fourier series, a direct computational algorithm for evaluation the optimal control and trajectory of linear singular systems with a quadratic cost functional is developed in this paper. The state variable, state- rate, and the control vector are expanded in Fourier orthogonal basis with unknown coefficients. The technique is straightforward and very convenient for computer programming. An illustrative example is given to demonstrate the applicability of the proposed method.

Keywords: *Optimal control; singular systems; Fourier series; operational matrix*

1. Introduction
Various orthogonal functions have been used to solve the problem of optimal control in recent years. Special attention has been given to applications of Walsh functions [1], block-pulse functions [2], Laguerre polynomials [3], Chebyshev polynomials [4], Legendre polynomials [5], and Fourier series [6].
The main characteristic of this technique is that it reduces these problems to those of solving a system of algebraic equations; thus greatly simplifying the problem and making it computationally plausible. The approach is based on converting the underlying differential equations into integral equations through integration, approximating various signals involved in the equations by truncated orthogonal series, and using the operational matrix of integration to eliminate the integral operations.
Singular systems, also commonly called generalized or descriptor systems in the literature appear in many practical situations including engineering systems, economic systems, network analysis, and biological systems (see e.g. [7, 8, 9]). In fact, many systems in the real life are singular in nature. They are usually simplified as or approximated by non-singular models because there is still lacking of efficient tools to tackle problems related to such systems. Significant results have been reported in diverse respects such as solvability [10,11], freqency-domain design [12], multiple-integaral observers [13] and integarted fault estimation and fault tolerant design [14]. Fourier series have been widely used to study the optimal control of linear systems with quadratic performance index. Campbell [15], Lewis and Mertzios [16], Marszalek [17], Paraskevopoulos [18], and Trzaska [19], applied the orthogonal functions for analysis of linear singular systems. Palanisamy and Balachandran [20, 21], and Balachandran and Murugresan [22], applied the single-term Walsh series (STWS) method to the analysis of linear singular system. This technique is also used to analyse the electronic circuits [23].In this paper we extend the Fourier series technique to study the problem of optimal control of linear singular systems with quadratic performance. The state variable $x(t)$, state rate $\dot{x}(t)$ and control variable $u(t)$ are expanded by Fourier series with unknown coefficients.
Also the properties of Fourier series are used to relate the unknown coefficients of $\dot{x}(t)$ to the coefficients of $x(t)$.
Using this method the dynamics of the system are converted to a system of algebraic equations. The necessary conditions of optimality are imposed to solve the quadratic programming by using the Lagrange multipliers.
The reminder of the paper is organized as follows: section (2) is about the preliminaries and problem statement; section (3) focuses on the main result, section (4) demonstrate a benchmark example. Finally section (5) is the conclusion.

2. Preliminaries and Problem Statement

2.1 Properties of the Fourier series
Suppose a signal $g(t)$ has finite energy over the interval $[0, L]$. Then $g(t)$ can be represented by a Fourier series as follows

$$g(t) = g_0 + \sum_{n=1}^{\infty} g_n \cos(\frac{2n\pi t}{L}) + g_n^* \sin(\frac{2n\pi t}{L}) \qquad (1)$$

Where the Fourier coefficients g_n, g_n^* are given by

$$g_0 = \frac{1}{L}\int_0^L g(t)\,dt \tag{2a}$$

$$g_n = \frac{2}{L}\int_0^L g(t)\cos\frac{2n\pi t}{L}dt, \quad n = 1,2,3,\ldots \tag{2b}$$

$$g_n^* = \frac{2}{L}\int_0^L g(t)\sin\frac{2n\pi t}{L}dt, \quad n = 1,2,3,\ldots \tag{2c}$$

We assume that the derivative of $g(t)$ in equation (1) is described by

$$f(t) = \dot{g}(t) = f_0 + \sum_{n=1}^{\infty}\left\{f_n\cos(\frac{2n\pi t}{L}) + f_n^*\sin(\frac{2n\pi t}{L})\right\} \tag{3}$$

An approximation to $f(t)$ and $g(t)$ are obtained by keeping those terms in (1) and (3) for which $1 \le n \le r$ and discarding others. This may be written in a compact form as

$$g(t) = g_0\phi_0(t) + \sum_{n=1}^{r}\left\{g_n\phi_n(t) + g_n^*\phi^*(t)\right\} = G^{\mathrm{T}}\Phi(t) \tag{4}$$

$$f(t) = f_0\phi_0(t) + \sum_{n=1}^{r}\left\{f_n\phi_n(t) + f_n^*\phi^*(t)\right\} = F^{\mathrm{T}}\Phi(t) \tag{5}$$

Where

$$\begin{aligned} G &= [g_0 \;\; g_1 \;\; g_2 \;\; \cdots \;\; g_r \;\; g_1^* \;\; g_2^* \;\; \cdots \;\; g_r^*]^{\mathrm{T}} \\ F &= [f_0 \;\; f_1 \;\; f_2 \;\; \cdots \;\; f_r \;\; f_1^* \;\; f_2^* \;\; \cdots \;\; f_r^*]^{\mathrm{T}} \\ \Phi(t) &= [\phi_0 \;\; \phi_1 \;\; \phi_2 \;\; \cdots \;\; \phi_r \;\; \phi_1^* \;\; \phi_2^* \;\; \cdots \;\; \phi_r^*]^{\mathrm{T}} \end{aligned} \tag{6}$$

With

$$\phi_n = \cos\frac{2n\pi t}{L}, \quad n = 0,1,2,3,\ldots$$

$$\phi_n^* = \sin\frac{2n\pi t}{L}, \quad n = 1,2,3,\ldots$$

The elements of $\phi(t)$ are orthogonal in the

Interval $t \in (0,L)$. i.e. $\int_0^L \phi_n\phi_m(t)dt = \begin{cases} 0 & n \neq m \\ \frac{L}{2} & n = m \end{cases}$

The integration of vector $\Phi(t)$ defined in equation (6) can be approximation by

$$\int_0^t \Phi(t')dt' = \mathrm{P}\Phi(t) \tag{7}$$

Where P is an $(2r+1)\times(2r+1)$ operational matrix of integration and is defined as [24].

$$P = L\begin{bmatrix} \frac{1}{2} & 0 & 0 & \ldots & 0 & 0 & \frac{-1}{\pi} & \frac{-1}{2\pi} & \ldots & \frac{-1}{(r-1)\pi} & \frac{-1}{r\pi} \\ 0 & 0 & 0 & \ldots & 0 & 0 & \frac{1}{2\pi} & 0 & \ldots & 0 & 0 \\ \vdots & \vdots & \vdots & & \vdots & \vdots & \vdots & \vdots & & \vdots & \vdots \\ 0 & 0 & 0 & \ldots & 0 & 0 & 0 & 0 & \ldots & \frac{1}{2(r-1)\pi} & 0 \\ 0 & 0 & 0 & \ldots & 0 & 0 & 0 & 0 & \ldots & 0 & \frac{1}{2r\pi} \\ \frac{1}{2\pi} & \frac{-1}{2\pi} & 0 & \ldots & 0 & 0 & 0 & 0 & \ldots & 0 & 0 \\ \frac{1}{4\pi} & 0 & \frac{-1}{4\pi} & \ldots & 0 & 0 & 0 & 0 & \ldots & 0 & 0 \\ \vdots & \vdots & \vdots & & \vdots & \vdots & \vdots & \vdots & & \vdots & \vdots \\ \frac{1}{2r\pi} & 0 & 0 & \ldots & 0 & \frac{-1}{2r\pi} & 0 & 0 & \ldots & 0 & 0 \end{bmatrix} \tag{8}$$

The cross-product of two Fourier series vectors is

$$\phi(t)\phi^T(t) = \begin{bmatrix} \phi_0^2 & \phi_0\phi_1 & \ldots & \phi_0\phi_r & \phi_0\phi_1^* & \ldots & \phi_0\phi_r^* \\ \phi_1\phi_0 & \phi_1^2 & \ldots & \phi_1\phi_r & \phi_1\phi_1^* & \ldots & \phi_1\phi_r^* \\ \vdots & \vdots & & \vdots & \vdots & & \vdots \\ \phi_r\phi_0 & \phi_r\phi_1 & \ldots & \phi_r^2 & \phi_r\phi_1^* & \ldots & \phi_r\phi_r^* \\ \phi_1^*\phi_0 & \phi_1^*\phi_1 & \ldots & \phi_1^*\phi_r & \phi_1^{*2} & \ldots & \phi_1^*\phi_r^* \\ \vdots & \vdots & & \vdots & \vdots & & \vdots \\ \phi_r^*\phi_0 & \phi_r^*\phi_1 & \ldots & \phi_r^*\phi_r & \phi_r^*\phi_1^* & \ldots & \phi_r^{*2} \end{bmatrix} \tag{9}$$

By using

$$\int_0^L \phi_n\phi_m(t)dt = \int_0^L \phi_n^*\phi_m^*(t)dt = \begin{cases} 0 & n \neq m \\ \frac{L}{2} & n = m \end{cases}$$

$$\int_0^L \phi_0^2(t)dt = L$$

Where m and n can assume any of the values 1,2,3,….we can easily obtain

$$D = \int_0^L \phi\phi^T(t)dt = L\begin{bmatrix} 1 & & & & & & \\ & \frac{1}{2} & & & 0 & & \\ & & \frac{1}{2} & & & & \\ & & & \frac{1}{2} & & & \\ & 0 & & & \ddots & & \\ & & & & & \frac{1}{2} & \end{bmatrix} \tag{10}$$

Where D is a $(2r+1)\times(2r+1)$ matrix. Thus D is a diagonal matrix and the simple structure of this matrix plays important role in the direct method for solving optimal control problem. Further, using equation (3) we get

$$g(t) - g(0) = \int_0^t f(t')dt'$$

And from equation (4), (5) and (7), using $g(0)=K^T\Phi(t)$, we have

$$(G^{\mathrm{T}}-K^{\mathrm{T}})\Phi(t)=F^T\mathrm{P}\Phi(t)$$

Where $\mathrm{K}^{\mathrm{T}}=\left[g(0)\ \ 0_1\ \ \ldots\ \ 0_r\ \ 0_1^*\ \ \ldots\ \ 0_r^*\right]$ thus we get

$$(G^{\mathrm{T}}-K^{\mathrm{T}})=F^T\mathrm{P} \tag{11}$$

2.2 Problem statement

Consider linear time invariant (LTI) singular system

$$E\dot{x}(t)=Ax(t)+Bu(t) \tag{12}$$
$$x(0)=x_0 \tag{13}$$

Where $x\in R^p$ is the state of the system, $u\in R^z$ is the input vector of the system, $E\in R^{p\times p}$ is assumed to be singular with $0<\mathrm{rank}(E)<p$, and A,B are real constant matrices of appropriate size. The problem is to find the optimal control $u(t)$ and the corresponding state trajectory $x(t)$, $0\le t\le L$, satisfying equation (12)-(13) while minimizing the cost function

$$J=\frac{1}{2}x^{\mathrm{T}}(L)Sx(L)+\frac{1}{2}\int_0^L\left[x^{\mathrm{T}}(t)Qx(t)+u^{\mathrm{T}}(t)Ru(t)\right]dt \tag{14}$$

In equation (14), T denotes transposition, S,Q and R are matrices of appropriate dimensions, S and Q are symmetric positive semi-definite matrices and R is a symmetric positive definite matrix.

3. Main result

3.1. Approximation of the singular system

By expanding $x_P(t)$, $u_Z(t)$ and $\dot{x}_P(t)$ in Fourier series of order r, we determine the following approximated values, i.e. for $P=1,2,3,\ldots p$, and $Z=1,2,3,\ldots z$ we get

$$x_P(t)=a_{P0}\phi_0(t)+\sum_{i=1}^{r}\left\{a_{Pi}\phi_i(t)+a_{Pi}^*\phi_i^*(t)\right\}=\mathrm{A}^{\mathrm{T}}\Phi(t) \tag{15}$$

$$u_Z(t)=b_{Z0}\phi_0(t)+\sum_{i=1}^{r}\left\{b_{Zi}\phi_i(t)+b_{Zi}^*\phi_i^*(t)\right\}=\mathrm{B}^{\mathrm{T}}\Phi(t) \tag{16}$$

$$\dot{x}_P(t)=c_{P0}\phi_0(t)+\sum_{i=1}^{r}\left\{c_{Pi}\phi_i(t)+c_{Pi}^*\phi_i^*(t)\right\}=C^{\mathrm{T}}\Phi(t) \tag{17}$$

Where $\{a_{Pi},a_{Pi}^*\}$, $\{b_{Zi},b_{Zi}^*\}$ and $\{c_{Pi},c_{Pi}^*\}$ are unknowns. Let

$$(Ax(t))_P=y_{P0}\phi_0(t)+\sum_{i=1}^{r}\left\{y_{Pi}\phi_i(t)+y_{Pi}^*\phi_i^*(t)\right\}=\mathrm{Y}^{\mathrm{T}}\Phi(t) \tag{18}$$

$$(Bu(t))_P=l_{P0}\phi_0(t)+\sum_{i=1}^{r}\left\{l_{Pi}\phi_i(t)+l_{Pi}^*\phi_i^*(t)\right\}=L^{\mathrm{T}}\Phi(t) \tag{19}$$

$$(E\dot{x}(t))_P=w_{P0}\phi_0(t)+\sum_{i=1}^{r}\left\{w_{Pi}\phi_i(t)+w_{Pi}^*\phi_i^*(t)\right\}=W^{\mathrm{T}}\Phi(t) \tag{20}$$

Using equation (18)-(20) for each $P,P=1,2,3,\ldots p$ the right-hand side of equation (12) has the form

$$W^{\mathrm{T}}\Phi(t)=(\mathrm{Y}^{\mathrm{T}}+L^{\mathrm{T}})\Phi(t)$$

By equating the coefficients of the same- order Fourier series, we obtain for $P=1,2,3,\ldots p$ and

$$W^{\mathrm{T}}=(\mathrm{Y}^{\mathrm{T}}+L^{\mathrm{T}}) \tag{21}$$

Also, by using equation (11) we get the constraints

$$F_{P0}=a_{P0}-x_P(0)-\left(\frac{1}{2}c_{P0}+\frac{1}{2\pi}\sum_{j=1}^{r}\frac{1}{j}c_{Pj}^*\right)L=0 \tag{22}$$

And for $i=1,2,3,\ldots r$ we have

$$F_{Pi}=a_{Pi}+\frac{L}{2\pi i}c_{Pi}^*=0 \tag{23}$$

$$F_{Pi}^*=a_{Pi}^*-\left(-\frac{1}{i\pi}c_{P0}+\frac{1}{2\pi i}c_{Pi}\right)L=0 \tag{24}$$

3.2. The performance index approximation

We now approximate the performance index J by using Fourier series.

Let

$$\alpha=\begin{pmatrix}(a_{10}\ \ a_{11}\ \ \ldots a_{1r}\ \ a_{11}^*\ \ a_{12}^*\ \ \ldots a_{1r}^*)^{\mathrm{T}}\\ \vdots\qquad\quad\vdots\qquad\qquad\vdots\\ (a_{P1}\ \ a_{P2}\ \ \ldots a_{Pr}\ \ a_{P1}^*\ \ a_{P2}^*\ \ \ldots a_{Pr}^*)^{\mathrm{T}}\end{pmatrix} \tag{25}$$

$$\beta=\begin{pmatrix}(b_{10}\ \ b_{12}\ \ \ldots b_{1r}\ \ b_{11}^*\ \ b_{12}^*\ \ \ldots b_{1r}^*)^{\mathrm{T}}\\ \vdots\qquad\quad\vdots\qquad\qquad\vdots\\ (b_{Z1}\ \ b_{Z2}\ \ \ldots b_{Zr}\ \ b_{Z1}^*\ \ b_{Z2}^*\ \ \ldots b_{Zr}^*)^{\mathrm{T}}\end{pmatrix} \tag{26}$$

And define the matrices:

$$\hat{\Phi}_1(t)=\begin{pmatrix}\Phi^{\mathrm{T}}(t)&&\\&\ddots&\\&&\Phi^{\mathrm{T}}(t)\end{pmatrix},\qquad \hat{\Phi}_2(t)=\begin{pmatrix}\Phi^{\mathrm{T}}(t)&&\\&\ddots&\\&&\Phi^{\mathrm{T}}(t)\end{pmatrix} \tag{27}$$

Note that α,β and $\hat{\Phi}_1(t)$ and $\hat{\Phi}_2(t)$ are matrices of order $P(2r+1)\times 1, Z(2r+1)\times 1$ and $P\times P(2r+1)$ and $Z\times Z(2r+1)$ respectively. Using equation (15) and (16) and (25)-(27) the state and control vector can be expressed as

$$x(t) = \hat{\Phi}_1(t)\alpha \tag{28}$$

$$u(t) = \hat{\Phi}_2(t)\beta \tag{29}$$

Substituting equation (28) and (29) in equation (14) we get

$$J = \frac{1}{2}\alpha^{\mathrm{T}}\hat{\Phi}_1^{\mathrm{T}}(L)S\hat{\Phi}_1(L)\alpha + \frac{1}{2}\alpha^{\mathrm{T}}\left[\int_0^L \hat{\Phi}_1^{\mathrm{T}}(t)Q\hat{\Phi}_1(t)dt\right]\alpha + \frac{1}{2}\beta^{\mathrm{T}}\left[\int_0^L \hat{\Phi}_2^{\mathrm{T}}(t)R\hat{\Phi}_2(t)dt\right]\beta \tag{30}$$

Equation (30) can be computed more efficiently by using equation (10) and writing J as

$$J = \frac{1}{2}\alpha^{\mathrm{T}}\left[\Phi(L)\Phi^{\mathrm{T}}(L)\otimes S\right]\alpha + \frac{1}{2}\alpha^{\mathrm{T}}(D\otimes Q)\alpha + \frac{1}{2}\beta^{\mathrm{T}}(D\otimes R)\beta \tag{31}$$

Where $\otimes$ denotes the Kronecker product [25].

Remark: As it is shown in (31) the dynamic cost function is converted to a statistic cost function and it simplifies the problem considerably.

3.3. Solution of the optimization problem

The optimal control problem has been reduced to a parameter optimization problem which can be stated as follows. Find α and β so that $J(\alpha,\beta)$ is minimized subject to the constraints in equations (21)-(24)
Let

$$L(\alpha,\beta) = J(\alpha,\beta) + \sum_{j=0}^{r}\lambda_j F_{P_j}(\alpha,\beta) + \sum_{j=1}^{r}\lambda_j^* F_{P_j}^* \tag{32}$$

where $\lambda = (\lambda_0 \ \ldots \ \lambda_r \ \lambda_r^* \ \ldots \ \lambda_r^*)$ represent the unknown Lagrange multiplier. Then necessary condition for stationary are given by

$$\frac{\partial L}{\partial a_{P_i}} = \frac{\partial J}{\partial a_{P_i}} + \sum_{j=0}^{r}\lambda_j\frac{\partial F_{P_j}}{\partial a_{P_i}} + \sum_{j=1}^{r}\lambda_j\frac{\partial F_{P_j}^*}{\partial a_{P_i}} \quad i=0,1,2,\ldots r \quad P=1,2,\ldots p \tag{33}$$

$$\frac{\partial L}{\partial a_{P_i}^*} = \frac{\partial J}{\partial a_{P_i}^*} + \sum_{j=1}^{r}\lambda_j\frac{\partial F_{P_j}}{\partial a_{P_i}^*} + \sum_{j=1}^{r}\lambda_j\frac{\partial F_{P_j}^*}{\partial a_{P_i}^*} \quad i=0,1,2,\ldots r \quad P=1,2,\ldots p \tag{34}$$

$$\frac{\partial L}{\partial b_{Z_i}} = \frac{\partial J}{\partial b_{Z_i}} + \sum_{j=0}^{r}\lambda_j\frac{\partial F_{P_j}}{\partial b_{Z_i}} + \sum_{j=1}^{r}\lambda_j\frac{\partial F_{P_j}^*}{\partial b_{Z_i}} \quad i=0,1,2,\ldots r \quad Z=1,2,\ldots z \tag{35}$$

$$\frac{\partial L}{\partial b_{Z_i}^*} = \frac{\partial J}{\partial b_{Z_i}^*} + \sum_{j=0}^{r}\lambda_j\frac{\partial F_{P_j}}{\partial b_{Z_i}^*} + \sum_{j=1}^{r}\lambda_j\frac{\partial F_{P_j}^*}{\partial b_{Z_i}^*} \quad i=0,1,2,\ldots r \quad Z=1,2,\ldots z \tag{36}$$

$$F_{Pj} = 0 \quad j = 0,1,2,\ldots r \tag{37}$$

$$F_{Pj}^* = 0 \quad j = 1,2,\ldots r \tag{38}$$

Remark: As it shown in (8) the operational matrix P has so many zeros and this fact results in a considerably saving of computing time.

4. Illustrative example

Consider the linear singular system [26]

$$\begin{bmatrix}0 & 1\\ 0 & 0\end{bmatrix}\begin{bmatrix}\dot{x}_1\\ \dot{x}_2\end{bmatrix} = \begin{bmatrix}1 & 0\\ 0 & 1\end{bmatrix}\begin{bmatrix}x_1\\ x_2\end{bmatrix} + \begin{bmatrix}0\\ 1\end{bmatrix}u \tag{39}$$

$$x(0) = \begin{bmatrix}1\\ -\frac{\sqrt{2}}{2}\end{bmatrix} \tag{40}$$

With the cost function

$$j = \frac{1}{2}\int_0^2\left[x^{\mathrm{T}}(t)x(t) + u^2(t)\right]dt \tag{41}$$

The problem is to find the optimal control $u(t)$ which minimizes equation (41) subject to (39) and (40). We determine the direct Fourier series approximation for $r = 10$
Let

$$x_1(t) = a_{10}\phi_0(t) + \sum_{i=1}^{10}\left\{a_{1i}\phi_i(t) + a_{1i}^*\phi_i^*(t)\right\} \tag{42}$$

$$x_2(t) = a_{20}\phi_0(t) + \sum_{i=1}^{10}\left\{a_{2i}\phi_i(t) + a_{2i}^*\phi_i^*(t)\right\} \tag{43}$$

$$u(t) = b_0\phi_0(t) + \sum_{i=1}^{10}\left\{b_i\phi_i(t) + b_i^*\phi_i^*(t)\right\} \tag{44}$$

$$\dot{x}_1(t) = c_{10}\phi_0(t) + \sum_{i=1}^{10}\left\{c_{1i}\phi_i(t) + c_{1i}^*\phi_i^*(t)\right\} \tag{45}$$

$$\dot{x}_2(t) = c_{20}\phi_0(t) + \sum_{i=1}^{10}\left\{c_{2i}\phi_i(t) + c_{2i}^*\phi_i^*(t)\right\} \tag{46}$$

Applying equation (30) we obtain the following approximation for J

$$J = a_{10}^2 + a_{20}^2 + b_0^2 + \frac{1}{2}\sum_{i=1}^{10}\left[(a_{1i}^2 + a_{2i}^2 + b_i^2) + (a_{1i}^{2^*} + a_{2i}^{2^*} + b_i^{2^*})\right] \tag{47}$$

Using equations (32)-(38) the direct method Fourier series approximation for $x_1(t), x_2(t)$ and $u(t)$ in equations (42)-(44) can be calculated.
In table I and Π, a comparison is made between the values of $x_1(t)$ and $u(t)$ using present method with $r = 10$, and the exact solution

Table I .Estimated and exact values of $x_1(t)$.

	$x_1(t)$		
Solution Number	time	exact solution	Fourier series $r=10$
1	0.00	1.00000	0.94543
2	0.25	0.70219	0.69577
3	0.50	0.49307	0.49945
4	0.75	0.34623	0.34457
5	1.00	0.24312	0.24095
6	1.25	0.17071	0.17384
7	1.50	0.11987	0.11834
8	1.75	0.08417	0.08314
9	2.00	0.05911	0.06488


Table Π .Estimated and exact values of $u(t)$

	$u(t)$		
Solution Number	time	exact solution	Fourier series $r=10$
1	0.00	0.70711	0.66852
2	0.25	0.49652	0.49199
3	0.50	0.34865	0.35316
4	0.75	0.24482	0.24364
5	1.00	0.17191	0.17038
6	1.25	0.12071	0.12292
7	1.50	0.08476	0.08368
8	1.75	0.05952	0.05879
9	2.00	0.04179	0.04588

5. Conclusion

The Fourier series and the associated matrix of integration (operational matrix) are applied to solve the optimal control of singular systems. The method is based upon reducing a linear singular quadratic optimization problem to a set of algebraic equations. The advantage of using Fourier series as compared to Laguerre polynomials, shifted Legendre polynomials and Chebyshev series is that in the present method the, most of the elements of the operational matrix given in (8) are zeros, and matrix D introduced in (10) is a diagonal matrix, hence making Fourier series computationally very attractive. As we can see from the tables, it is shown that with a relatively low r , we have a very accurate solution.

6. Acknowledgements

The authors wish to express their sincere thanks to the referee for valuable suggestions which improved the final manuscript.

7. References

[1] MS. Corrington. Solutions of differential and integral equations with Walsh function. IEEE Transactions on Circuit Theory, 20**:** 470-476, 1973.

[2] C. Hwang and YP. Shih. Optimal control of delay systems via block pulse functions. Journal of Optimization Theory and Application, 45*:* 101-112, 1985.

[3] C. Hwang and YP. Shih. Solution of integral equations via Laguerre polynomials. Computers and Electrical Engineering , 9: 123-129, 1982.

[4] M. Razzaghi and M. Razzaghi. Solution of linear two-point boundary value problem and optimal control of time-varying systems by shifted Chebyshev. Journal of the Franklin Institute, 327:321-328, 1990.

[5] HM. Perng. Direct approach for the optimal control of linear time-delay systems via shifted Legendre polynomials. International Journal of Control, 43**:** 1897-1904, 1986.

[6] M. Razzaghi and M. Razzaghi. Fourier series direct method for variationl problem. Int. J. control,48: 887-895, 1988.

[7] L. Dai, singular control system, Springer, Berlin, 1989

[8] M. Kuijper, First Order Representation of Linear systems, Birkhauser, Boston, 1994.

[9] F. L. Lewis, A survey of linear singular systems, Circuits, Systems Signal Process. 5 (1): 3-36, 1986.

[10] SL. Campbell. *Singular Systems of Differential Equations*. Pitman: London, 1980.

[11] SL. Campbell, CD Meyer and NJ, Rose. Application of the Drazian inverse to linear systems of differential equations with singular constant coefficient. SIMA Journal of Applied Mathematics, 31: 425-611, 1976.

[12] Z. Gao, and A. T. P, So. A general doubly coprime factorization for descriptor systems, Systems and Control Letters, 49(3): 213-224, 2003.

[13] Gao, Z and D. W. C, Ho. Proportional multiple-integral observer design for descriptor systems with measurement output disturbances, IEE Proc.-Control Theory Appl, 151(3):.279-288, 2004.

[14] Gao, Z. , and S. X, Ding,. Actuator fault robust estimation and fault-tolerant control for a class of nonlinear descriptor systems, Automatica, 43: (5), 912-920, 2007.

[15] S.L. Campbell. On using orthogonal function with singular systems, proc. IEE Pt. D, 131: 267-268, 1984.

[16] F.L. Lewis and B. G. Mertzios , Analysis of singular systems using orthogonal functions, IEEE Trans. Auto Control ,32: 527-530, 1987.

[17] W. Marszalek, On using orthogonal functions for the analysis of singular systems, proc. IEE Pt. D, 132: 131-132, 1985.

[18] P. N. Paraskevopoulos. Analysis of singular systems using orthogonal function. Proc. IEE Pt. D, 131: 37-38, 1984.

[19] Z. Trzaska, Computation of the block pulse solution of singular systems, IEE Pt. D, 133: 191-192, 1986.

[20] K. R. Palannisamy and Balachandran, Single-term Walsh series approach to singular systems, Int.J.Control, 46: 1931-1934, 1987.

[21] K. R. Palannisamy and Balachandran, Analysis of time-varying singular systems via Single-term Walsh series approach proc. IEE Pt. D, 135: 461-462, 1988.

[22] K. Balachandran, and K. Murugesan, Analysis of Different systems via Single-term Walsh series method, Int. J. Comp. Math. 33: 171-179, 1990.

[23] K. Balachandran, and K. Murugesan, Analysis of electronic circuits using the Single-term Walsh series approach. Int. J. Electronics, 69: 327-332, 1990.

[24] P. N. Paraskevopoulos, P. D. Sparis, and S.G Mouroutsos. Int. J. Systems Sci.16: 171-181, 1985.

[25] P Lancaster. Theory of Matrices. Academic Press: New York, 1969.

[26] K. Balachandran and K. Murugesan. optimal control of singular system via single-term Walsh series. International Journal of computer Mathematics. 43: 153-159, 1992.

Ramazan Ebrahimi, He is a M.Sc student in control engineering in electrical Dept in Bahonar University of Kerman.

Mahmoud Samavat, He got his B.Sc and M.Sc all in electrical engineering in 1982 and 1985 respectively from North Dakota state university in USA. Also he got his Ph.D in control engineering from Dep of Automatic control and system engineering from university of Sheffield, England in Dec 2000. Since 1985 he is a faculty member of electrical Dept in Bahonar university of Kerman. his research area is stabilization, identification, model reduction and optimal control.

Mohammed Ali Valim, He got his B.Sc in pure mathematics in 1985 from Esfahan University in IRAN. he got his M.Sc in pure mathematics (Analysis) in Bahonar university of Kerman in 1987. Also he got his Ph.D in pure mathematics (optimal control) in 1999 from Bahonar university of Kerman in IRAN. Since 1987 he has been a faculty member of Math Dep. Of Bahonar university of Kerman. His research area is analysis, Linear algebra and optimal control.

www.icgst.com

A Hybrid Genetic-Simulated Annealing Approach to TCPS based Hydrothermal System under Open Market System

C. Srinivasa Rao[1], S. Siva Nagaraju[2], P. Sangameswara Raju[3]
[1] Assistant Professor at G. Pulla Reddy Engineering College, Kurnool, Andhra Pradesh, India
[2] Associate Professor at J.N.T.U College of Engg., Kakinada, Andhra Pradesh , India.
[3] Associate Professor at S.V.University, Tirupati, Andhra Pradesh, India.
E-mail: csr_bit@yahoo.co.in

Abstract
This paper presents the analysis of Automatic generation control (AGC) of a two-area interconnected hydrothermal system with Thyristor controlled phase shifter (TCPS) in series with the tie-line under open market system. It also involves the optimization of integral controller employing a hybrid approach of modified Genetic algorithm and Simulated Annealing method (HMGASA) modified genetic algorithm method. Open transmission access and the evolving of more socialized companies for generation, transmission and distribution affects the formulation of AGC problem. So the traditional AGC two-area system is modified to take into account the effect of bilateral contracts on the dynamics. It is possible to stabilize the system frequency and tie-power oscillations by controlling the phase angle of TCPS which is expected to provide a new ancillary service for the future power systems. A control strategy using TCPS is proposed to provide active control of system frequency. Gain settings of the integral controllers without and with TCPS are optimized using the HMGASA technique following a step load disturbance in either of the areas. Analysis reveals that a TCPS is quite capable of suppressing the frequency and tie-power oscillations effectively as compared to that obtained without TCPS

Key Words: *AGC, Hydrothermal, TCPS, HMGASA algorithm, Disco participation matrix, open market system*

1. Introduction
Large scale power systems are normally composed of control areas or regions representing coherent groups of generators. In a practically interconnected power system, the generation normally comprises of a mix of thermal, hydro, nuclear and gas power generation. However, owing to their high efficiency, nuclear plants are usually kept at base load close to their maximum output. Gas power generation is ideal for meeting the varying load demand. Thus the natural choice of AGC falls on either thermal or hydro units. A realistic situation may arise where an area regulated by hydro generation is interconnected to another area regulated by thermal generation. Nowadays worldwide, the electric power industry is in a transition from Vertically integrated utility (VIU) scenario, where a single utility owned and operated the generation, transmission and distribution systems and provided power at regulated rates to the deregulated scenario, where, competitive companies sell unbundled power at lower rates. Furthermore, various kinds of apparatus with large capacity and fast power consumption such as testing plants for nuclear fusion, steel factories etc increase significantly. When these loads are concentrated in power systems, they may cause a serious problem of frequency oscillations. Therefore, it is very important to consider how the control services of system frequency should be implemented. In a deregulated environment, any power system control such as frequency, will serve as an ancillary service. Thus, stabilization of frequency oscillations in an interconnected power system becomes challenging when implemented in the future competitive environment. A new frequency stabilization service which emphasis not only efficiency, reliability and economics, but also, advanced and improved controls for satisfying the requirements of power system operation, is much in demand.

On the other hand, the concept of utilizing power electronic devices for power system control has been widely accepted in the form of Flexible AC Transmission Systems (FACTS) which provide more flexibility in power system operation and control [4]. This extra flexibility permits the independent adjustment of certain system variables such as power flows, which are not normally controllable. A Thyristor Controlled Phase Shifter (TCPS) is expected to be an effective apparatus for the tie-line power flow control of an interconnected power system In the analysis of an interconnected power system, some areas are considered as the channels of disturbances and in this situation, the conventional frequency control i.e., the governor may no longer be able to attenuate the large frequency oscillations due to its slow response [5, 6]. On the other hand, tie-line power flow control by a TCPS installed in series with the tie-line in between two areas of an interconnected power

system has the possibility to control the system frequency positively. The proposed control strategy will be a new ancillary service for the stabilization of frequency oscillations of an interconnected power system. Literature survey shows ample applications of TCPS for the improvement of dynamic and transient stabilities of power systems[3],[7]and[8]. However, no attempt has been made to improve the performance of AGC of interconnected power system under open market system considering TCPS in series with the tie-line. In the present work, analysis has been carried out for the AGC of interconnected hydrothermal power system under open market system considering a TCPS in series with the tie-line. An interconnected hydrothermal system involves widely different characteristics for the hydro and thermal subsystems. The characteristics of hydro turbines differ from steam turbines in that the relatively large water inertia used as a source of energy causes a considerably greater time lag in the response of the change in the prime mover torque to a change in gate position, and also an initial tendency for the torque to change in a direction opposite to that finally produced. The speed governor characteristics of the hydro units are widely different from that of the turbo governor. Moreover, the maximum permissible generation rate constraint for the hydro units is relatively much higher than the thermal units. Further, the effects of different Generation Rate Constraints (fairly slow response for the thermal plant and quite fast response for the hydro plant) on the selection of optimum controller settings for the thermal and hydro areas and on the system dynamic performance considering a TCPS in series with the tie-line is yet to be established. In view of the above, the main objectives of the present work are:

1)To study the effect of a Thyristor Controlled Phase Shifter (TCPS) in a tie-line on the AGC dynamics of a hydrothermal system
2)To develop a linearised model of a two area interconnected hydrothermal system under open market scenario considering a TCPS in series with the tie-line
3)To optimize the gain settings of the integral controllers with and without considering TCPS employing HMGASA method
4)To compare the dynamic responses with and without considering the TCPS.

2.Tie Line Power flow model Considering TCPS

Under open market system the power system structure changed in such a way that would allow the evolving of more specialized industries for generation (Genco), transmission (Transco) and distribution (Disco). A detailed study on the control of generation in deregulated power systems is given in [9]. The concept of independent system operator (ISO) as an unbiased coordinator to balance reliability with economics has also emerged [10,11]. The assessment of Automatic Generation control in an open market environment is given in detail in [12,13] and also provides a detailed review over this issue and explains how an AGC system could be simulated after deregulation. The recent advances in power electronics have led to the development of the Flexible Alternating Current Transmission Systems (FACTS). FACTS devices are designed to overcome the limitations of the present mechanically controlled power systems and enhance power system stability by using reliable and high-speed electronic devices. One of the promising FACTS devices is the Thyristor Controlled Phase Shifter (TCPS). A TCPS is a device that changes the relative phase angle between the system voltages. Therefore, the real power flow can be regulated to mitigate the frequency oscillations and enhance power system stability. In this study, a two-area hydrothermal power system interconnected by a tie-line under open market scenario is considered.

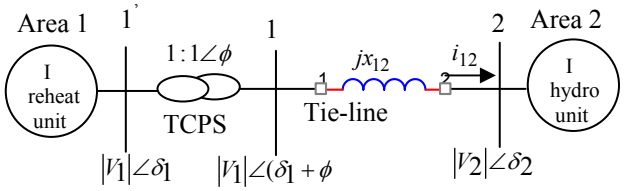

Figure1: Interconnected hydrothermal two area system with TCPS in series with the Tie-line

Figure1 shows the schematic of the two-area interconnected hydrothermal system considering a TCPS in series with the tie-line. TCPS is placed near area 1. Area 1 is the thermal area comprising of three reheat units and area 2 is the hydro area consisting of three hydro units. Without TCPS, the incremental tie-line power flow from area 1 to area 2 under open market system can be expressed as [1]

$$\Delta P^{o}_{tie12} = \frac{2\pi T^{o}_{12}}{s}(\Delta f_1 - \Delta f_2) \qquad \text{.....(1)}$$

When a TCPS is placed in series with the tie line as in Fig 1, a current flowing from area 1 to area 2 can be written as

$$i_{12} = \frac{|V_1|\angle(\delta_1+\phi) - |V_2|\angle\delta_2}{jX_{12}} \qquad \text{.....(2)}$$

From Figure 1 it can also be written as

$$P_{tie12} - jQ_{tie12} = |V_1|\angle -(\delta_1+\phi)\left(\frac{|V_1|\angle(\delta_1+\phi) - |V_2|\angle\delta_2}{jX_{12}}\right) \qquad \text{.....(3)}$$

Separating the real part of Eqn (3), we get

$$P_{tie12} = \frac{|V_1||V_2|}{X_{12}}\sin(\delta_1 - \delta_2 + \phi) \qquad \text{.....(4)}$$

But in Eqn (4) moving δ_1, δ_2 and ϕ from their nominal values δ_1^o, δ_2^o and ϕ^o respectively, we get

$$\Delta P_{tie12} = \frac{|V_1||V_2|}{X_{12}}\cos(\delta_1^o - \delta_2^o + \phi^o)\sin(\Delta\delta_1 - \Delta\delta_2 + \Delta\phi) \qquad \text{.....(5)}$$

But $(\Delta\delta_1 - \Delta\delta_2 + \Delta\phi)$ is very small and hence, $\sin(\Delta\delta_1 - \Delta\delta_2 + \Delta\phi) \approx (\Delta\delta_1 - \Delta\delta_2 + \Delta\phi)$

So Eqn (5) can be written as

$$\Delta P_{tie12} = \frac{|V_1||V_2|}{X_{12}} \cos(\delta_1^o - \delta_2^o + \phi^o)(\Delta\delta_1 - \Delta\delta_2 + \Delta\phi) \quad \text{.....(6)}$$

Let $T_{12} = \frac{|V_1||V_2|}{X_{12}} \cos(\delta_2^0 - \delta_2^0 + \varphi^0)$ .....(7)

Thus,Eqn.(6) reduces to $\Delta P_{tie12} = T_{12}(\Delta\delta_1 - \Delta\delta_2 + \Delta\varphi)$ .....(8)

Therefore, $\Delta P_{tie12} = T_{12}(\Delta\delta_1 - \Delta\delta_2) + T_{12}\Delta\varphi$ .....(9)

We also know that, $\Delta\delta_1 = 2\pi\int \Delta f_1 dt$ and $\Delta\delta_2 = 2\pi\int \Delta f_2 dt$ .....(10)

From Eqns.(9) and (10), it can be written as

$$\Delta P_{tie12} = 2\pi T_{12}(\int \Delta f_1 dt - \int \Delta f_2 dt) + T_{12}\Delta\varphi \quad \text{.....(11)}$$

Taking the laplace transform of Eqn.(11), it can be written as

$$\Delta P_{tie12}(s) = \frac{2\pi T_{12}}{s}\left[\Delta F_1(s) - \Delta F_2(s)\right] + T_{12}\Delta\varphi(s) \quad \text{.....(12)}$$

As per Eqn.(12), it can be observed that the tie-line power flow can be controlled by controlling the phase shifter angle $\Delta\varphi$. The phase shifter angle $\Delta\varphi$ (s) can be represented as [12-14]:

$$\Delta\varphi(s) = \frac{K_\phi}{1 + sT_{ps}} \Delta Error_1(s) \quad \text{.....(13)}$$

Where K_φ and T_{ps} are the gain and time constants of the TCPS. Thus, Eqn.(12)can be rewritten as

$$\Delta P_{tie12}(s) = \frac{2\pi T_{12}}{s}\left[\Delta F_1(s) - \Delta F_2(s)\right] + T_{12}\frac{K_\phi}{1 + sT_{ps}} \Delta Error_1(s) \quad \text{.....(14)}$$

If the frequency deviation Δf_1 is sensed, it can be used as the control signal (i.e., $\Delta Error_1 = \Delta f_1$) to the TCPS unit to control the TCPS phase shifter angle which in turn, controls the tie-line power flow. Thus,

$$\Delta\varphi(s) = \frac{K_\phi}{1 + sT_{ps}} \Delta F_1(s) \quad \text{.....(15)}$$

and the tie-line power flow perturbation becomes

$$\Delta P_{tie12}(s) = \frac{2\pi T_{12}}{s}\left[\Delta F_1(s) - \Delta F_2(s)\right] + T_{12}\frac{K\varphi}{1 + sT_{ps}} \Delta F_1(s) \quad \text{.....(16)}$$

But in the open market system the actual tie-line power flow also includes the demand from Discos in one area to Gencos in another area. It can be represented as follows.

$\Delta P_{\text{tie 1-2, actual}} = \Delta P_{tie12}(s)$ + (demand of Discos in area 2 from Gencos in area 1) – (demand of Discos in area 1 from Gencos in area2)

3. System Investigation

The AGC system investigated is composed of an interconnection of two areas under open market system. Area 1 comprises of a reheat system and area 2 comprises of hydro system. The detailed transfer function models of speed governors and turbines are discussed and developed in the IEEE committee report on Dynamic models for Steam and Hydro turbines in Power systems[14]. The detailed small perturbation transfer function block diagram model of two area hydrothermal system under open market scenario along with the incremental model of TCPS in series with the tie-line is shown in Figure 2. Nominal parameters of the TCPS system are given in the Appendix.

4. Optimization of Integral Gain Settings

Modified genetic algorithm method is used to obtain the optimum integral gain settings. A performance index which is denoted by $J = \int_0^t (\alpha\Delta f_1^2 + \beta\Delta f_2^2 + \Delta P_{tie12}^2)dt$ is minimized in the presence of GRCs to obtain the optimum values of K_{i1} and K_{i2}. A value of 0.65 is considered for both α and β. The modified genetic algorithm method resembles the normal traditional genetic algorithm which takes into account the nature of genetics [15]. But in modified genetic algorithm there are 3 modifications i.e (a) Modification in parent selection (b) Improvement in child string (c) Elitism. The algorithm for modified genetic algorithm method can be written as shown below.

Step 1: As the genetic algorithm takes pairs of strings, we create a random number of strings depending upon our necessity and also note down their decoded values along with setting a maximum allowable generation number $t_{\max}$

Step 2: Using the mapping rule we next find out the corresponding values of K_I for the corresponding decoded values.

Step 3: Using these values of K_I the fitness function values are found out.

Step 4: Next the process of reproduction is carried out on the strings to create a mating pool

Step 5: The process of crossover and mutation is also carried out on the strings with probabilities of 0.8 and 0.05 respectively.

Step 6: After the termination criteria is met with, the value of K_I with minimum fitness function value is considered as optimum value.

Here the following modifications are applied for the selection of parents so that the strings with large values of fitness are copied more into the mating pool.

1. The first parent in each reproduction is the string having the best fitness value. The second parent is selected from the ordered population using normal selection technique.
2. At the i^{th} reproduction, first parent is the i^{th} string of the population arranged in the order of fitness values. Second parent is selected from the ordered population using normal selection technique.

To improve the quality of child strings, the strings having fitness values less than average fitness values of the previous generation are identified first. Their quality is improved by selecting a number of bits at random with probability P_{m1} and complimenting. In order to avoid losing of best results during the selection, elitism is used. So here the best solution of every generation is copied to the next so that the possibility of its destruction is eliminated.


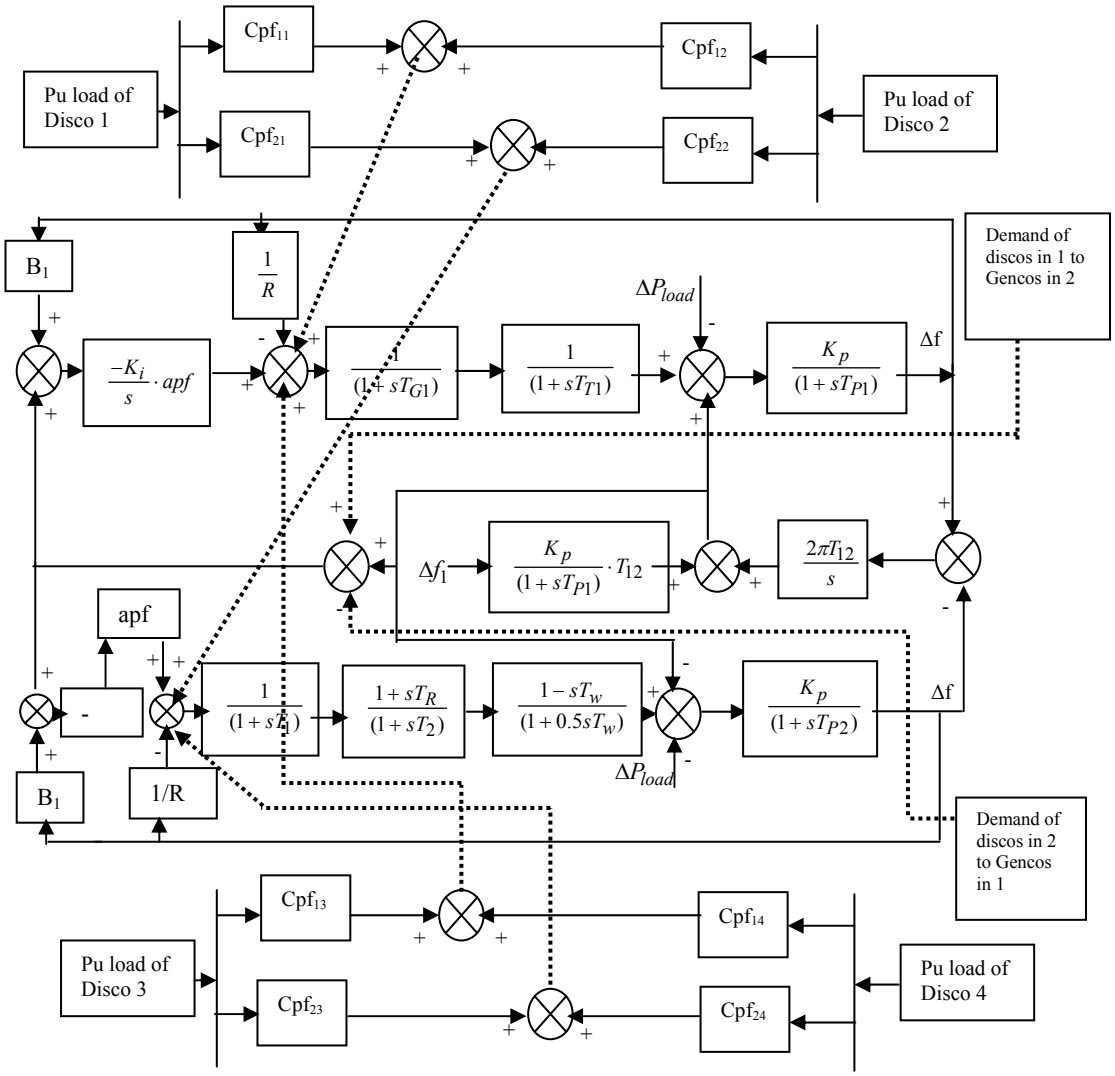

Figure 2: Two area hydrothermal system under open market scenario

A new hybrid method based on the combination of modified Genetic algorithm and simulated annealing has been proposed wherein the simulated annealing takes over the optimization of integral controller once the genetic algorithm terminates. This new method is called as hybrid modified Genetic- Simulated annealing method (HMGASA) which indeed gives good results than the techniques considered separately.
The simulated annealing method resembles the cooling process of molten metals through annealing. The algorithm for simulated annealing method can be written as shown below.

Step 1: Choose an initial point $x^{(0)}$, a termination criterion ε .Set T a sufficiently high value, number of iterations to be performed at a particular temperature n ,and set t=0.

Step 2: Calculate a neighbouring point $x^{(t+1)} = N(x^{(t)})$. Usually a random point in the neighborhood is created

Step 3: If $\Delta E = E(x^{(t+1)}) - E(x^{(t)}) < 0$, set t = t+1; else create a random number (r) in the range (0,1). If $r \le \exp(-\frac{\Delta E}{T}) set = t+1$; else go to step 2

Step 4: If $\left| x^{(t+1)} - x^{(t)} \right| < \varepsilon$ and T is small, **Terminate** else if (t mod n)= 0 then lower T according to a cooling schedule. And go to step 2. Else go to step 2.

Optimum values of integral gain settings of area 1 and area 2 without and with TCPS in series with the tie-line are tabulated in Table-1

Table 1. Optimum values of Integral Gain Settings

Area	Without TCPS	With TCPS inseries with tie-line
Thermal	k_{i1} = 0.650	k_{i1} =0.940
Hydro	k_{i2} = 0.470	k_{i2} =0.570

From Table-1 it is seen that the optimum values of the integral gain settings in areas 1 and 2 considering TCPS are higher than those obtained without TCPS.

5. Dynamic Responses and Discussions

Considering GRCs, simulation studies are performed to investigate the performance of the two-area hydrothermal system under open market system without and with TCPS in series with the tie-line. A

step load disturbance of 0.04 pu MW is considered in either of the areas. Also an additional case is also considered when contract violation occurs in either area. So in this contact violation an additional load of 0.03 pu MW is considered in both the areas after the time span of 30 sec. In this contract violation the Gencos which are present in that particular area where the violation has taken place indeed take up that extra load while the remaining generators of other area generate the power which they had been generating before. It can also be seen that this contract violation does not effect the systems frequency response and altogether the system comes back to its original state after some disturbance initially.

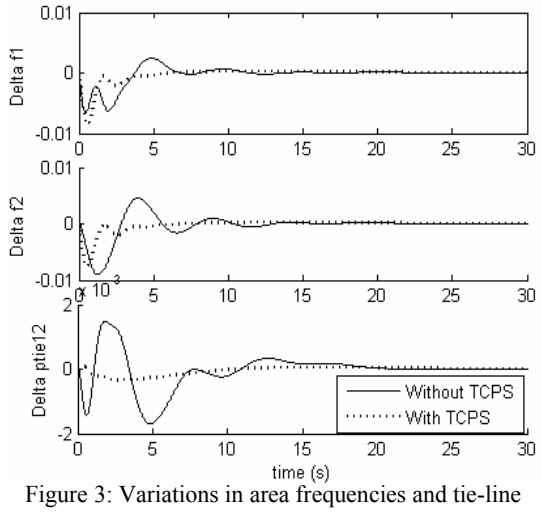

Figure 3: Variations in area frequencies and tie-line power

It is seen from Figure 3 that, with the TCPS in series with the tie-line, dynamic responses for Δf_1, Δf_2 have improved significantly and it can be observed that the oscillations in area frequencies have decreased to a considerable extent with the use of TCPS. Depicted in Figure 4 are the generations of Gencos in first area and Figure 5 depicts the generation of Gencos in second area for a load of 0.004 p.u Mw in both areas. This idea has been implemented in the block diagram and it has also been represented in block diagram of Figure 2.

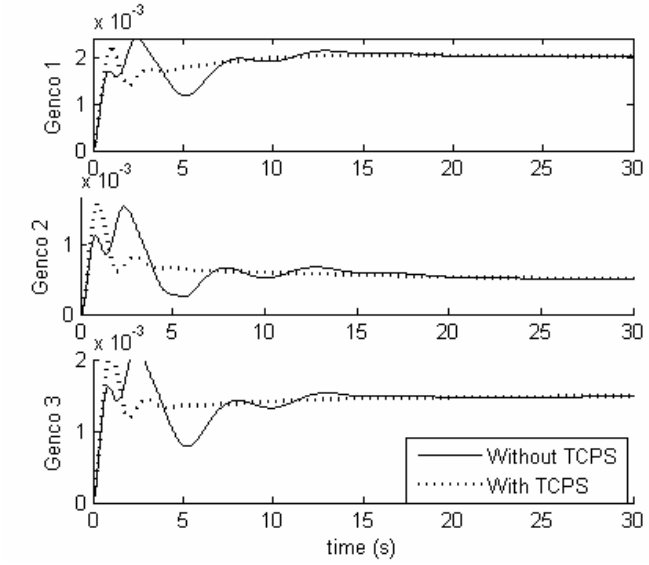

Figure 4: Generations of Gencos in area 1

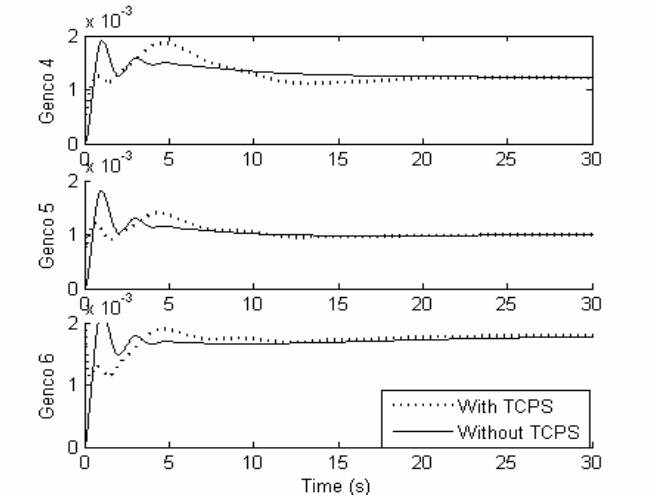

Figure 5: Generations of Gencos in area 2

Figures 6-8 shown below show the case of contract violation where an additional load of 0.03 pu MW is demanded in each area. As mentioned earlier it can be seen in Figure 6 that the frequency error has some transients and after some time it comes back to its original zero position after some time. Figures 6-7 depict the generations of Gencos in both areas during contract violation and also with the use of TCPS the oscillations are reduced drastically

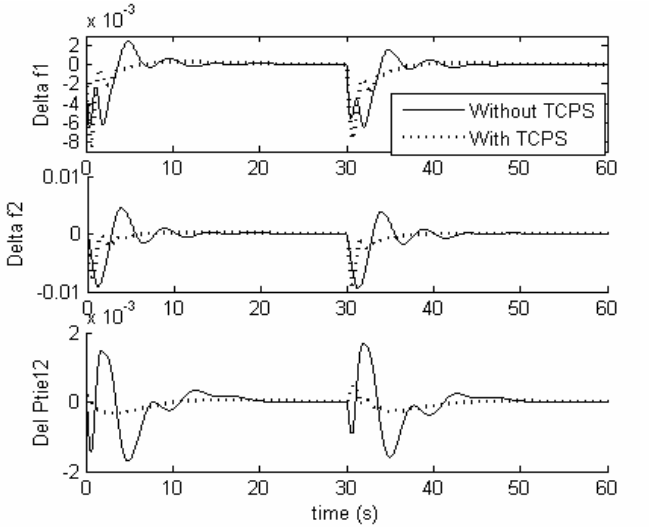

Figure 6: Variations in area frequencies and tie-line power deviations during contract violation

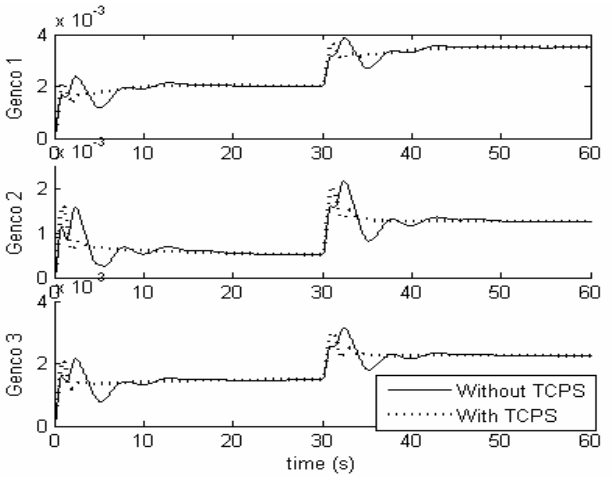

Figure 7: Generations of Gencos in area 1 during contract violation in area 1

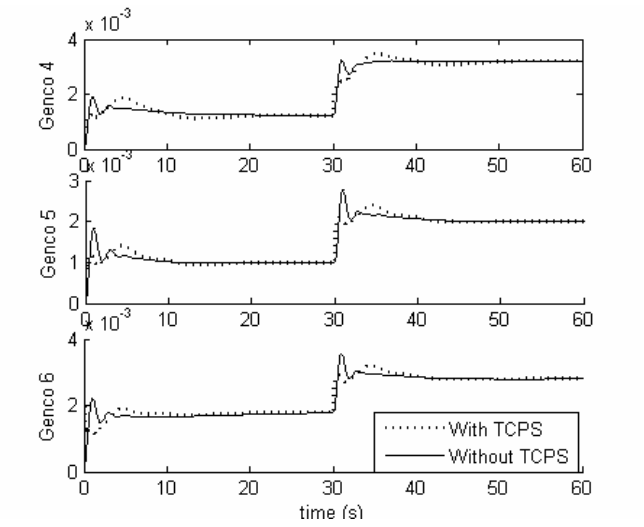

Figure 8: Generation of Gencos in area 2 during contract violation in area 2

Depicted in Fig 9 are the frequency deviations for the various values of integral controllers generated during the process of HMGASA algorithm. The optimum values of integral controllers without and with TCPS have already been tabulated in Table 1. Here also the oscillations in area frequencies have been greatly reduced by the use of TCPS

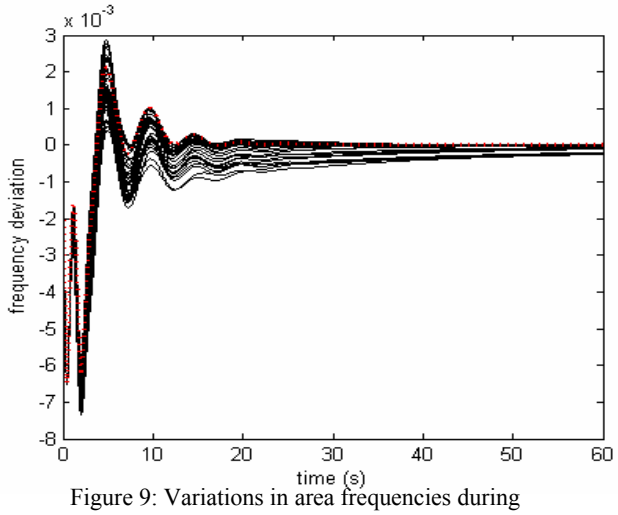

Figure 9: Variations in area frequencies during various values of integral controller

6. Conclusions

In this paper, a tie-line power flow control technique by TCPS has been proposed for a two-area interconnected hydrothermal power system under open market scenario. Gain settings of the integral controllers are optimized using HMGASA algorithm in the presence of GRCs by minimizing a quadratic performance index. A control strategy has been proposed to control the TCPS phase angle which in turn controls the inter-area tie-line power flow. Simulation results reveal that frequencies and tie-power oscillations following sudden load disturbance in either of the areas can be suppressed by controlling the phase angle of TCPS. It may be therefore concluded that, the tie-line power flow control by a TCPS can be expected to be utilized as a new ancillary service for stabilization of frequencies and tie power oscillations in the deregulated environment of power systems.

7. Appendix

All the notations carry the usual meanings

TCPS data:

$T_{PS} = 0.1s$

$K_{\phi} = 1.5rad / Hz$

$\phi_{\max} = 10^{o}$

$\phi_{\min} = -10^{o}$

8. References

Journal papers:

[1] Y. L. Karnavas and D. P. Papadopoulos, "AGC for autonomous power system using combined intelligent techniques," *International Journal of Electric Power System Research, vol. 62,* pp. 225– 239, 2002.

[2] Y. H. Moon, H. S. Ryu, J. G. Lee, K. B. Song, and M. C. Shin, "Extended integral control for load - frequency control with the consideration of generation rate constraints," *International Journal of Electrical Power and Energy Systems, vol. 24,* pp. 263–269, 2002.

[3] H. F. Wang, F. J. Shift, and M. Li, "Analysis of thyristor controlled phase shifter applied in damping power system oscillations," *International Journal of Electrical Power and Energy Systems, vol. 19,* no. 1, pp. 1–9, 1997.

[4] N. G. Hingorani, "Flexible ac transmission," *IEEE Spectrum,* pp. 40–45, Apr. 1993.

[5] O. I. Elgerd and C. Fosha, "Optimum megawatt frequency control of multi-area electric energy systems," *IEEE Transactions on Power Apparatus and Systems,* vol. PAS-89,no.4, pp. 556–563, Apr. 1970.

[6] N. Jaleeli, L. S. Vanslycn, D. N. Ewart, L. H. Fink, and A. G. Hoffmann, "Understanding automatic generation control," *IEEE Transactions on Power Systems,* vol. 7, pp. 1106–1122, 1999.

[7] K. Xing and G. Kusic, "Application of thyristor controlled phase shifters to minimize real power losses and augment stability of power systems,"*IEEE Transactions on Energy Conversion,* vol. 3, no. 4, pp. 792–798, 1988.

[8] R. Baker, G. Guth, W. Egli, and P. Eglin, "Control algorithm for a static phase shifting transformer to enhance transient and dynamic stability of large power systems," *IEEE Transactions on Power Apparatus and Systems,* vol. PAS-101, no. 9, pp. 3532–3542, 1982.

[9] Robert P. Schulte, "Automatic generation Control modification for present demands on interconnected power systems", *IEEE Trans. On Power Systems,* August 1996,pp.1286-1291.

[10] Jayant Kumar, Kah-Koeng and Gerald Sheble, "AGC simulator for price based operation

Part1", *IEEE Transactions on Power Systems,* vol.12,no.2, May 1997,pp. 527-532.

[11] Jayant Kumar, Kah-Hoeng and Gerald Sheble, "AGC simulator for price based operation part-2", *IEEE Transactions on Power Systems,* Vol.12, no. 2, May1997, pp 533-538.

[12] Bjorn H.Bakken and OvesGrande, "Automatic generation control in a deregulated environment", *IEEE Transactions on Power Systems,* vol.13, no.4,Nov1998,pp. 1401-1406.

[13] Vaibhav Donde, M.A.Pai and Ian A.Hiskens, "Simulation and optimization in an AGC system after deregulation", *IEEE Transaction on Power system,* vol.16, no.3, Aug.2001, pp.481-489.

[14] I. C. Report, "Dynamic models for steam and hydro turbines in power system studies," *IEEE Transactions on Power Apparatus and Systems,* vol. PAS-92, no. 6, pp. 1904–1915, Nov/Dec 1973.

[15] T. Ghose, "Solution of price based unit commitment problem by modified genetic algorithm" *IEE Transactions on IT in power*, pp. 50-53, Jan 2005.

[16] N. Cohn, "Techniques for improving the control of bulk power transfers on interconnected systems," *IEEE Transactions on Power Apparatus and Systems,* vol. PAS-90, no. 6, pp. 2409–2419, 1971.

[17] S. M. Miniesy and E. V. Bohn, "Two level control of interconnected power plants," *IEEE Transactions on Power Apparatus and Systems,* vol. PAS-90, pp. 2742–2748, June 1971.

[18] R. K. Green, "Transformed automatic generation control," *IEEE Transactions on Power Systems,* vol. 11, no. 4, pp. 1799–1804, 1996.

[19] M. Reformat, E. Kuffel, D. Woodford, and W. Pedrycz, "Application of genetic algorithms for control design in power systems,"*Proc. IEE,Generation, Transmission & Distribution,* vol. 145, no. 4, pp. 345–354, 1998.

[20] T. Hiyama, "Design of decentralized load - frequency regulators for interconnected power systems," *Proc. IEE,* vol. 129, Pt. C, no. 1, pp. 17– 22, 1982.

[21] A. Bose and I. Atiyyah, "Regulation Error in Load- Frequency Control, "*IEEE Transactions on Power Apparatus and Systems,* vol. PAS-99, no. 2, pp. 650– 657, 1980.

Bibliographies

C.Srinivasa Rao graduated from J.N.T University in 2002, Masters in 2004 from Birla Institute of Technology, Mesra and currently pursuing his Ph.D from J.N.T.University. Working as Assistant Professor in the Department of Electrical Engineering, G.Pulla Reddy Engineering college (Autonomous), Kurnool, Andhra Pradesh since June 2004. His areas of interest are in Genetic Algorithm applications, power system operation and control and Deregulated market

Dr.S.Sivanagaraju, graduated in 1998, Masters in 2000 from IIT, Kharagpur and did his Ph.D from J.N.T.University in 2004. Presently he is working as Associate Professor in the Department of Electrical Engineering, J.N.T.U College of Engg. (Autonomous), Kakinada. He is Referee for IEE Proceedings- Generation Transmission and Distribution and International Journal of Emerging Electric Power System. He has about 40 publications in National and International Journals and Conferences to his credit. His areas of interest are in Distribution Automation, Genetic Algorithm applications to distribution systems and power system.

Dr.P.Sangameswararaju did his Ph.D from S.V.University. Presently he is working as Associate Professor in the Department of Electrical Engineering, S.V.University. Tirupathi, Andhra Pradesh. He has about 20 publications in National and International Journals and Conferences to his credit. His areas of interest are in Distribution systems and power systems.

www.icgst.com

Fuzzy Dynamic Output Feedback Control for Nonlinear Systems Integrated with H_∞ and Quadratic D-Stability Strategies

Mourad KCHAOU, Mansour SOUISSI, Ahmed TOUMI
National School of Engineers of Sfax,
BP: W, 3038 Sfax, Tunisia,
Mouradkchaou@isetma.rnu.tn, mansour.souissi@ipeis.rnu.tn, ahmad.tomi@enis.rnu.tn,

Abstract

This paper deals with the design of a dynamic output feedback controller for nonlinear and uncertain systems. The proposed controller is based on the Takagi-Sugeno (TS) fuzzy approach. Both stabilities in a pre-specified LMI stability region and H_∞ control synthesis have been developed. The control laws are derived considering the so-called dynamic output feedback parallel-distributed compensation (DOPDC). The resolution of the problem associated with the controller synthesis has been achieved considering an LMI approach. The capability of the proposed approach is illustrated through a numerical example.

Keywords: *Fuzzy system, Robust H_∞ control, dynamic output feedback, robust D-stability, linear matrix inequality (LMI).*

1 Introduction

Over the past two decades, fuzzy logic control has been given an increasing attention. The implementation of fuzzy control strategies has led to successful applications. Of particular interest are the Takagi-Sugeno (TS) fuzzy models which are currently considered as universal approximator for any nonlinear function [22]. The (TS) fuzzy model represents a nonlinear system by a set of local linear models, which is smoothly blended together through membership functions. This representation offers the possibility of using conventional linear systems for the analysis and design of the fuzzy controller. Being an interesting procedure of the control design framework, the parallel distributed compensation (PDC) is applied in the present paper. The PDC control structure uses a nonlinear state feedback controller, which mirrors the structure of the associated (TS) model. The gains of the controller can be determined automatically using an LMI formulation [1, 3, 5, 6, 13, 20, 23]. Since the parametric uncertainty is a crucial factor from the point of view of stability and performance, it's very important to consider the robust stability against parametric uncertainty in the (TS) fuzzy controller [4, 7, 10, 11, 21, 23, 26]. Recently, many works on (TS) fuzzy model-based control of nonlinear systems were developed to stabilize the (TS) fuzzy model with an adequate level of performance such as the H_2 performance [8], H_∞ performance [10, 13, 14, 17, 20] or the mixed H_2/H_∞ performance [9]. In this paper, we extend the LMI based approach to develop a dynamic output feedback controller for a class of fuzzy uncertain systems. These are described by (TS) fuzzy models in which both robust D-stability and prescribed H_∞ performance are required to be achieved. The paper is organized as follow:
Problem formulation and definitions are presented in section 2. The analysis and the synthesis of the results of the proposed fuzzy dynamic output feedback controller, which guarantees the H_∞ performance and quadratic D-stability, are developed in section 3. In section 4, numerical example is provided to confirm the design effectiveness and to illustrate the desired performance.

2 System description and definitions

A convenient and flexible tool for handling complex nonlinear systems is the (TS) fuzzy model, where the consequent parts are linear models connected by IF-THEN rules [3, 5, 6]. A discrete-time (TS) fuzzy model with uncertainties is composed of r plant rules that can be represented as

Plant Rule i:

$$\begin{aligned}\text{If } \theta_1(k) \text{ is } M_{1_i} \text{ and } \ldots \text{ and } \theta_p(k) \text{ is } M_{p_i} \text{ Then} \quad (1)\\ x(k+1) = (A_i + \Delta A_i)x(k) + (B_{1_i} + \Delta B_{1_i})u(k)\\ + (B_{2_i} + \Delta B_{2_i})w(k)\\ z(k) = C_{1_i}x(k) + D_{1_i}u(k)\\ y(k) = C_{2_i}x(k) + D_{2_i}w(k)\\ \text{for i} = 1, 2, \ldots, r\end{aligned}$$

where M_{j_i} is the fuzzy set; $x(k) \in \mathbb{R}^n$ is the state, $u(k) \in \mathbb{R}^m$ is the control input, $y(k) \in \mathbb{R}^p$ is the output, $z(k) \in \mathbb{R}^q$ is the control output and $w(k) \in \mathbb{R}^l$ is the exogenous disturbance input with $\{w(k)\} \in L_2[0, \infty)$.
A_i, B_{1_i}, B_{2_i}, C_{1_i},D_{1_i},C_{2_i} and D_{2_i} are known real constant matrices and ΔA_i, ΔB_{1_i} and ΔB_{2_i} are time-varying but norm bounded uncertainties with the following form:

$$\left[\Delta A_i \; \Delta B_{1_i} \; \Delta B_{2_i}\right] = HF(k)\left[E_i \; E_{1_i} \; E_{2_i}\right] \quad (2)$$

where H, E_i, E_{1_i} and E_{2_i} are known constant matrices of appropriate dimensions and $F(k)$ is an unknown real time varying matrix with Lebesgue-measurable elements satisfying $F^T(k)F(k) \leq I$.
The dynamic fuzzy model can be represented by the following overall model, which combines all the local models through membership functions.

$$\begin{aligned}x(k+1) = \sum_{i=1}^{r} h_i(\theta(k))\Big((A_i + \Delta A_i)x(k)\\ +(B_{1_i}+\Delta B_{1_i})u(k) + (B_{2_i} + \Delta B_{2_i})w(k)\Big)\\ z(k) = \sum_{i=1}^{r} h_i(\theta(k))\Big(C_{1_i}x(k) + D_{1_i}w(k)\Big) \quad (3)\\ y(k) = \sum_{i=1}^{r} h_i(\theta(k))\Big(C_{2_i}x(k) + D_{2_i}w(k)\Big)\end{aligned}$$

where $h_i(\theta(k))$ is the normalized weight for each rule, that is:

$$0 \leq h_i(\theta(k)) \leq 1 \quad \text{and} \quad \sum_{i=1}^{r} h_i(\theta(k)) = 1 \quad (4)$$
$$\text{for} \quad i = 1, 2, \cdots, r$$

Conformably to the description (1), it is quite natural to seek a dynamic output feedback parallel-distributed compensation (DOPDC),[6, 24, 25] in the form:

$$\begin{aligned}\text{If } \theta_1(k) \text{ is } M_{1_j} \text{ and } \ldots \text{ and } \theta_p(k) \text{ is } M_{p_j} \text{ Then} \quad (5)\\ \widehat{x}(k+1) = \widehat{A}_j\,\widehat{x}(k) + \widehat{B}_j\,y(k)\\ u(k) = \widehat{C}_j\,\widehat{x}(k)\\ \text{for j} = 1, 2, \ldots, r\end{aligned}$$

The overall (DOPDC) controller can be rewritten as

$$\begin{aligned}\widehat{x}(k+1) = \sum_{j=1}^{r} h_j(\theta(k))\Big(\widehat{A}_j\,\widehat{x}(k) + \widehat{B}_j\,y(k)\Big) \quad (6)\\ u(k) = \sum_{j=1}^{r} h_j(\theta(k))\widehat{C}_j\,\widehat{x}(k)\end{aligned}$$

The closed-loop system obtained by connecting the dynamic controller (6) and the uncertain fuzzy system (3) can be expressed as

$$\begin{aligned}\widetilde{x}(k+1) = \sum_{i=1}^{r}\sum_{j=1}^{r} h_i h_j\Big(\overline{A}_{ij}\,\widetilde{x}(k) + \overline{B}_{ij}\,w(k)\Big) \quad (7)\\ z(k) = \sum_{i=1}^{r}\sum_{j=1}^{r} h_i h_j \overline{C}_{ij}\,\widetilde{x}(k)\end{aligned}$$

where

$$\overline{A}_{ij} = \widetilde{A}_{ij} + \widetilde{H}F(k)\widetilde{E}_{ij},\ \overline{B}_{ij} = \widetilde{B}_{ij} + \widetilde{H}F(k)\widetilde{E}_{1_i},\ \overline{C}_{ij} = \widetilde{C}_{ij} \quad (8)$$

with

$$\widetilde{A}_{ij} = \begin{bmatrix} A_i & B_{1_i}\widehat{C}_j \\ \widehat{B}_j C_{2_i} & \widehat{A}_j \end{bmatrix},\ \widetilde{B}_{ij} = \begin{bmatrix} B_{2_i} \\ \widehat{B}_j D_{2_i} \end{bmatrix},$$
$$\widetilde{C}_{ij} = \begin{bmatrix} C_{1_i} \; D_{1_i}\widehat{C}_j \end{bmatrix},\ \widetilde{E}_{ij} = \begin{bmatrix} E_i \; E_{1_i}\widehat{C}_j \end{bmatrix},$$
$$\widetilde{E}_{1_i} = E_{2_i},\ \widetilde{H} = \begin{bmatrix} H \\ 0 \end{bmatrix}, \text{ and } \quad \widetilde{x}(k) = \begin{bmatrix} x(k) \\ \widehat{x}(k) \end{bmatrix}$$

Now, we recall the following definitions.
Definition 2.1 *: Suppose γ is a given positive number. A system of the form (7) is said to have L_2 gain less than equal to γ if*

$$\sum_{k=0}^{k=\infty} z^T(k)z(k) \leq \gamma^2 \sum_{k=0}^{k=\infty} w^T(k)w(k) \quad (9)$$

Definition 2.2 *: A subset D of the complex plane is called an LMI region if there exists a symmetric matrix $\Gamma \in \mathbb{R}^{g\times g}$ and a matrix $\Pi \in \mathbb{R}^{g\times g}$ such that*

$$\mathcal{D} = \{z = x + iy \in \mathbb{C}; f_{\mathcal{D}}(z) < 0\} \quad (10)$$

where the characteristic function $f_{\mathcal{D}}$ is given as follows:

$$f_{\mathcal{D}}(z) = \Gamma + \Pi z + \Pi^T \overline{z} \quad (11)$$

The uncertain system $x(k+1) = (A+\Delta A)x(k)$ is said to be quadratically D-stable if there exists a symmetric positive-definite matrix P such that for all admissible perturbation ΔA, the following matrix inequality

$$\Gamma \otimes P + \Pi \otimes P(A + \Delta A) + \Pi^T \otimes (A + \Delta A)^T P < 0$$

is true, where the LMI region is defined in (11)


Problem formulation: The aim of this paper is to design a full order fuzzy dynamic output feedback controller of the form (6) such that the resulting closed loop fuzzy system (7) is quadratically D-stable in the given LMI region while satisfying a prescribed H_∞ performance level irrespective of the parameters uncertainties.

3 Dynamic output feedback fuzzy controller design with D-stability constraints

In this section, we develop the (DOPDC) controller (6) for uncertain (TS) fuzzy model (3), taking into account the formulation of the previous section.
We first give the following results which will be used in the proof of our results.

Lemma 3.1 *[25] Given any matrices X, Y and Z with appropriate dimensions such that $Y > 0$ then, we have*

$$X^TZ + Z^TX \le X^TYX + Z^TY^{-1}Z$$

Lemma 3.2 *[15, 26] Let A, H, E, P and F be real matrices of appropriate dimensions such that $P > 0$ and $F^TF \le I$. Then, for any scalar $\varepsilon > 0$ such that $P - \varepsilon HH^T > 0$, we have*

$$\begin{aligned}(A+HFE)^TP^{-1}(A+HFE) \le & A^T(P-\varepsilon HH^T)^{-1}A \\ & + \varepsilon^{-1}E^TE\end{aligned}$$

Theorem 3.1 *For a prescribed H_∞ performance $\gamma > 0$ and LMI stability region $\mathcal{D}$, the system (7) is D-stable with H_∞ norm bound γ if there exists a matrix $P > 0$ such that satisfying the following matrix inequalities:*

$$\begin{pmatrix} -P & * & * & * & * & * \\ 0 & -\gamma^2 I & * & * & * & * \\ \widetilde{A}_{ii} & \widetilde{B}_{ii} & -P^{-1} & * & * & * \\ \widetilde{C}_{ii} & 0 & 0 & -I & * & * \\ \widetilde{E}_{ii} & \widetilde{E}_{1_i} & 0 & 0 & -\varepsilon_{ii} I & * \\ 0 & 0 & \widetilde{H}^T & 0 & 0 & -\varepsilon_{ii}^{-1} I \end{pmatrix} < 0 \qquad (12)$$

$$\begin{pmatrix} \Theta_{ii} & * & * \\ (L_2 \otimes \widetilde{E}_{ii}) & -\varepsilon_{0_{ii}} I & * \\ (L_1 \otimes \widetilde{H}^T P) & 0 & -\varepsilon_{0_{ii}}^{-1} I \end{pmatrix} < 0 \qquad (13)$$

$$i = 1, \ldots, r$$

$$\begin{pmatrix} -4P & * & * & * & * & * & * \\ 0 & -4\gamma^2 I & * & * & * & * & * \\ \widetilde{A}_{ij} + \widetilde{A}_{ji} & \widetilde{B}_{ij} + \widetilde{B}_{ji} & -P^{-1} & * & * & * & * \\ \widetilde{C}_{ij} + \widetilde{C}_{ji} & 0 & 0 & -I & * & * & * \\ \widetilde{E}_{ij} & \widetilde{E}_{1_i} & 0 & 0 & -\varepsilon_{ij} I & * & * \\ \widetilde{E}_{ji} & \widetilde{E}_{1_j} & 0 & 0 & 0 & -\varepsilon_{ij} I & * \\ 0 & 0 & H_c^T & 0 & 0 & 0 & -\varepsilon_{ij}^{-1} I \end{pmatrix} < 0 \qquad (14)$$

$$\begin{pmatrix} \phi_{ij} & * & * \\ (L_2 \otimes M_{cij}) & -\varepsilon_{0_{ij}} I & * \\ (L_1 \otimes H_c^T P) & 0 & 0 \; -\varepsilon_{0_{ij}}^{-1} I \end{pmatrix} < 0 \qquad (15)$$

$1 \le i < j \le r$
where

$$\Theta_{ii} = \Gamma \otimes P + \Pi \otimes P\widetilde{A}_{ii} + (\Pi \otimes P\widetilde{A}_{ii})^T,$$
$$\phi_{ij} = 2\Gamma \otimes P + \Pi \otimes P(\widetilde{A}_{ij} + \widetilde{A}_{ji}) + (\Pi \otimes P(\widetilde{A}_{ij} + \widetilde{A}_{ji}))^T$$
$$H_c = \begin{bmatrix} \widetilde{H} \; \widetilde{H} \end{bmatrix}, \quad M_{cij} = \begin{bmatrix} \widetilde{E}_{ij} \\ \widetilde{E}_{ji} \end{bmatrix} \quad \text{and} \quad \Pi = L_1^T L_2$$

Proof: Firstly, we show that for any non zero $w(k) \in L_2$, the uncertain system (7) satisfies (9) under zero initial condition. To this end, we introduce the criterion:

$$J = \sum_{k=0}^{\infty} \left(z^T(k)z(k) - \gamma^2 w^T(k)w(k) \right) \qquad (16)$$

Noting the zero initial condition and the system (7), we can deduce

$$\begin{aligned} J = & \sum_{k=0}^{\infty} \left[V(\widetilde{x}(k+1)) - V(\widetilde{x}(k)) + z^T(k)z(k) \right. \\ & \left. - \gamma^2 w^T(k)w(k) \right] - V(x(\infty)) \\ \le & \sum_{k=0}^{\infty} \left[\Delta V(\widetilde{x}(k)) + z^T(k)z(k) - \gamma^2 w^T(k)w(k) \right] \\ = & \sum_{k=0}^{\infty} \Big\{ \sum_{i=1}^{r}\sum_{j=1}^{r}\sum_{u=1}^{r}\sum_{v=1}^{r} h_i h_j h_u h_v \big([\overline{A}_{ij}\widetilde{x}(k) + \overline{B}_{ij}w(k)]^T \\ & \times P[\overline{A}_{uv}\widetilde{x}(k) + \overline{B}_{uv}w(k)] + [\overline{C}_{ij}\widetilde{x}(k)]^T [\overline{C}_{uv}\widetilde{x}(k)] \big) \\ & - \widetilde{x}^T(k)P\widetilde{x}(k) - \gamma^2 w^T(k)w(k) \Big\} \end{aligned} \qquad (17)$$

where $V(\widetilde{x}(k)) = \widetilde{x}^T(k)P\widetilde{x}(k)$ is a Lyapunov function candidate.
By Lemma (3.1), we have

$$\begin{aligned} & \sum_{i=1}^{r}\sum_{j=1}^{r}\sum_{u=1}^{r}\sum_{v=1}^{r} h_i h_j h_u h_v [\overline{C}_{ij}\widetilde{x}(k)]^T [\overline{C}_{uv}\widetilde{x}(k)] \\ = & \frac{1}{4} \sum_{i=1}^{r}\sum_{j=1}^{r}\sum_{u=1}^{r}\sum_{v=1}^{r} h_i h_j h_u h_v [(\overline{C}_{ij} + \overline{C}_{ji})\widetilde{x}(k)]^T \\ & \times [(\overline{C}_{uv} + \overline{C}_{vu})\widetilde{x}(k)] \\ \le & \frac{1}{4} \sum_{i=1}^{r}\sum_{j=1}^{r} h_i h_j [(\overline{C}_{ij} + \overline{C}_{ji})\widetilde{x}(k)]^T [(\overline{C}_{ij} + \overline{C}_{ji})\widetilde{x}(k)] \end{aligned} \qquad (18)$$


and

$$\begin{aligned}
&\sum_{i=1}^{r}\sum_{j=1}^{r}\sum_{u=1}^{r}\sum_{v=1}^{r} h_i h_j h_u h_v [\overline{A}_{ij}\widetilde{x}(k)+\overline{B}_{ij}w(k)]^T \\
&\times P[\overline{A}_{uv}\widetilde{x}(k)+\overline{B}_{uv}w(k)] \\
&= \frac{1}{4}\sum_{i=1}^{r}\sum_{j=1}^{r}\sum_{u=1}^{r}\sum_{v=1}^{r} h_i h_j h_u h_v [(\overline{A}_{ij}+\overline{A}_{ji})\widetilde{x}(k) \\
&+ (\overline{B}_{ij}+\overline{B}_{ji})w(k)]^T \\
&\times P[(\overline{A}_{uv}+\overline{A}_{vu})\widetilde{x}(k)+(\overline{B}_{uv}+\overline{B}_{vu})w(k)] \\
&\leq \frac{1}{4}\sum_{i=1}^{r}\sum_{j=1}^{r} h_i h_j [(\overline{A}_{ij}+\overline{A}_{ji})\widetilde{x}(k)+(\overline{B}_{ij}+\overline{B}_{ji})w(k)]^T \\
&\times P[(\overline{A}_{ij}+\overline{A}_{ji})\widetilde{x}(k)+(\overline{B}_{ij}+\overline{B}_{ji})w(k)]
\end{aligned} \tag{19}$$

Therefore

$$\begin{aligned}
J \leq \sum_{k=0}^{\infty}\frac{1}{4}\Big\{ &\sum_{i=1}^{r}\sum_{j=1}^{r} h_i h_j \Big(\\
&[(\overline{A}_{ij}+\overline{A}_{ji})\widetilde{x}(k)+(\overline{B}_{ij}+\overline{B}_{ji})w(k)]^T \\
&\times P[(\overline{A}_{ij}+\overline{A}_{ji})\widetilde{x}(k)+(\overline{B}_{ij}+\overline{B}_{ji})w(k)] \\
&[(\overline{C}_{ij}+\overline{C}_{ji})\widetilde{x}(k)]^T[(\overline{C}_{ij}+\overline{C}_{ji})x(k)] \\
&-4\widetilde{x}^T(k)P\widetilde{x}(k)-4\gamma^2 w^T(k)w(k)\Big)\Big\}
\end{aligned} \tag{20}$$

This implies

$$\begin{aligned}
J \leq \frac{1}{4}\sum_{k=0}^{\infty}\Big\{ &\sum_{i=1}^{r}\sum_{j=1}^{r} h_i h_j \xi^T(k)\big((\overline{\Upsilon}_{cij}+\overline{\Upsilon}_{cji})^T(\overline{\Upsilon}_{cij}+\overline{\Upsilon}_{cji}) \\
&+(\overline{\Gamma}_{cij}+\overline{\Gamma}_{cji})^T P(\overline{\Gamma}_{cij}+\overline{\Gamma}_{cji})+4P_\gamma\big)\xi(k)\Big\} \\
= \sum_{k=0}^{\infty}\Big\{ &\sum_{i=1}^{r} h_i^2 \xi^T(k)\big(\overline{\Upsilon}_{cii}^T\overline{\Upsilon}_{cii}+\overline{\Gamma}_{cii}^T P\overline{\Gamma}_{cii}+P_\gamma\big)\xi(k)\Big\} \\
+\frac{1}{2}\sum_{k=0}^{\infty}\Big\{ &\sum_{i=1}^{r}\sum_{j>i}^{r} h_i h_j \xi^T(k)\Big[(\overline{\Upsilon}_{cij}+\overline{\Upsilon}_{cji})^T(\overline{\Upsilon}_{cij}+\overline{\Upsilon}_{cji}) \\
&+(\overline{\Gamma}_{cij}+\overline{\Gamma}_{cji})^T P(\overline{\Gamma}_{cij}+\overline{\Gamma}_{cji})+4P_\gamma\Big]\xi(k)\Big\}
\end{aligned} \tag{21}$$

where

$$\begin{aligned}
&\overline{\Upsilon}_{cij}=\left[\overline{C}_{ij}\ 0\right],\ \overline{\Gamma}_{cij}=\left[\overline{A}_{ij}\ \overline{B}_{ij}\right],\ P_\gamma=-\begin{bmatrix}P & 0\\ 0 & \gamma^2 I\end{bmatrix} \\
&\text{and}\quad \xi^T(k)=\left[\widetilde{x}^T(k)\, w^T(k)\right]
\end{aligned} \tag{22}$$

Set for $1 \leq i \leq j \leq r$

$$\begin{aligned}
&\Upsilon_{cij}=\left[\widetilde{C}_{ij}\ 0\right],\ \Gamma_{cij}=\left[\widetilde{A}_{ij}\ \widetilde{B}_{ij}\right],\ N_{cij}=\left[\widetilde{E}_{ij}\ \widetilde{E}_{1_{ij}}\right] \\
&\text{and}\quad E_{cij}=\begin{bmatrix}N_{cij}\\ N_{cji}\end{bmatrix}
\end{aligned} \tag{23}$$

Then, applying the Schur complement to (14) gives

$$P^{-1}-\varepsilon_{ij}H_c H_c^T>0 \tag{24}$$

and

$$\begin{aligned}
&(\Gamma_{cij}+\Gamma_{cji})^T(P^{-1}-\varepsilon_{ij}H_cH_c^T)^{-1}(\Gamma_{cij}+\Gamma_{cji})+\varepsilon_{ij}^{-1}E_{cij}^T E_{cij} \\
&\quad+(\Upsilon_{cij}+\Upsilon_{cji})^T(\Upsilon_{cij}+\Upsilon_{cji})+4P_\gamma<0
\end{aligned} \tag{25}$$

Considering (24) and using lemma (3.2), we have for $1 \leq i < j \leq r$

$$\begin{aligned}
&(\Gamma_{cij}+\Gamma_{cji}+H_c\overline{F}(k)E_{cij})^T P(\Gamma_{cij}+\Gamma_{cji}+H_c\overline{F}(k)E_{cij}) \\
&\quad+(\Upsilon_{cij}+\Upsilon_{cji})^T(\Upsilon_{cij}+\Upsilon_{cji})+4P_\gamma \\
&\quad=(\overline{\Gamma}_{cij}+\overline{\Gamma}_{cji})^T P(\overline{\Gamma}_{cij}+\overline{\Gamma}_{cji})+ \\
&\quad(\overline{\Upsilon}_{cij}+\overline{\Upsilon}_{cji})^T(\overline{\Upsilon}_{cij}+\overline{\Upsilon}_{cji})+4P_\gamma<0
\end{aligned} \tag{26}$$

where $\overline{F}(k)=\begin{bmatrix}F(k) & 0\\ 0 & F(k)\end{bmatrix}$

Using (12), and following a similar way to the derivation of (26), we can obtain

$$\overline{\Gamma}_{cii}^T P\overline{\Gamma}_{cii}+\overline{\Upsilon}_{cii}^T\overline{\Upsilon}_{cii}+P_\gamma<0 \tag{27}$$

Therefore, the inequality in (21) together with (26) and (27) gives that for any $\xi(k)\neq 0 \quad J<0$, which implies $\sum_{k=0}^{k=\infty} z^T(k)z(k) < \gamma^2\sum_{k=0}^{k=\infty} w^T(k)w(k)$ for any zeros $w(k)\in L_2[0,\infty)$ Next, we establish the D-stability performance, we assume $w(k)\equiv 0$. Then the closed-loop system (7) is given by

$$\widetilde{x}(k+1)=\sum_{i=1}^{r}\sum_{j=1}^{r} h_i h_j \overline{A}_{ij}\,\widetilde{x}(k) \tag{28}$$

Now, we introduce

$$\begin{aligned}
F_{Dij} &= \sum_{i=1}^{r}\sum_{j=1}^{r} h_i h_j\Big(\Gamma\otimes P+\Pi\otimes P\overline{A}_{ij}+(\Pi\otimes P\overline{A}_{ij})^T\Big) \\
&= \frac{1}{2}\sum_{i=1}^{r}\sum_{j=1}^{r} h_i h_j\Big(2\Gamma\otimes P+\Pi\otimes P(\overline{A}_{ij}+\overline{A}_{ji}) \\
&\qquad+(\Pi\otimes P(\overline{A}_{ij}+\overline{A}_{ji}))^T\Big) \\
&= \sum_{i=1}^{r} h_i^2\Big(\Gamma\otimes P+\Pi\otimes P\overline{A}_{ii}+(\Pi\otimes P\overline{A}_{ii}))^T\Big)+ \\
&\sum_{i=1}^{r}\sum_{j>i}^{r} h_i h_j\Big(2\Gamma\otimes P+\Pi\otimes P(\overline{A}_{ij}+\overline{A}_{ji})+(\Pi\otimes P(\overline{A}_{ij}+\overline{A}_{ji}))^T\Big)
\end{aligned} \tag{29}$$

On the other hand by the Schur complement, we have from (15)

$$\phi_{ij}+\varepsilon_{0_{ij}}^{-1}(L_2\otimes M_{cij})^T(L_2\otimes M_{cij})+\varepsilon_{0_{ij}}(L_1^T\otimes PH_c)(L_1^T\otimes PH_c)^T<0 \tag{30}$$

Using the matrix fact $HFE + E^T F^T H^T < \varepsilon HH^T + \varepsilon^{-1} E^T E$, we have

$$\begin{aligned}
&\phi_{ij} + (L_1^T \otimes PH_c)(I \otimes \overline{F}(k))(L_2 \otimes M_{cij}) \\
&\quad + (L_2 \otimes M_{cij})^T (I \otimes \overline{F}(k))^T (L_1^T \otimes PH_c)^T \\
&= \phi_{ij} + L_1^T L_2 \otimes PH_c \overline{F}(k) M_{cij} + (L_1^T L_2 \otimes PH_c \overline{F}(k) M_{cij})^T \\
&\quad = 2\Gamma \otimes P + \Pi \otimes P(\widetilde{A}_{ij} + \widetilde{A}_{ji} + H_c \overline{F}(k) M_{cij}) \\
&\quad + (\Pi \otimes P(\widetilde{A}_{ij} + \widetilde{A}_{ji} + H_c \overline{F}(k) M_{cij}))^T \\
&= 2\Gamma \otimes P + \Pi \otimes P(\overline{A}_{ij} + \overline{A}_{ji}) + (\Pi \otimes P(\overline{A}_{ij} + \overline{A}_{ji}))^T < 0
\end{aligned} \tag{31}$$

Using (13), and following a similar way to the derivation of (31), we can obtain

$$\Gamma \otimes P + \Pi \otimes P\overline{A}_{ii} + (\Pi \otimes P\overline{A}_{ii}))^T < 0 \tag{32}$$

Then, it follows from (31), (32) and (29) that $F_{D_{ij}} < 0$. Hence, the uncertain system (28) is quadratically D-stable. This end the proof. □

Now, we are in position to give the main results on the solvability of the robust output feedback H_∞ control problem with pole placement constraints.

Theorem 3.2 *Consider the uncertain discrete fuzzy system (3). Given a scalar* $\gamma > 0$ *and any LMI stability region* $\mathcal{D}$*, then there exists a full-order fuzzy dynamic output feedback controller (6) such that the closed-loop system (7) is quadratically D-stable and the prescribed* H_∞ *performance is guaranteed if there exist matrices* $X > 0$, $Y > 0$, Ω_i, Φ_i *and* Ψ_i, $1 \le i \le r$, *such the following LMIs hold for some scalars* ε_{ij} *and* $\varepsilon_{0_{ij}}$.

$$\begin{pmatrix}
-J_1 & * & * & * & * & * \\
0 & -J_2 & * & * & * & * \\
M_{1_{ii}} & M_{5_{ii}} & -J_1 & * & * & * \\
M_{2_{ii}} & 0 & 0 & -I & * & * \\
M_{3_{ii}} & M_{6_i} & 0 & 0 & -J_{3_{ii}} & * \\
0 & 0 & N & 0 & 0 & -J_{4_i}
\end{pmatrix} < 0 \tag{33}$$

$$\begin{pmatrix}
\vartheta_{ii} & * & * \\
L_2 \otimes M_{3_{ii}} & -J_{5_i} & * \\
L_1 \otimes N & 0 & -J_{6_i}
\end{pmatrix} < 0 \tag{34}$$

$$\begin{pmatrix}
-4J_1 & * & * & * & * & * & * & * & * \\
0 & -4J_2 & * & * & * & * & * & * & * \\
\Xi_{1_{ij}} & \Xi_{5_{ij}} & -J_1 & * & * & * & * & * & * \\
\Xi_{2_{ij}} & 0 & 0 & -I & * & * & * & * & * \\
M_{3_{ij}} & M_{6_i} & 0 & 0 & -J_{3_{ij}} & * & * & * & * \\
M_{3_{ji}} & M_{6_j} & 0 & 0 & 0 & -J_{3_{ij}} & * & * & * \\
0 & 0 & M & 0 & 0 & 0 & -J_{4_{ij}} & * & * \\
M_{4_{ij}} & 0 & 0 & 0 & 0 & 0 & 0 & -I & * \\
0 & 0 & M_{7_{ij}}^T & 0 & 0 & 0 & 0 & 0 & -I
\end{pmatrix} < 0 \tag{35}$$

$$\begin{pmatrix}
\varphi_{ij} & * & * & * & * \\
L_2 \otimes M_{8_{ij}} & -J_{5_{ij}} & * & * & * \\
L_1 \otimes M & 0 & -J_{6_{ij}} & * & * \\
L_2 \otimes M_{4_{ij}} & 0 & 0 & -I & * \\
L_1 \otimes M_{7_{ij}}^T & 0 & 0 & 0 & -I
\end{pmatrix} < 0 \tag{36}$$

where

$\Xi_{1_{ij}} = M_{1_{ij}} + M_{1_{ji}}$, $\Xi_{2_{ij}} = M_{2_{ij}} + M_{2_{ji}}$, $\Xi_{5_{ij}} = M_{5_{ij}} + M_{5_{ji}}$,
$\varphi_{ij} = 2\Gamma \otimes J_1 + \Pi \otimes (M_{1_{ij}} + M_{1_{ji}}) + \Pi^T \otimes (M_{1_{ij}} + M_{1_{ji}})^T$
$\vartheta_{ii} = \Gamma \otimes J_1 + \Pi \otimes M_{1_{ii}} + \Pi^T \otimes M_{1_{ii}}^T$
$J_1 = \begin{bmatrix} Y & I \\ I & X \end{bmatrix}$, $J_2 = \gamma^2 I$, $J_{3_{ij}} = \varepsilon_{ij} I$, $J_{4_i} = \varepsilon_{ii}^{-1} I$
$J_{4_{ij}} = diag(\varepsilon_{ij}^{-1} I, \varepsilon_{ij}^{-1} I)$, $J_{5_i} = \varepsilon_{0_{ii}} I$, $J_{5_{ij}} = diag(\varepsilon_{0_{ij}} I, \varepsilon_{0_{ij}} I)$,
$J_{6_i} = \varepsilon_{0_{ij}}^{-1} I$, $J_{6_{ij}} = diag(\varepsilon_{0_{ij}}^{-1} I, \varepsilon_{0_{ij}}^{-1} I)$
$M_{1_{ij}} = \begin{bmatrix} A_i Y + B_i \Psi_j & A_i \\ \Omega_i & XA_i + \Phi_j C_{2i} \end{bmatrix}$, $M_{2_{ij}} = \begin{bmatrix} C_i + D_i \Psi_j \, C_i \end{bmatrix}$,
$M_{3_{ij}} = \begin{bmatrix} E_i Y + E_{1_i} \Psi_j \, E_i \end{bmatrix}$, $M_{4_{ij}} = \begin{bmatrix} \Psi_j - \Psi_i & 0 \\ (C_{2_i} - C_{2_j}) Y & 0 \end{bmatrix}$,
$M_{5_{ij}} = \begin{bmatrix} B_{2_i} \\ XB_{2_i} + \Phi_j D_{2_i} \end{bmatrix}$, $M_{6_i} = \begin{bmatrix} E_{2_i} \end{bmatrix}$,
$M_{7_{ij}} = \begin{bmatrix} 0 & 0 \\ X(B_{1_i} - B_{1_j}) \, \Phi_j - \Phi_i \end{bmatrix}$, $M_{8_{ij}} = \begin{bmatrix} M_{3_{ij}} \\ M_{3_{ji}} \end{bmatrix}$
$N = \begin{bmatrix} H^T \, H^T X \end{bmatrix}$, $M = \begin{bmatrix} H^T \, H^T X \\ H^T \, H^T X \end{bmatrix}$

Furthermore, a desired robust dynamic output feedback H_∞ *controller is given in the form of (6) with parameters as follows:*

$$\widehat{A}_i = S^{-1}(\Omega_i - XA_iY - XB_{1_i}\Psi_i - \Phi_i C_{2_i} Y) W^{-T} \tag{37}$$

$$\widehat{B}_i = S^{-1}\Phi_i \tag{38}$$

$$\widehat{C}_i = \Psi_i W^{-T} \tag{39}$$

where S *and* W *are any nonsingular matrices satisfying*

$$SW^T = I - XY \tag{40}$$

Proof: Recall that our goal is to derive the expressions of the controller parameters from (12)-(15). To do this, we partition P and P^{-1} as

$$P = \begin{pmatrix} X & S \\ S^T & X_{22} \end{pmatrix}, P^{-1} = \begin{pmatrix} Y & W \\ W^T & Y_{22} \end{pmatrix} \tag{41}$$

where the partitioning of P and P^{-1} is compatible with that of $\widetilde{A}_{ij}$ defined in (8).
Now define

$$T_1 = \begin{pmatrix} Y & I \\ W^T & 0 \end{pmatrix}, T_2 = \begin{pmatrix} I & X \\ 0 & S^T \end{pmatrix} \tag{42}$$

which imply that $PT_1 = T_2$ and $T_1^T P T_1 = T_1^T T_2$
By applying the Schur complement to (35), we obtain

$$\begin{pmatrix} -4J_1 & * & * & * & * & * \\ 0 & -4J_2 & * & * & * & * \\ \Xi_{1_{ij}} & \Xi_{5_{ij}} & -J_1 & * & * & * \\ \Xi_{2_{ij}} & 0 & 0 & -I & * & * \\ M_{3_{ij}} & M_{6_{ij}} & 0 & 0 & -J_{3_{ij}} & * \\ 0 & 0 & M & 0 & 0 & -J_{4_{ij}} \end{pmatrix} + \begin{pmatrix} 0 \\ 0 \\ M_{7_{ij}} \\ 0 \\ 0 \\ 0 \end{pmatrix} \begin{pmatrix} 0 \\ 0 \\ M_{7_{ij}} \\ 0 \\ 0 \\ 0 \end{pmatrix}^T + \begin{pmatrix} M_{4_{ij}}^T \\ 0 \\ 0 \\ 0 \\ 0 \\ 0 \end{pmatrix} \begin{pmatrix} M_{4_{ij}}^T \\ 0 \\ 0 \\ 0 \\ 0 \\ 0 \end{pmatrix}^T < 0 \tag{43}$$

By lemma (3.1), we can be deduce from (43) that for $1 \leq i < j \leq r$

$$\begin{pmatrix} -4J_1 & * & * & * & * & * \\ 0 & -4J_2 & * & * & * & * \\ \Xi_{1_{ij}} + \mathcal{M}_{ij} & \Xi_{5_{ij}} & -J_1 & * & * & * \\ \Xi_{2_{ij}} & 0 & 0 & -I & * & * \\ M_{3_{ij}} & M_{6_{ij}} & 0 & 0 & -J_{3_{ij}} & * \\ 0 & 0 & M & 0 & 0 & -J_{4_{ij}} \end{pmatrix} < 0 \tag{44}$$

where

$$\mathcal{M}_{ij} = \begin{pmatrix} 0 & 0 \\ X(B_{1_i} - B_{1_j})(\Psi_j - \Psi_i) + (\Phi_j - \Phi_i)(C_{2_i} - C_{2_j})Y & 0 \end{pmatrix} = M_{7_{ij}} M_{4_{ij}}$$

Using the relationship

$$\begin{aligned} &(XA_iY + XB_{1_i}\Psi_j + \Phi_j C_{2_i}Y) \\ &\quad + (XA_jY + XB_{1_j}\Psi_i + \Phi_i C_{2_j}Y) = \\ &\quad (XA_iY + XB_{1_i}\Psi_i + \Phi_i C_{2_i}Y) \\ &\quad + (XA_jY + XB_{1_j}\Psi_j + \Phi_j C_{2_j}Y) + \\ &X(B_{1_i} - B_{1_j})(\Psi_j - \Psi_i) + (\Phi_j - \Phi_i)(C_{2_i} - C_{2_j})Y \end{aligned}$$

and considering the notations in (8) with $\widehat{A}_i$, $\widehat{B}_i$ and $\widehat{C}_i$ for $1 \leq i \leq r$ in (37)-(39), we can verify that the matrix inequality in (44) can be written as

$$diag(T_1^T, I, T_2^T, I, I, I, I) \times (14) \times diag(T_1, I, T_2, I, I, I, I) < 0 \tag{45}$$

In the same way, it is easy to check as the inequality(33) can be written as

$$diag(T_1^T, I, T_2^T, I, I, I) \times (12) \times diag(T_1, I, T_2, I, I, I,) < 0 \tag{46}$$

Now, by applying the Schur complement to (36), we obtain

$$\begin{pmatrix} \varphi_{ij} & * & * \\ L_2 \otimes M_{8_{ij}} & -J_{5_{ij}} & * \\ L_1 \otimes M & 0 & -J_{6_{ij}} \end{pmatrix} + \begin{pmatrix} (L_1^T \otimes M_{7_{ij}}) \\ 0 \\ 0 \end{pmatrix} \begin{pmatrix} (L_1^T \otimes M_{7_{ij}}) \\ 0 \\ 0 \end{pmatrix}^T + \begin{pmatrix} (L_2 \otimes M_{4_{ij}})^T \\ 0 \\ 0 \end{pmatrix} \begin{pmatrix} (L_2 \otimes M_{4_{ij}})^T \\ 0 \\ 0 \end{pmatrix}^T < 0 \tag{47}$$

Therefore, by lemma (3.1) and by performing a Kronecker product property, the inequality (47) implies that

$$\begin{pmatrix} \varphi_{ij} & * & * \\ L_2 \otimes M_{8_{ij}} & -J_{5_{ij}} & * \\ L_1 \otimes M & 0 & -J_{6_{ij}} \end{pmatrix} + \begin{pmatrix} (L_1^T \otimes M_{7_{ij}}) \\ 0 \\ 0 \end{pmatrix} \begin{pmatrix} (L_2 \otimes M_{4_{ij}})^T \\ 0 \\ 0 \end{pmatrix}^T + \begin{pmatrix} (L_2 \otimes M_{4_{ij}})^T \\ 0 \\ 0 \end{pmatrix} \begin{pmatrix} (L_1^T \otimes M_{7_{ij}}) \\ 0 \\ 0 \end{pmatrix}^T = \begin{pmatrix} \mathcal{G}_{ij} & * & * \\ L_2 \otimes M_{8_{ij}} & -J_{5_{ij}} & * \\ L_1 \otimes M & 0 & -J_{6_{ij}} \end{pmatrix} < 0 \tag{48}$$

where

$$\mathcal{G}_{ij} = 2\Gamma \otimes J_1 + \Pi \otimes (\Xi_{1_{ij}} + \mathcal{M}_{ij}) + (\Pi \otimes (\Xi_{1_{ij}} + \mathcal{M}_{ij}))^T$$

We can verify that the matrices inequalities in (48) and (34) respectively can be written as

$$diag((I \otimes T_1^T), I, I) \times (15) \times diag((I \otimes T_1^T), I, I) < 0 \tag{49}$$

$$diag((I \otimes T_1^T), I, I) \times (13) \times diag((I \otimes T_1^T), I, I) < 0 \tag{50}$$

From (45), (46), (49) and (50), we conclude that with controller parameters (37)-(39) the closed-loop system (7) is robustly quadratically D-stable and (9) is satisfied.This end the proof. □

Remarks 3.1 *1. Theorem (3.2) provides a sufficient conditions for the solvability of the robust H_∞ output feedback control problem with pole placement constraints. We note that (33)-(36) are LMIs in $X > 0$, $Y > 0$, Ω_i, Φ_i and Ψ_i, $1 \leq i \leq r$, when $\gamma > 0$, $\varepsilon_{ij} > 0$ and $\varepsilon_{0_{ij}} > 0$ are given. In this case, these LMIs can be solved efficiently by resorting to some standard numerical algorithm.*

2. Note that a pole placement for each linear models of (TS) model in LMI region does not allow

specifying exactly the dynamics of the nonlinear model in closed loop. However, it is still a very interesting way of tuning the close loop dynamics.

4 Numerical example

In this section, a numerical example is presented to illustrate the effectiveness of the proposed controller design technique. Consider the following discrete-time Lorenz system given in [7] with a sampling time $T_s = 0.002s$

$$\begin{aligned} x(k+1) &= \sum_{i=1}^{2} h_i(x_1(k))\Big\{(A_i + \Delta A_i)x(k) \\ &\quad + (B_1 + \Delta B_{1_i})u(k) + (B_{2_i} + \Delta B_{2_i})w(k)\Big\} \\ z(k) &= \sum_{i=1}^{2} h_i(x_1(k))\Big\{C_{1_i}x(k) + D_{1_i}u(k)\Big\} \\ y(k) &= C_2x(k) + D_2w(k) \end{aligned} \tag{51}$$

where $x(k) = \left[x_1^T(k)\, x_2^T(k)\, x_3^T(k)\right]^T$
Similar to [7], we assume that $x_1(k) \in [M_1, M_2]$, and select the membership functions as $h_1 = \frac{M_2 - x_1(k)}{M_2 - M_1}$; $h_2 = 1 - h_1$ with $M_1 = -20$ and $M_2 = 30$
The disturbance input signal $w(k)$ is given by $w(k) = 0.5sin(2\pi kTs)$.
The system matrices are

$$A_1 = \begin{pmatrix} 1-\sigma T_s & \sigma T_s & 0 \\ rT_s & 1-T_s & -M_1T_s \\ 0 & M_1T_s & 1-bT_s \end{pmatrix},$$

$$A_2 = \begin{pmatrix} 1-\sigma T_s & \sigma T_s & 0 \\ rT_s & 1-T_s & -M_2T_s \\ 0 & M_2T_s & 1-bT_s \end{pmatrix},$$

$$B_1 = B_2 = \begin{pmatrix} 1 \\ 0 \\ 0 \end{pmatrix},\ B_{2_1} = \begin{pmatrix} 0.1 \\ -0.1 \\ 0.1 \end{pmatrix},\ B_{2_2} = \begin{pmatrix} 0.1 \\ 0.1 \\ -0.1 \end{pmatrix},$$

$$C_{1_1} = C_{1_2} \begin{pmatrix} 0.005 & 0 & 0 \\ 0 & 0.005 & 0 \\ 0 & 0 & 0.005 \end{pmatrix},\ D_{1_1} = D_{1_2} \begin{pmatrix} 0.1 \\ 0 \\ 0 \end{pmatrix},$$

$$C_2 = \begin{pmatrix} 1\,1\,0 \\ 0\,1\,1 \end{pmatrix},\ D_2 = \begin{pmatrix} 0.1 \\ 0.1 \end{pmatrix}$$

The nominal value of $(\sigma, r, b) = (10, 28, \frac{8}{3})$ for chaos to emerge. We assume that all system parameters are uncertain but bounded within 30% of their nominal values. The uncertain matrices are the following

$$H = \begin{pmatrix} 0.06 & 0 & 0 \\ 0 & 0.06 & 0 \\ 0 & 0 & 0.06 \end{pmatrix},$$

$$E_1 = E_2 = \begin{pmatrix} -\sigma\ \sigma T_s & 0 \\ r & 0 & -M_2T_s \\ 0 & 0 & -b \end{pmatrix} \times 10^{-3},$$

$$E_{1_1} = E_{1_2} = \begin{pmatrix} 0.1\,0.1\,0.1 \end{pmatrix},\ E_{2_1} = E_{2_2} = 0$$

In this example, we choose the H_∞ level $\gamma = 1$ and we would place all its closed-loop poles within LMI disk region of radius $r_0 = 0.6$ and center $C_0(-q_0, 0) = (-0.4, 0)$.
In order to design a fuzzy H_∞ output feedback controller for the (TS) model, we first choose $\varepsilon_{11} = 1.5$, $\varepsilon_{12} = 1.2$, $\varepsilon_{22} = 1.2$ and $\varepsilon_{0_{11}} = 1.3$, $\varepsilon_{0_{12}} = 1.1$, $\varepsilon_{0_{22}} = 1.1$
Then, using the Matlab LMI Control Toolbox with starting point $x_0 = \begin{bmatrix} 10 & -10 & -10 \end{bmatrix}$ and the theorem (3.2), we obtain

$$X = \begin{pmatrix} 55.396 & 21.341 & -26.531 \\ 21.341 & 25.134 & -3.052 \\ -26.531 & -3.052 & 28.171 \end{pmatrix},$$

$$Y = \begin{pmatrix} 126.34 & -43.164 & 4.6949 \\ -43.164 & 123.93 & -0.35455 \\ 4.6949 & -0.35455 & 120.36 \end{pmatrix},$$

$$\widehat{A}_1 = \begin{pmatrix} 0.065816 & -0.070841 & 0.31372 \\ -0.091508 & 0.35792 & 0.072845 \\ -0.085573 & 0.15074 & 0.92246 \end{pmatrix},$$

$$\widehat{A}_2 = \begin{pmatrix} 0.097458 & -0.16722 & 0.28155 \\ -0.06961 & 0.34856 & 0.24871 \\ -0.073245 & 0.10855 & 0.90052 \end{pmatrix},$$

$$\widehat{B}_1 = \begin{pmatrix} 0.50427 & -0.29683 \\ 0.17445 & 0.10098 \\ 0.048336 & -0.071547 \end{pmatrix},$$

$$\widehat{B}_2 = \begin{pmatrix} 0.50256 & -0.29948 \\ 0.17522 & 0.10008 \\ 0.04769 & -0.072213 \end{pmatrix},$$

$$\widehat{C}_1 = \begin{pmatrix} -0.29909 & -0.15427 & 0.45631 \end{pmatrix},$$

$$\widehat{C}_2 = \begin{pmatrix} -0.29872 & -0.15202 & 0.44942 \end{pmatrix},$$

Using SVD algorithm, we have

$$S = \begin{pmatrix} -73.713 & -6.794 & 16.899 \\ -17.48 & -43.027 & -15.033 \\ 48.112 & -26.042 & 20.428 \end{pmatrix},$$

$$W = \begin{pmatrix} 76.39 & 11.157 & -14.525 \\ 2.6467 & 44.994 & 14.07 \\ -47.027 & 20.656 & -22.802 \end{pmatrix}$$

Figure 1 shows the state responses and the ratio of the regulated output energy to the disturbance energy $(\sum_{k=0}^{kf} z^T(k)z(k) / \sum_{k=0}^{kf} w^T(k)w(k))$ for the chaotic system. We can note that the ratio tends to a constant value which is about 0.06488 which is less the


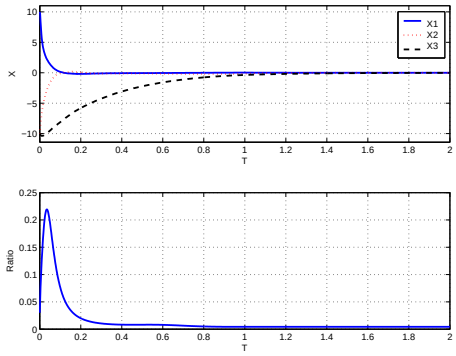

Figure 1: Control results of the chaotic Lorenz system.

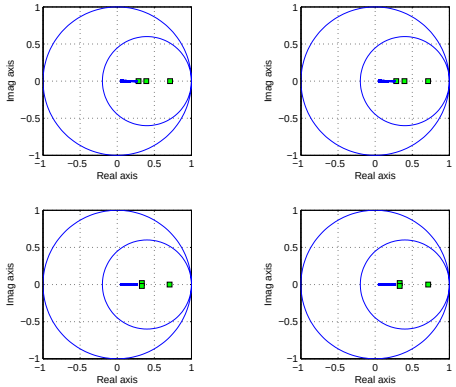

Figure 2: Closed-loop poles of each subsystem .

prescribed value γ.
Figures 2 shows that the fuzzy controller place all its closed-loop poles within prespecified LMI disk region.

5 Conclusion

In this paper, we have presented a stabilizing dynamic output feedback controller which is devoted to uncertain nonlinear systems. The (TS) fuzzy model is employed to describe a nonlinear system with uncertainties. The H_∞ performance and quadratic D-stability have been considered and a sufficient conditions, which are formulated in terms of LMI, is derived. Simulation results have clearly shown that the desired specifications for nonlinear systems can be achieved using the proposed method.

References

[1] B.S.Chen, C.S.Tseng and H.J.Uang. Robustness Design of nonlinear dynamic systems via fuzzy linear control. IEEE transaction on fuzzy systems, vol. 7, no 5, October 1999.

[2] C.Sherer, P.Gahinet and M.Chilali. Multi objective output feedback control via LMI optimization. IEEE transaction on automatic control, vol. 42, no 7, July 1997.

[3] C.S.Tseng, B.S.Chen and H.J.Uang.Fuzzy tracking control design for nonlinear dynamic systems via T-S fuzzy model. IEEE transaction on automatic control, vol. 9, no 3, June 2001.

[4] F.Liu, W.Xu and J.Chu. Robust fuzzy LQ-H_∞ control for uncertain nonlinear Systems with delay 15th Triennial world congress, Barcelona-Spain, IFAC 2002.

[5] H.D.Tuan, P.Apkarian and Y. Yamamoto. Parameterized linear matrix inequality techniques in fuzzy contol system design. IEEE transaction on fuzzy systems, vol. 9, no 2, April 2001.

[6] H.Duong, P.Apkarian, T.Narikiyo and M.Kanota. New fuzzy control model and dynamic output feedback parallel distributed compensation. IEEE transaction on fuzzy systems, vol. 12, no 1, February 2004.

[7] H.j.Lee, J.B.Park and G.Chen. Robust fuzzy control of nonlinear systems with parametric uncertainties. IEEE transaction on fuzzy systems, vol. 9, no 2, April 2001.

[8] H.N.Wu and K.Y.Cai. H_2 guaranteed cost fuzzy control for uncertain nonlinear systems via linear matrix inequalities. Fuzzy sets and systems Journal, vol. 148, pp. 411-429, 2004.

[9] J.Doyle,K.Glover and B.Bodenheimer: Mixed H_2/H_∞ performance objectives II optimal control IEEE transaction on automatic control, vol. 39, no 8, August 1994.

[10] J.C.Loo and M.L.Lin. Robust H $_\infty$ nonlinear modelling and control via uncertain fuzzy systems. Fuzzy sets and systems Journal, vol. 143, pp. 189-209, 2004.

[11] J.H.Chou and S.H.Chen. Stability analysis of the discrete T-S fuzzy model with time varying consequent uncertainties. Fuzzy sets and systems Journal, vol. 118, pp. 271-279, 2001.

[12] K.Tanaka and M.Sano. A Robust stabilization problem of fuzzy control systems and its application to Backing up control of Truck-Trailer. IEEE transaction on fuzzy systems, vol. 24, no 2, May 1994.

[13] K.Tanaka, T.Iked and H.O.Wang. Robust stabilisation of a class of uncertain nonlinear systems via fuzzy control Quadratic stabilizability, H_∞ control, and linear Matrix inequalities. IEEE transaction on fuzzy systems, vol. 4, no 1, February 1996.

[14] K.R.Lee, E.T.Jeung and H.B.Park. Robust fuzzy H_∞ control for uncertain nonlinear systems via state feedback an LMI approach. Fuzzy sets and systems Journal, vol. 120, pp. 123-134, 2001.

[15] L. Xie. Output feedback H_∞ control of systems with parameters uncertainties. International Jounal of Control, vol. 63, no 4, pp. 741-750, 1996.

[16] L.Yu, G.Chen and Y.an. Design of output feedback guaranteed cost controllers with disk closed loop pole constraints for uncertain discrete-time systems. 15th Triennial world congress, Barcelona-Spain, IFAC 2002.

[17] M.Chilali and P.Gahinet H_∞ design with pole placement constraints An LMI approach. IEEE transaction on automatic control, vol. 41, no 3, March 1996.

[18] M. Chilali, P. Gahinet and P. Apkarian Robust pole placement in LMI regions. IEEE transaction on automatic control, vol. 44, no 12, December 1999.

[19] S.boyd, V.Balakrishnan, E.Feron and L.Elghaoui. Control system analysis and synthesis via linear matrix inequalities . In proc. ACC, pp. 2147-2154, 1993.

[20] S.Kiong Nguang and P.Shi. Robust H_∞ output feedback control design for fuzze dynamic systems with quadratic D stability constraints An LMI approach. Information sciences Article in press (2005)

[21] S.Tong and H.H.Li. Observer based robust fuzzy control of non linear systems with parametric uncertainties. Fuzzy sets and systems Journal, vol. 131, pp. 165-184, 2002.

[22] T.Takagi and M.Sugeno. Fuzzy identification of systems and its applications to modelling and control. IEEE trans. system Man Cybern. (SMC), vol. 15, no 1, pp. 116-132, 1985.

[23] W.Chang, J.B.Park, Y.H.Joo and G.Chen Output feedback fuzzy control for uncertain nonlinear systems. Journal of dynamic systems, measurement and control, vol. 125-521, December 2003.

[24] W.Assawinchaichote and S.K.Nguang. Fuzzy H_∞ Output Feedback Control Design for Singularly Perturbed Systems With Pole Placement Constraints: An LMI Approach . IEEE transaction on fuzzy systems, vol. 14, no 3, June 2006.

[25] S.Xu and J Lam. Robust H_∞ Control for Uncertain Discrete-time-Delay fuzzy systems Via Output Feedback Controllers. IEEE transaction on fuzzy systems, vol. 13, no 1, Februart 2005.

[26] Y.Y.Cao and P.M.Frank. Robust H_∞ disturbance attenuation for a class of uncertain discrete-time fuzzy systems. IEEE transaction on fuzzy systems, vol. 8, no 4, August 2000.

Mourad KCHAOU was born in Sfax, Tunisia in 1968. He received his Mastery of Sciences from ENSET of Tunis, Tunisia in 1993. In 2004 he obtained his Master degree in Automatic and industrial Computing Sfax Engineering National School (ENIS). He is currently an Assistant in the Electronic Engineering department of Soussa High Institute of Applied Sciences and Technology. The main research area concerns the fuzzy modeling and robust fuzzy control. E-mail : mouradkchaou@isetma.rnu.tn or mouradkchaou@yahoo.fr

Mansour SOUISSI Mansour suissi (born in 1955), Professor in Preparatory Institute of Engineers Study of Sfax (IPEIS) Tunisia, received the DEA (Master) in electrotechnics from ENSET (Tunisia) and the Doctoral Thesis from the University of Tunis in 1987, In 2002, he obtained the University Habilitation (HDR) from Tunisia, Faculty of Sciences. He is at present the Director of studies in (IPEIS). The main research area concerns the green house modeling and control and the fuzzy logic control. Tel : 0216 74860209 E-mail : mansour.souissi@ipeis.rnu.tn

Ahmed TOUMI (born in 1952), Professor in the Sfax Engineering National School (ENIS), received the Electrical Engineering Diploma from (ENIS/Tunisia), the DEA (Master) in Instrumentation and Measurement from University of Bordeaux-1/France in 1981 and the Doctoral Thesis from the University of Tunis in 1985. He joined the Sfax Engineering National School (ENIS), as an Associate Professor of Electric Engineering, since October 1981. In 2000, he obtained the University Habilitation (HDR) from the Sfax Engineering School (ENIS). He is at present the Director of the Electrical Engineering Department in ENIS. The main research area concerns the modelling, the stability of the electric machines, the electrical networks, the fuzzy logic control. He is the Head of the Research Unit of Industrial Processes Control (UCPI) of the Sfax University. Since 2002, he is the President of the international conference on Sciences and Techniques of Automatic control (STA) which have taken place in a number of tourist cities of Tunisia. Tel. : 0216 74 27 40 88 Fax : +216 74 27 55 95 E-mail : ahmad.tomi@enis.rnu.tn

www.icgst.com

Line Flow Constrained Evaluation of Optimal Bilateral Real Power Contracts/Transactions

K. Vaisakh, G. V.Siva Krishna Rao
Department of Electrical Engineering, AU College of Engineering
Andhra University, Visakhapatnam-530 003,AP, India
vaisakh_k@yahoo.co.in

Abstract
Under a deregulated environment, electricity consumers and suppliers generally establish various bilateral power transactions/contracts. The transmission company normally honors and executes these bilateral contracts as far as the system design and operating conditions permit. This paper describes studies of optimal the bilateral contracts by using Line Flow Factors (LFFs). A generalized linear programming formulation is then proposed to solve system operation under a deregulated environment subjected to the steady-state security constraints (e.g. generation and line flow limits). Examples are presented to illustrate how to use this formulation to minimize the cost of any bilateral contract to comply with the security requirements. It was concluded that the proposed methodology will be an effective tool to study the intricate relationships between the bilateral contracts and system security.

Keywords: *generation, load distribution factors and real power transaction.*

1. Introduction
The open access transmission regime is spearheading the rapid disintegration of the well-entrenched vertically integrated structure of the electric power industry. The entry of a large number of new players and the unbundling of electricity services has pushed the industry toward the widespread use of transactions to meet customer demands. The driving forces of deregulation are aiming to establish a more competitive market in order to achieve lower rates for the consumers and higher efficiency for the suppliers. Traditional power companies are therefore gradually divested into independent business entities by unbundling and privatization of their generation, transmission and distribution functions [1, 2].

Power suppliers, both the conventional utilities as well as the Independent Power Producers (IPP), are actively competing with one another for customers. The consumers can therefore establish various service contracts with any supplier in order to obtain the lowest rate and most desirable service. Bilateral contracts specifying the amount of power, the time and duration of the service and the associated rate and possible compensation are negotiated and agreed upon between the suppliers and consumers.

The next step of course is to deliver the power from the suppliers to their respective consumers. Power transmission under a deregulated environment is generally handled by an independent entity whose network is open to all users. Although there are different rules governing the role and responsibility of the transmission company [2], a basic requirement is to serve the needs of all users in the network as much as the system design and operating conditions permit. In the competitive electrical power market, large-scale customers can select Power Producers and Suppliers (PPSs), and decide the amount of electrical power to purchase. This paper develops optimal bilateral transactions/contracts for customers for minimum cost taking into line limits.

The line flow constraints are accounted for as a maiden attempt in determination of optimal bilateral transactions by expressing line flows in terms of active power contracts using line flow factors and are elegantly evaluated from existing load flow information. The proposed approach for optimal bilateral transactions with constraints on active power generations and line flows is tested on 4-bus sample system and 24-bus real life Indian system. The results obtained show great promise for practical application of the proposed algorithm on a real-time basis.

The paper is organized as follows: Section (2) focuses on bilateral transaction model; section (3) presents the development of line flow factors,section (4) presents the evaluation of line flow factors and section (5) emphasizes the application of linear programming to obtain the optimal bilateral transactions.

2. Bilateral Contract/Transaction Model

The electric power transactions are classified into pool transactions and bilateral contracts as well as security transactions. A certain transaction level of, for example, bilateral contracts may affect pool transactions by causing transmission congestion etc. Under the assumption that both the bilateral and market power transacted through pool (or power) market are coexisted and the generated power is supplied to customers through the transmission network management of power transmission company and the system operation of System Operator (SO). This paper proposes a method for determination of optimal bilateral contracts using linear programming with or without coexistence of pool market in a system for a given load condition.

Bilateral transactions are contracts between power sellers (say GENCOS) and buyers (say DISCOS or large customers). This type of power trading would therefore entail injection of bulk power into the transmission system by the power producer, and withdrawal of an equal amount of power, from the network by the customer. This scenario is simulated as the output of a generator, at a generator bus, and a corresponding load, at a load bus. Following assumptions are resorted to:

- there are multiple candidate power suppliers, being included in the generation set;
- there are multiple candidate power customers, being included in the load set;
- the reactive power of load is compensated locally, only real power transaction is supplied by the transaction;

The system model can be shown as in the following graph:

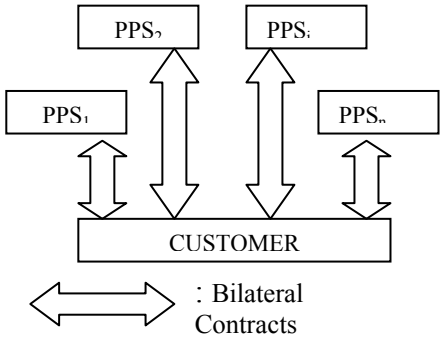

Figure 1: The model for the bilateral transaction

The goal of this paper is to find the optimal supplier customer combination for a particular transaction, such that the cost of transaction will have minimum value. The algorithm achieves these optimal bilateral transactions by considering all the transactions at a time. As the focus of the algorithm in this paper is on the determination of optimal bilateral power contracts, the actual flow path is of less importance. Therefore, a loss formula is preferred to the accumulation of all line losses.

This paper focuses on the power dispatch problem under open access and is confined to the dispatch of active power, keeping bus voltages and reactive power constant when appropriate, The distributed slack bus concept where the amount of real power imbalance in the system can be distributed among transactions based on participation factors [3] resembles actual operation of power system and is easy to include but this is not done here to keep the presentation simple.

The market design in the paper envisages participants who specify hourly quantities of demand, locations of generators supplying individual and group contracts, and willingness to pay for transmission services. At this stage the model does not take into account the co-existence of these bilateral and multilateral contracts with pool type dynamic supplies and demands based on bids and market clearing prices. This more complex issue of reconciling pool and bilateral contracts in an open access system is discussed in outline in [4-6]. Charging for Vars and other ancillary services is also an extension that stands outside the scope of this paper.

3. Development of line flow factors

To illustrate the proposed approach, a sample four-bus network shown in Fig.2 is considered. The system has two generators/suppliers, P_{g1} and P_{g2} at buses 1, 2 and two customers/loads, P_{d3} and P_{d4} at buses 3, 4 respectively. The system data is given in Appendix.

Let

P_{gi} : Supplier at bus i,

P_{dj} : Customer at bus j

P_{dj}^{gi} : Power contract of customer at bus j from supplier at bus i

P_{l-k} : Actual power flow in line l-k due to all customers and suppliers

P_{l-k}^{gi} : Power flow in line l-k due to supplier at bus i

P_{l-k}^{ij} : Power flow in line l-k with supplier at bus i and customer at bus j

L_{l-k}^{ij} : Line Flow Factor of a line l-k when the supplier at bus i and customer at bus j

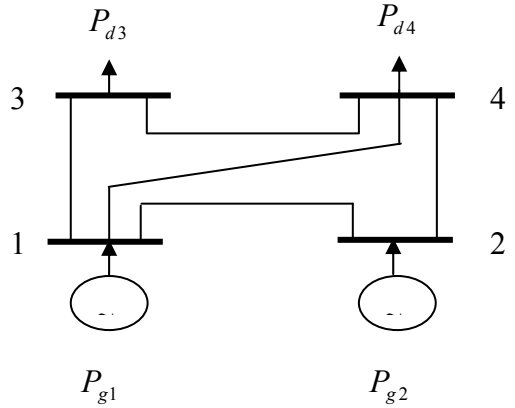

Figure2. Sample 4- bus system For the sample network, it is assumed that the loads at buses 4 and 5 are supplied by both the suppliers. Therefore, we can write

$$P_{d3} = P_{d3}^{g1} + P_{d3}^{g2}$$
$$P_{d4} = P_{d4}^{g1} + P_{d4}^{g2} \quad (1)$$

Where

P_{d3}^{g1} , P_{d4}^{g1} = Power contracts of customers at buses 3 and 4 from supplier at bus1 respectively.

P_{d3}^{g2} , P_{d4}^{g2} = Power contracts of customers at buses 3 and 4 from supplier at bus 2 respectively.

Now the actual power flow in the line1-2 can be expressed as

$$P_{1-2} = P_{1-2}^{g1} + P_{1-2}^{g2} \quad (2)$$

Where

P_{1-2}^{g1} , P_{1-2}^{g2} = Power flow in the line1-2 due to power contracts from supplier1 and supplier2 respectively.

The power flow P_{1-2}^{g1} can be expressed again as

$$P_{1-2}^{g1} = P_{1-2}^{13} + P_{1-2}^{14} \quad (3)$$

where

P_{1-2}^{13} , P_{1-2}^{14} = Power flow in the line 1-2 due to power contracts of customers at bus 3 and bus 4 from supplier at bus 1 respectively.

Re-writing the above equation as

$$P_{1-2}^{g1} = (P_{1-2}^{13} / P_{d3}^{g1}) P_{d3}^{g1} + (P_{1-2}^{14} / P_{d4}^{g1}) P_{d4}^{g1}$$
$$P_{1-2}^{g1} = (LF_{1-2}^{13}) P_{d3}^{g1} + (LF_{1-2}^{14}) P_{d4}^{g1} \quad (4a)$$

Where

LF_{1-2}^{13} = Line Flow Factor of line1-2 or fraction of power flow in line 1-2 when supplier1 contributes power P_{d3}^{g1} to customer at bus3.

LF_{1-2}^{14} = Line Flow Factor of line1-2 or fraction of power flow in line 1-2 when supplier1 contributes power P_{d4}^{g1} to customer4

Similarly the power flow P_{1-2}^{g2} can be expressed as

$$P_{1-2}^{g2} = (P_{1-2}^{24} / P_{d4}^{g2}) P_{d4}^{g2} + (P_{1-2}^{25} / P_{d5}^{g2}) P_{d5}^{g2}$$
$$P_{1-2}^{g2} = (L_{1-2}^{23}) P_{d3}^{g2} + (L_{1-2}^{24}) P_{d4}^{g2} + (L_{1-2}^{25}) P_{d5}^{g2} \quad (4b)$$

where

L_{1-2}^{24} = Line Flow Factor of line1-2 or fraction of power flow in line 1-2 when the supplier at bus 2 contributes power P_{d4}^{g2} to customer at bus 4.

L_{1-2}^{25} = Line Flow Factor of line1-2 or fraction of power flow in line 1-2 when the supplier at bus 2 contributes power P_{d5}^{g2} to customer at bus 5.

Similarly the power flow P_{1-2}^{g2} can be expressed as

$$P_{1-2}^{g2} = (P_{1-2}^{23} / P_{d3}^{g2}) P_{d3}^{g2} + (P_{1-2}^{24} / P_{d4}^{g2}) P_{d4}^{g2}$$
$$P_{1-2}^{g2} = (LF_{1-2}^{23}) P_{d3}^{g2} + (LF_{1-2}^{24}) P_{d4}^{g2} \quad (4b)$$

where

LF_{1-2}^{23} = Line Flow Factor of line1-2 or fraction of power flow in line1-2 when supplier2 contributes power P_{d3}^{g2} to customer3.

LF_{1-2}^{24} = Line Flow Factor of line1-2 or fraction of power flow in line 1-2 when the supplier2 contributes power P_{d4}^{g2} to customer 4.

From the equations 4(a) and 4(b)

$$P_{1-2} = P_{1-2}^{g1} + P_{1-2}^{g2}$$
$$= (LF_{1-2}^{13}) P_{d3}^{g1} + (LF_{1-2}^{14}) P_{d4}^{g1} + (LF_{1-2}^{23}) P_{d3}^{g2} + (LF_{1-2}^{24}) P_{d4}^{g2} \quad (5)$$

Similarly the actual power flow in the remaining lines have been expressed and represented in matrix form as

$$\begin{bmatrix} P_{1-2} \\ P_{1-3} \\ P_{1-4} \\ P_{2-4} \\ P_{3-4} \end{bmatrix} = \begin{bmatrix} L_{1-2}^{13} & L_{1-2}^{14} & L_{1-2}^{23} & L_{1-2}^{24} \\ L_{1-3}^{13} & L_{1-3}^{14} & L_{1-3}^{23} & L_{1-3}^{24} \\ L_{1-4}^{13} & L_{1-4}^{14} & L_{1-4}^{23} & L_{1-4}^{24} \\ L_{2-4}^{13} & L_{2-4}^{14} & L_{2-4}^{23} & L_{2-4}^{24} \\ L_{3-4}^{13} & L_{3-4}^{14} & L_{3-4}^{23} & L_{3-4}^{24} \end{bmatrix} \begin{bmatrix} P_{d3}^{g1} \\ P_{d4}^{g1} \\ P_{d3}^{g2} \\ P_{d4}^{g2} \end{bmatrix} \quad (6)$$

In general, the relationship between line flow and the transaction power at a bus via LFFs can be expressed as follows:

$$P_{l-k} = [L_{l-k}^{ij}][P_{dj}^{gi}] \quad (7)$$

4. Evaluation of line flow factors

The proposed approach for calculating Line Flow Factors starts from the power flows, as given by a load flow solution, with the assumption that the network consists of one supplier and one customer at a time, as illustrated in Figure .2. A dominion is obtained for each supplier and each customer and is a directed graph consisting of one supplier and one customer. The Line Flow Factors for the customer at a bus j and supplier at bus i are calculated by dividing the real power flow in a line P_{l-k} by the load P_{dj} at the bus j i.e., $L_{l-k}^{ij} = P_{l-k} / P_{dj}$ .The value of P_{dj} is any arbitrarily selected value and need not be the actual value. If the given system is a lossless system then $P_{dj} = P_{gi}$ otherwise $P_{gi} > P_{dj}$.

The coefficient L_{l-k}^{ij} , which is the sensitivity of the flow on the line l-k with respect to the supplier at bus -i and customer at bus -k, implies the fraction of power flow in the transmission line l-k when a unit power transaction is at bus-j.

For example, if we assume that the given system is lossless, and that 100MW is the only customer at bus3 (P_{d3}) and the supplier at bus1, then the line flows are obtained as given by a load flow solution and the line flow factor of line 1-2 for this dominion is

L_{1-2}^{13} =16.35/100.=0.1635.Here the line flow $P_{1-2}(=P_{l-k})$ in the line 1-2 is 16.35MW and $P_{d3}(=P_{dj})$ is 100MW. The subscript 1-2 indicates the line connected between buses 1 and 2 and the superscript 1-3 indicates that supplier is at bus 1 and customer is at bus 3. Similarly the line flow factors for other dominions are calculated and are given in Table I.

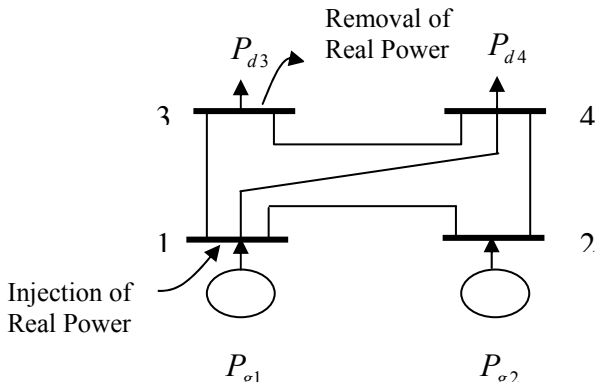

Figure 3: A domain

Table 1: Line Flow Factors of Each Dominion

Lines l-k	LUFs L_{l-k}^{ij}	Supplier at bus1 (i=1)		Supplier at bus2 (i=2)	
		Customer at bus		Customer at bus	
		3 (j=3)	4 (j=4)	3 (j=3)	4 (j=4)
1-2	L_{1-2}	0.1635	0.3000	-0.3052	-0.1687
1-3	L_{1-3}	0.6180	0.3007	0.3906	0.0725
1-4	L_{1-4}	0.2177	0.3993	-0.0854	0.0962
2-4	L_{2-4}	0.1635	0.3000	0.6949	0.8313
3-4	L_{3-4}	-0.3811	0.3007	-0.6093	0.0725

The negative sign indicates that, the real power flow is opposite to the convention used. Once the line flow factors are obtained, these factors remain constant, and can be used for calculating line flows without running load flows whenever load/generation at a bus is increased or decreased.

5. Optimal Bilateral Transactions/Contracts (OBT) Problem Formulation

The optimal bilateral transactions problem is considered as a general minimization problem with constraints, and can be written in the following way:

$$\underset{x}{Min}\ Z = f^T x \tag{8}$$

Such that $Ax \le b$

$$A_{eq}\, x \le b_{eq}$$

$$lb \le x \le ub \tag{9}$$

where f, x, b, b_{eq}, lb, and ub are vectors and A and A_{eq} are matrices.

For the four- bus test system the cost coefficients vector $\underline{f}$ and $\underline{x}$ is given by:

$$\underline{f} = \begin{bmatrix} 15 \\ 15 \\ 17 \\ 17 \end{bmatrix}, \qquad \underline{x} = \begin{bmatrix} P_{d3}^{g1} \\ P_{d4}^{g1} \\ P_{d3}^{g2} \\ P_{d4}^{g2} \end{bmatrix}$$

The elements of the vector $\underline{f}$ represents marginal cost coefficients, and the elements of the vector $\underline{x}$ represents the bilateral contracts between each supplier and customer.

The objective function of our linear program is the sum of marginal cost of real power suppliers at buses 1, and 2. We denote the objective function of the linear program as Z:

$$Z = 15P_{d3}^{g1} + 15_{d4}^{g1} + 17p_{d3}^{g2} + 17P_{d4}^{g2} \tag{10}$$

Equality Constraints:

Denoting the total load to be supplied as LOAD, the original equality constraint is that the sum of the bilateral power contracts must equal the total load to be supplied, i.e.,

$$P_{d3}^{g1} + P_{d4}^{g1} + P_{d3}^{g2} + P_{d4}^{g2} = LOAD = 500\text{MW} \tag{11}$$

Also the power supplied to the customer from a supplier should be equal to the load power i.e.

$$P_{d3}^{g1} + P_{d3}^{g2} = P_{d3} = 300\text{MW}, \tag{12}$$

$$P_{d4}^{g1} + P_{d4}^{g2} = P_{d4} = 200\text{MW} \tag{13}$$

Inequality Constraints:

The original inequality constraints are

$$100 \le P_{g1} \le 500,\ 50 \le P_{g2} \le 150,$$

However, in order to utilize 4 variables, the above constraints on the two-generation levels are converted to constraints on the 4 new variables.

$$A=\begin{bmatrix} LF_{1-2}^{13} & LF_{1-2}^{14} & LF_{1-2}^{23} & LF_{1-2}^{24} \\ LF_{1-3}^{13} & LF_{1-3}^{14} & LF_{1-3}^{23} & LF_{1-3}^{24} \\ LF_{1-4}^{13} & LF_{1-4}^{14} & LF_{1-4}^{23} & LF_{1-4}^{24} \\ LF_{2-4}^{13} & LF_{2-4}^{14} & LF_{2-4}^{23} & LF_{2-4}^{24} \\ LF_{3-4}^{13} & LF_{3-4}^{14} & LF_{3-4}^{23} & LF_{3-4}^{24} \end{bmatrix}, \; b=\begin{bmatrix} P_{1-2} \\ P_{1-3} \\ P_{1-4} \\ P_{2-4} \\ P_{3-4} \end{bmatrix}$$

The equations (11)-(13) form the additional constraints represented in the matrix A_{eq}

Lower Bounds: It should be recognized that all of the new variables must be non-negative. This comes from the fact that we cannot have a negative amount of generation increment. But we can have any amount of generation increment between zero and the upper bound. So the lower bound on all 4 variables is zero.

Upper bounds: The upper bounds on the variables can be taken as the maximum load at that particular load bus. For the four-bus system it is taken as 200 MW.

The results of the linear programming are given by

$$\begin{bmatrix} P_{d3}^{g1} \\ P_{d4}^{g1} \\ P_{d3}^{g2} \\ P_{d4}^{g2} \end{bmatrix}=\begin{bmatrix} 200.0 \\ 200.0 \\ 100.0 \\ 0.0 \end{bmatrix}, \; f=7700$$

The summary of the results obtained using the LFF method are given in the Tables 6.7.and 6.8.

Table 2: Real Power Transactions & Cost

Real Power Contracts	Transaction (MW)	Cost of Transaction ($/MWhr)
P_{d3}^{g1} (MW)	200	3000
P_{d3}^{g2} (MW)	100	1700
P_{d4}^{g1} (MW)	200	3000
P_{d4}^{g2} (MW)	0	0
Total Cost ($/MWhr)		7700

Table 3: Real Power Generation Levels & Cost

	Generation levels (MW)	Cost of Generation ($/MWhr)
G1 (MW)	400	6000
G2 (MW)	100	1700
Total Cost ($MWhr)		7700

6. Real-Life Indian System studies

The proposed approach is applied for a practical Indian system of 24-bus equivalent EHV power system and is shown in Fig.4. The system has 4 generator buses and 20 other buses. The load is represented at 220 kV sides of 400 kV / 220 kV nodes at 8 numbers of buses. The system peak load is 2620MW; 980MVAR.It is assumed that all the generators are having thermal units. .

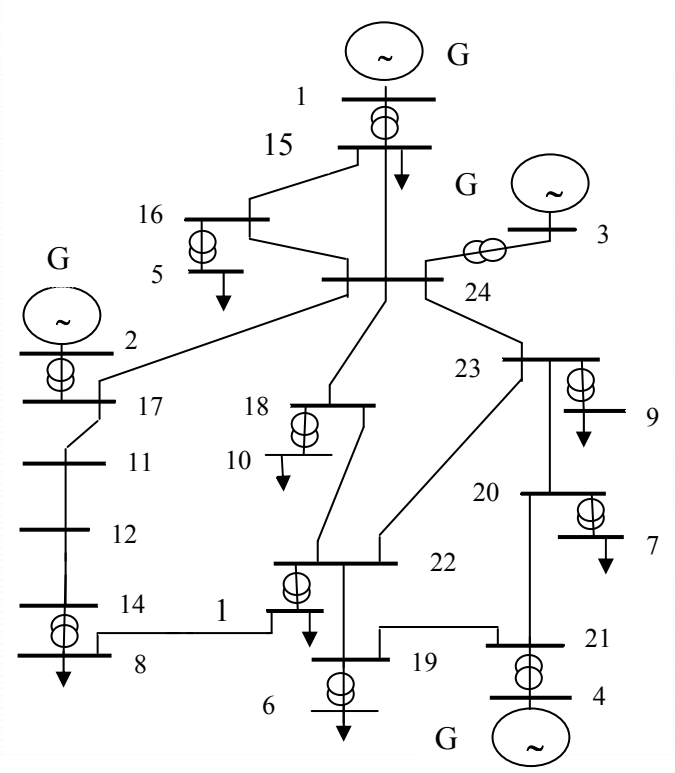

Figure 4 Real-Life 24-bus Equivalent EHV system

Table 4: Generating unit's data

Generator Bus No.	No. of Units	$P_{g\max}$	$P_{g\min}$
1	10	200	40
2	2	200	40
3	4	200	40
4	4	200	40

Table 4: Cost characteristics of generating units

Generator Bus No.	a -MW^2	b -MW	c
1	0.8	400	8000
2	0.8	400	8000
3	0.8	400	8000
4	0.8	400	8000

7. Conclusions

In this paper, a new set of line flow factors are developed. In the developed framework, one can directly evaluate the flow on a line and optimal bilateral real power contracts. The method is conceptually simple. The linear programming concept is used to determine the optimal bilateral contracts, which minimizes the marginal

cost. For the sample 4-bus network and real –life 24-bus Indian systems, the method has been demonstrated with the encouraging results.

Table 6: Real Power contracts

Load Bus No.	Real power contracts from each load each bus (MW)			
	G1	G2	G3	G4
5	187.2724	46.8410	163.0704	36.5883
6	29.1313	31.7595	55.2295	184.8875
7	42.3607	34.1981	80.3218	186.2895
8	28.6762	52.0084	54.3807	66.9826
9	24.9035	18.2312	47.2200	39.6016
10	13.2460	10.4365	25.1163	16.5207
13	73.0557	106.3393	138.5519	180.5350
15	531.3374	31.6870	110.3275	24.7549

Table 7: Generation levels (MW) and cost (Rs./hr)

Generator	Method	Cost of generation Rs./hr
G1	929.95	521160
G2	331.53	044280
G3	674.23	115820
G4	736.16	167130
P. Loss (MW)	51.87	Total Cost: 848390

8. References

[1] C.W.Yu and A.K.David," Pricing transmission services in the context of industry deregulation", IEEE Trans. on PS, Vol.12, No.1, Feb 1997, pp52-60.

[2] HB Rudnic, R Palma and J E Fenandez," Marginal pricing and supplement cost allocation in transmission open access", IEEE Trans. on power Systems, Vol.10, No.2, pp 1125-1142, May 1995.

[3] J. Pan, Y Teklu, and S.Rahman, "Review of usage-based transmission cost allocation", IEEE Trans. On PS, Vol.15, No.4, November 2000, pp1218-1224.

[4] F.Galiana, and M Illic," A mathematical frame work for the analysis and management of power transactions under open access", in IEEE Winter Power meeting, Feb.1998.

[5] W.Y.Ng," Generalized Generation Distribution Factors for Power System Security Evaluation", IEEE Trans. On PAS, Vol.PAS-100, No.3, March 1981, pp1001-1005.

[6] J.Bialek," Topological generation and Load distribution factors for Supplement Charge Allocation in Transmission Open Access", IEEE Trans. on power Systems, Vol.12, No.3, pp 1185-1193, April 1997.

Appendix

Table A: The four- bus system data

Transmission line data				Generation and Load data		
From Bus	To Bus	R (Ω)	X (Ω)	Bus No.	Pg (MW)	Pd (MW)
1	2	12.75	97			
1	3	6	69.5	1	400	0
1	4	11.7	96	2	100	0
2	4	3.5	30.8	3	0	300
3	4	5.75	58	4	0	200

K.Vaisakh received the BE degree in Electrical Engg. from Osmania University, Hyderabad in 1994, M.Tech degree in Electrical Power Systems from JNT University Hyderabad in 1999 and Ph.D degree from Indian Institute of Science, Bangalore in 2005. He is currently Professor in Department of Electrical Engineering, A.U. College of Engg., A.U., Visakhapatnam INDIA. His research interests include computer aided power system analysis, reactive power optimization, voltage stability, and deregulation.

G. V. Siva Krishna Rao received the B.Tech degree in Electrical & Electronics Engineering and M Tech degree in power system operation and control both from S V University, Tirupati in 1992 and 1996 respectively. He is doing PhD degree in the Department of Electrical Engineering, Andhra University, Visakhapatnam INDIA where he is currently Associate Professor. His research interests include deregulation and computer aided power system analysis.

www.icgst.com

Employing Particle Swarm Optimizer and Genetic Algorithms for Optimal Tuning of PID Controllers: A Comparative Study

Mohammed El-Said El-Telbany
Computers & Systems Department, Electronics Research Institute
El-Tahrir St. Dokki, Giza, Egypt
telbany@eri.sci.eg
http://www.amman.edu/members/engineering/telbani.htm

Abstract

The proportional-integral-derivative (PID) controllers were the most popular controllers of this century because of their remarkable effectiveness, simplicity of implementation and broad applicability. However, PID controllers are poorly tuned in practice with most of the tuning done manually which is difficult and time consuming. The computational intelligence has purposed genetic algorithms (GA) and particle swarm optimization (PSO) as opened paths to a new generation of advanced process control. These advanced techniques to design industrial control systems are, in general, dependent on achieving *optimum performance* with the controller when facing with various types of disturbance that are unknown in most practical applications. This paper presents a comparison study of using two algorithms for the tuning of PID-controllers for processes which represents a subsystem of complex industrial processes, known to be *non-linear* and *time variant*. Simulation results showed that the PID control tuned by PSO provides an adequate closed loop dynamic for the Ball and Hoop system experiment in wide range operations.

Keywords: *Particle swarm optimisation; genetic algorithms, intelligent control; PID control*

1. Introduction

Currently, the most of industrial processes are controlled by the well-established PID control. The standard PID control configuration is as shown in Figure 1. These parameters K_p, K_i, K_d are chosen to meet prescribed performance criteria, classically specified in terms of rise and settling times, overshoot, and steady state error, following a step change in the demand signal. The popularity of PID control can be attributed to its simplicity (in terms of design and from the point of view of parameter tuning) and to its good performance in a wide range of operating conditions. Moreover, the controllers designed with the aid of modern control techniques are usually of high order, difficult to implement, and virtually impossible to re-tune on line. Also, the design procedures of PID controllers are simple, although, the tuning parameters are the most challenging ones in a PID controller, as optimal tuning parameters are difficult to find. Therefore, researchers introduced advanced controllers such as PID auto-tuning or self-tuning, model-based adaptive control, model predictive control, fuzzy control, artificial neural networks, optimal control, expert control, robust control, etc. Although fuzzy control has great potential for solving complex control problems, it has, at least, these limitations

1. Its design procedure is complicated and requires a great deal of specialty.
2. As a rule-based system, criteria for control system stability are complicated and usually conservative. A bad-rule or an out-dated rule may cause the fuzzy controlled system to become unstable.
3. If the process changes, it is necessary to modify the rules, which is time-consuming.

The other methods including optimal control, expert control, neural networks, etc., have been developed to address the issues of complexity. However, most require some kind of process model and high-level expertise. It is difficult to develop a general-propose, user-friendly, smart control system based on these control methods.

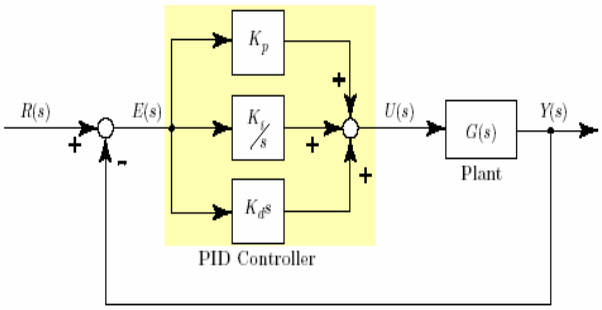

Figure 1: PID Controlled System.

There are a variety of PID controllers tuning methods have been developed such as Ziegler-Nichols rules, Cohen-Coon rule and so on [1, 2, 11]. These methods are applied directly since they provide simple tuning rules to determine the PID parameters. However, since they rely

on a minimum amount of dynamic information by making a certain assumption about nature of the controlled process, such as linearity, weak interactions within the process, absence of noise, etc. The realized closed loop response is less than optimum since the real world processes are *non-linear* and *very complex*. Recently, the computational intelligence has purposed *genetic algorithms* (GA) [9, 18] and *particle swarm optimization* (PSO) [15, 16] as opened paths to a new generation of advanced process control. These advanced techniques to design industrial control systems are, in general, dependent on achieving *optimum performance* with the controller when facing with various types of disturbance that are unknown in most practical applications. Usually such an optimum system performance is defined by a continuous function which is obtained by minimizing the sum of the square of the error between the actual and desired output. The GA and PSO are *non-gradient* based optimization and search algorithm and belongs to probabilistic search algorithms, which have attracted much attention from the research community. These algorithms generally mimic some natural phenomena, for example GA model the evolution of a species, based on Darwin's principle of survival of the fittest and *competition* to produce better adapted generations in their problem solution space while the PSO in contrast relies on *cooperation* rather than *competition* and good solutions in the problem set are shared with their less-fit brethren so that the entire population improves and poorly performing members are not killed off as in GA. Although these probabilistic search algorithms generally require many more function evaluations to find an optimal solution, as compared to *gradient-based* algorithms (i.e., simple gradient descent, conjugate gradient descent, etc.), they are promising approaches due to their effectiveness in searching very large spaces and the ability to perform global search for best forecasting model. Moreover, they are generally easy to program, can efficiently make use of large numbers of processors, do not require continuity in the problem definition, and generally are better suited for finding a global, or near global, solution. Genetic algorithms have been extensively applied to the *off-line/on-line* design of controllers. GA was first investigated as an alternative means of tuning PID controllers. Oliveira *et al.* [19] used a standard GA to determine initial estimates for the values of PID parameters. Genetic algorithms are tested for PID controller for nonlinear process and showed robustness and efficiency [22, 12, 10]. Lennon and Passino [17] developed a more complex optimization known as a general genetic adaptive controller (GGAC). Other several applications of GA appeared in [4, 7, 21]. The PSO have also been used for tuning PID controller [8, 20; 6, 23] and have proved successful results. The primary contribution of this paper is to evaluate the two algorithms in the tuning of PID-controllers in the ball and hoop system which represents a system of complex industrial processes, known to be *non-linear* and *time variant*. Such comparative analysis is very important for identifying both the advantages and their possible disadvantages. The rest of the paper is organized in the following manner. In Section 2, a problem formulation is presented. In sections 3 and 4, the particle swarm optimization algorithm and genetic algorithms which will be applied in this paper are described briefly. In section 5, we provide an overview of control problem which we will be used in this paper. Detailed experiments results are provided in section 6. Finally, Section 7 concludes the paper.

2. Problem Formulation

By formulating the PID controller design problem as an optimization and search problem, we frequently have a complicated function to be optimized. This function can be represented as follows:

$$f : S \to R \tag{1}$$

Where S is the set of solutions and best choices are that for the function f is optimal. In the context of controller, *a candidate system* can be represented by a uniform parametric vector given by

$$S_i = \{g_1, g_2, \ldots, g_n\} \in \Re^n \tag{2}$$

Where i stands for the i^{th} possible candidate solution, n the number of parameters required by the solution, $g_j \in \Re$ the j^{th} parameter of the i^{th} candidate solution with $j \in \{1, \ldots, n\}$, and $\Re^n$ the n-dimensional real Euclidean space. We have a complicated objective function $Q(S)$ needs to be optimized. Where $Q(S)$ represents the quality measurement for a solution S_i given $\forall S_i \; Q(S_i) > 0$. The problem is to find the best solution (i.e., controller) $\check{S}$ such that:

$$Q(\tilde{S}) = \underset{S}{Max}\, Q(S) \tag{3}$$

3. Particle Swarm Optimization

The particle swarm optimization algorithms are based on two socio-metric principles. Particles fly through the solution space and are influenced by both the best particle in the particle population and the best solution that a current particle has discovered so far. The best particle in the population is typically denoted by (gobal best), while the best position that has been visited by the current particle is donated by (local best). The (global best) individual conceptually connects all members of the population to one another. That is, each particle is influenced by the very best performance of any member in the entire population. The (local best) individual is conceptually seen as the ability for particles to remember past personal success. The particle swarm optimisation makes use of a velocity vector to update the current position of each particle in the swarm. The position of each particle is updated based on the social behaviour that a population of individuals adapts to its environment by returning to promising regions that were previously discovered [14]. Let the i-th particle of the swarm is represented by the D–dimensional vector $X_i = (x_{i1}, x_{i2}, \ldots, x_{iD})$ and the best particle in the swarm, i.e. the particle with the smallest function value,


is denoted by the index *g*. The best previous position (the position giving the best function value) of the *i*-th particle is recorded and represented as $P_i = (p_{i1}, p_{i2}, ..., p_{iD})$, and the position change (velocity) of the *i*-th particle is $V_i = (v_{i1}, v_{i2}, ..., v_{iD})$. The particles are manipulated according to the equations

$$v_{id} = w \cdot v_{id} + c_1 \cdot r_1 \cdot (p_{id} - x_{id}) + c_2 \cdot r_2 \cdot (p_{gd} - x_{id}) \quad (4)$$

$$x_{id} = x_{id} + v_{id} \quad (5)$$

where $d = 1, 2, \ldots, D$; $i = 1, 2, \ldots, N$ and N is the size of population; w is the inertia weight; c_1 and c_2 are two positive constants; r_1 and r_2 are two random values in the range [0, 1]. The first equation is used to calculate *i*-th particle's new velocity by taking into consideration three terms: the particle's previous velocity, the distance between the particle's best previous and current position, and, finally, the distance between swarm's best experience (the position of the best particle in the swarm) and *i*-the particle's current position. Then, following the second equation, the *i*-the particle flies toward a new position. In general, the performance of each particle is measured according to a predefined fitness function, which is problem–dependent. The role of the inertia weight w is considered very important in PSO convergence behaviour. The inertia weight is employed to control the impact of the previous history of velocities on the current velocity. In this way, the parameter w regulates the trade–off between the global (wide–ranging) and local (nearby) exploration abilities of the swarm. A large inertia weight facilitates global exploration (searching new areas); while a small one tends to facilitate local exploration, i.e. fine–tuning the current search area. A suitable value for the inertia weight w usually provides balance between global and local exploration abilities and consequently a reduction on the number of iterations required to locate the optimum solution. A general rule of thumb suggests that it is better to initially set the inertia to a large value, in order to make better global exploration of the search space, and gradually decrease it to get more refined solutions, thus a time decreasing inertia weight value is used. The main steps of the PSO algorithm are shown in Table 1, where there are three main steps 1) initialize a population of particles (position and velocities); 2) updating velocities; 3) updating positions.

Table 4. The main steps for PSO algorithm.

```
Function PSO(Particles, Fitness-FN) returns a controller
inputs: Particles, a set of PID-controllers
Fitness-Fn, a function that controller response according Eq. (7).
repeat
Loop for i from I to Size (Particles) do
        Find the personal best & global best position of each Particle.
        Update each Particle according to Eq. (4) & Eq. (5).
 until some controller is fit enough, or enough time has elapsed
return the best controller in Particles, according to Fitness-Fn
```

4. Genetic Algorithm

The GA is an optimization routine based on the principles of Darwinian Theory and natural genetics. It has primarily been utilized as an *off-line* technique for performing a directed search for the optimal solution to a problem. The GA performs a parallel, directed, random search for the fittest element of a population within a search space. The population simply consists of strings of numbers, called chromosomes that hold possible solutions of a problem. The members of a population are manipulated cyclically through three primary genetic operators called *selection*, *crossover*, mutation, and *replacement,* to produce a new generation (a new population) that tends to have higher overall fitness evaluation. By creating successive generations which continue to evolve, the GA will tend to search for a global optimal solution. The key to the search is the fitness evaluation. The fitness of each of the members of the population is calculated using a fitness function that characterizes how well each particular member solves the given problem. Parents for the next generation are selected based on the fitness value of the strings. That is, strings that have a higher fitness value are more likely to be selected as parents, and, thus, are more likely to survive to the next generation. The main steps of the GA algorithm are shown in Table 2.

Table 4. The main steps for GA algorithm.

```
Function GA(Population, Fitness-FN) returns a controller
inputs: Population, a set of PID-controllers
Fitness-Fn, a function that controller response according Eq. (7).
repeat
New-Population <— empty set
Loop for i from I to Size (Population) do
        Father  <— Random-Selection (Population, Fitness-Fn)
        Mother <— Random-Selection (Population, Fitness-Fn)
        Child   <— Crossover (Father, Mother)
if (small random probability) then
         Child <— Mutate (child)
add Child to New-Population
Population <— New-Population
until some controller is fit enough, or enough time has elapsed
return the best controller in Population, according to Fitness-Fn
```

5. Plant System

The *Ball and Hoop* system [3] illustrates the dynamics of a steel ball that is free to roll on the inside of a rotating circular hoop. There is a groove on the inside edge of the hoop so that a steel ball can roll freely inside the hoop. This introduces the complexity of the rolling radius of the ball being different to the actual radius of the ball as illustrated in Figure 2, where the angle, θ, is the hoop angular position. The position of the ball is given by:

1. y, the position of the ball on the hoop periphery with respect to a datum point.
2. ψ, the slosh angle which measures the deviation of the ball from its rest position.


A fourth order system was selected as the Ball and Hoop system is of order four with the following transfer function [10].

$$G(s)=\frac{1}{s^4+6\cdot s^3+11\cdot s^2+6\cdot s} \quad (6)$$

The ball and hoop apparatus is difficult to control optimally using a PID controller because the system parameters are constantly changing. The Ziegler-Nichols tuning method [24] using root-locus to evaluate the PID gains for the system, and the resulted gains are: $K_p=6$, $K_i=1.91$, and $K_d=4.74$.

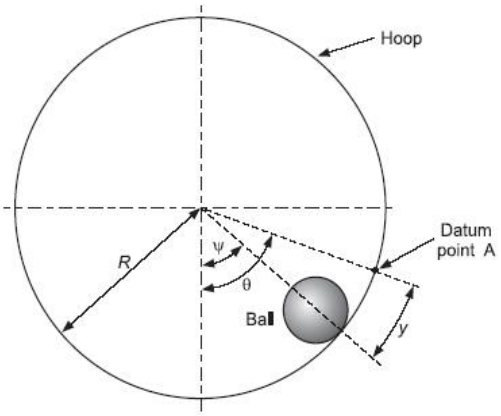

Figure 2: The Ball and Hoop System

6. PID Process Control Design

The PID controller will be tuned *offline* using both of GA and PSO as shown in Figure 3.

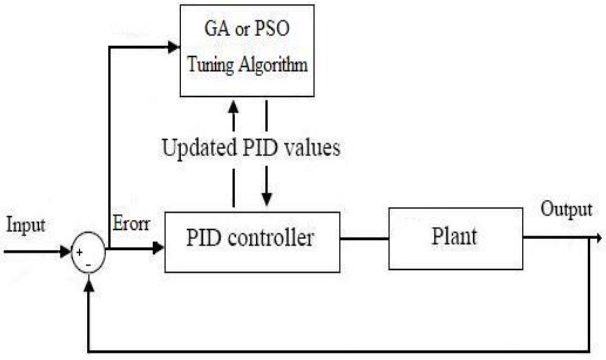

Figure 3: The structure of GA or PSO of PID tuning system.

Where the performance index ISE is used to estimates the parameters of PID controller is given by:

$$I_{ISE}=\int_0^T e^2(t)dt \quad (7)$$

The tuning of PSO-based PID controller' results will be compared to those obtained from the GA and traditional techniques. The PSO and GA tuning algorithms are conducted several pre-experiments to determine the parameters setting per algorithm that yields the best performance. For PSO, all swarm particles start at a random position in the range [-100.0, 100.0] for each dimension. The velocity of each particle is randomized to a small value to provide initial random impetus to the swarm. The swarm size was limited to 20 particles. The must important factor is *maximum velocity* parameter which affect the convergence speed of the algorithm is set to 100.0. The c_1 and c_2 are 2.0 and 2.0 respectively. For GA, the GAOT is used [13] with population size of 50, the search range [-100.0, 100.0] and with other default parameters. The two algorithms are runs of 100 iterations. Figure 3 presents the step response of different PID controller using ISE performance index. As shown in Figure 4, the best results when used in conjunction with a particle swarm optimization. Table 3, describes the steady state characteristics of each of the controlled systems.

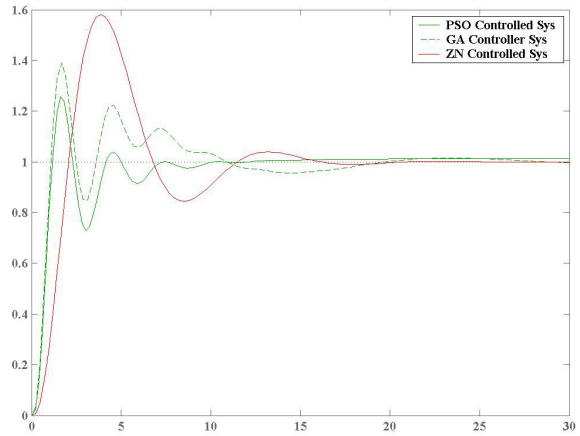

Figure 4: The step response of different tuning algorithms.

Table 1: Comparisons of Steady State Responses

	PSO	GA	ZN
Rise Time	**1.2000**	**1.2000**	**2.1000**
% Overshoot	**24.345**	**28.5908**	**58.1561**
Settling Time	**10.0**	**20.4000**	**19.8000**

The PSO-tuned PID controllers outperform the GA-tuned and Ziegler-Nichols tuned controller in terms of settling time and overshoot. However the rise time of both PSO and GA are equal. Analyzing the transfer function of the ball and hoop system is stable as it has three poles located on the left hand side of the s-plane and one critically stable pole located at the origin. The presence of a critically stable pole will result in a more oscillatory open loop response. From the transfer function, it is clear that there will be an open-loop steady state gain of 1.84. This gain is shown in Figure 5 when the open loop response of the system is plotted against a PID controlled system using the PSO tuned controller which gave the best performance.

Figure 6 compares the performance of the Ziegler-Nichols tuned designed controller with the PID tuned controller by the PSO and GA. The ISE performance criteria were improved by 35% for the GA and 52% for the PSO.

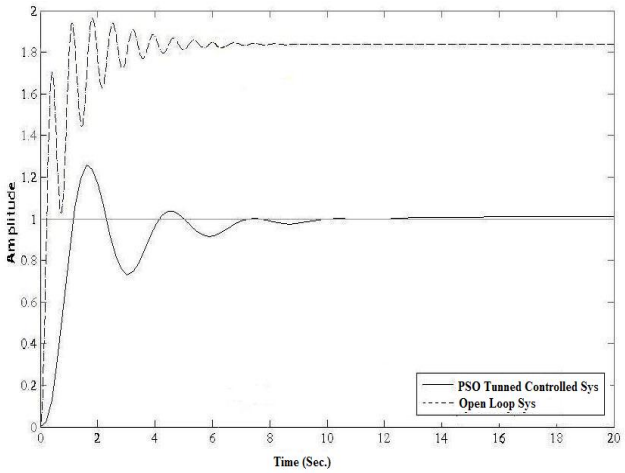

Figure 5: The open and PID closed loop response of the Ball and Hoop system tuned by PSO.

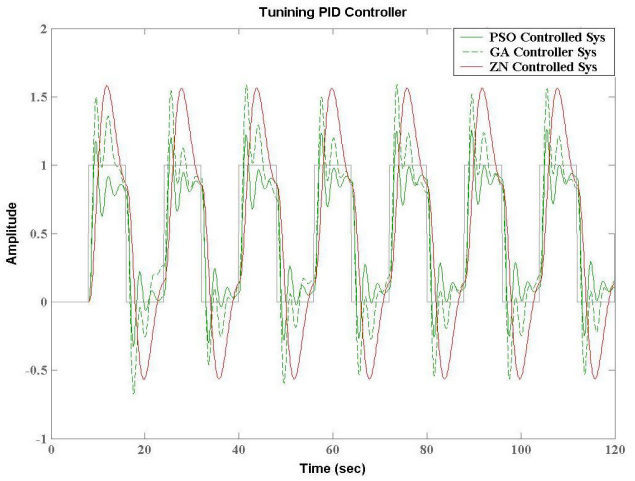

Figure 6: The Ball and Hoop System

7. Control System Stability Criterion

In control systems, which is a linear time-invariant system its stability is determined by its characteristic polynomial and its corresponding roots, which are eigenvalues or poles. A linear time-invariant system is asymptotically stable if and only if all the roots of its characteristic polynomial are in the open left half of the *s*-plane. The potential for closed-loop pole location is determined by the flexibility available to compute acceptable three-term controller coefficients to achieve arbitrarily chosen stable closed-loop pole positions. For a discrete system the poles of the overall closed loop equation must lie with the unit circle. Any set of PID parameters that gave poles that were outside the unit circle had there weighted error value set really high so that they would not be chosen for selection in the GA or PSO learning process. As the poles obtained for the overall closed loop transfer function for the different sets of PID parameters can be real and imaginary the absolute value of each pole is taken. If this absolute value is greater than one then the pole is outside the unit circle hence the overall system is unstable. When the system is unstable for a set of PID values the fitness evaluation gives this set of PID parameters a low fitness value.

8. Discussion and Conclusions

In this work, we have presented a comparison study of using PSO and GA algorithms for the tuning of PID-controllers for processes which represents a subsystem of complex industrial processes, known to be *non-linear* and *time variant*. Simulation results showed that the PID control tuned by PSO provides an adequate closed loop dynamic for the Ball and Hoop system experiment in wide range operations. This work can be extended by tuning the PID controller *online* so that the controller adaptively changing its setpoint based on the current situation.

References

[1]. Astrom K., and T. Hagglund T., "The future of PID control", *Control Engineering Practice*, 9, pp-1163-1175, 2001.

[2]. Astrom, K., and Hagglund, T., *PID controllers: Theory, design, and tuning*. 2nd Edition, Instrument Society of America, 1995.

[3]. Ball and Hoop White Paper, URL: http://www.control-systemsprinciples.co.uk

[4]. Cipperfield A. Flemming P., and Fonscea C., "Genetic Algorithms for Control System Engineering", in Proceedings Adaptive Computing in Engineering Design Control, pp- 128-133, 1994.

[5]. Conradie A., Miikkulainen R., and Aldrich C., Adaptive Control Utilizing Neural Swarming. In Proceedings of the Genetic and Evolutionary Computation Conferences, USA, 2002.

[6]. Easter S., Subramanian S., and Solomon S., (2003). Novel technique for PID tuning by particle swarm optimization, in *Proeedings 7th Annu. Swarm Users/Researchers Conf.*

[7]. Flemming P., and Purshouse R., Evolutionary Algorithms in Control System Engineering: A Survey, Control Engineering Practice, Vol. 10. pp. 1223-1241, 2002.

[8]. Gaing, Z.-L., "A particle swarm optimization approach for optimum design of PID controller in AVR system," *IEEE Transactions on Energy Conversion*, vol. 19, no. 2, pp. 384-391, 2004.

[9]. Goldberg D., Genetic Algorithms in Search, optimization, and Machine Learning. Addison-Wesley, 1989.

[10]. Griffin I., "*On-line PID Controller Tuning using Genetic Algorithms",* MSc. thesis School of Electronic Engineering, Dublin City University, 2003.

[11]. Halevi, Y., Palmor, Z.J., and Efrati, T., Automatic tuning of decentralized PID controllers for MIMO processes. *Journal of Process Control*, 7, 2, 119–128, 1997.

[12]. Herrero J., Blasco X., M. Martinez, J.V. Salcedo, "*Optimal PID Tuning with Genetic Algorithms For Non Linear Process Models*" 15th Ifac, Span, 2002.

[13]. Houck, C., Joines J., and Kay M., A Genetic Algorithm for Function Optimization: A MATLAB Implementation. ACM Transactions on Mathematical Software, 1996.

[14]. Kennedy J., and Spears M., "Matching Algorithms to Problems: An Experimental Test of the Particle

Swarm and Some Genetic Algorithms on the Multimodal Problem generator", Proceedings IEEE International Conference of Evolutionary Computation, 1998.
[15]. Kennedy, J. and Eberhart, C., Particle Swarm Optimization. Proceedings of the 1995 IEEE International Conference on Neural Networks, Australia, pp. 1942-1948, 1995.
[16]. Kennedy, J. and Eberhart, C., Swarm Intelligence Morgan Kaufman, 2001.
[17]. Lennon W., and Passino K.,. Genetic Adaptive Identifcation and Control.", Engineering Application of Artificail Intelligence, Vol. 12 pp. 185-200, 1999.
[18]. Michalewicz Z. and Dasgupta D., Evolutionary Algorithms in Engineering Applications. Springer-Verlag, 1997.
[19]. Oliveira, P. M., Cunha, J. B., and Coelho, J. o. P. Design of PID controllers using the particle swarm algorithm. Twenty-First IASTED International Conference: Modelling, Identification, and Control (MIC 2002), Innsbruck, Austria. 2002.,
[20]. Oliveira, P., Sequeira, J., and Sentieiro, J., *Selection of Controller Parameters using Genetic Algorithms*, Engineering Systems with Intelligence. Concepts, Tools, and Applications, Kluwer Academic Publishers, Dordrecht, Netherlands, pp431-438, 1991.
[21]. Wang Q., Spronck P., and Tracht R., "An Overview of Genetic Algorithms Applied To Control Engineering Problems", in Proceedings of the 2nd International Conference on Machine Learning and Cybernetics, 2003.
[22]. Wang, P., and Kwok, D.P., Optimal Design of PID process controllers based on genetic algorithms. *Control Engineering Practice*, 2, 4, 641–648, 1994.
[23]. Zheng, Y., Ma, L., Zhang, L., and Qian, J. Robust PID Controller Design using Particle Swarm Optimizer. Proceedings of IEEE International Symposium on Intelligence Control 2003, pp. 974-979, 2003
[24]. Ziegler, J., and Nichols, N., "Optimum settings for automatic controllers", *Transations of ASME*, 64, pp.759-768, 1942.

Mohammed El-Telbany was born in Dammitta, Egypt, in 1968. He received the B.S. degree in computer engineering and science from the University of Minufia in 1991 and the M.Sc. and PhD degree in Computer Engineering, from Electronics and Communication Department, Cairo University, Faculty of Engineering, in 1997 and 2003 respectively. He has been a Researcher at the Electronics Research Institute since 1993 till now. He has also worked at the ESA at European Space Research Institute (ESRIN), 1998-1999, Frascati, Italy, at the Faculty of Engineering, Al-Ahliyya Amman University, Jordan, 2004-2005 and College of Computer Sciences, King Khalid University, KSA, 2005-2008. He has been involved in the field of autonomous mobile robots and machine leaning. His pervious research includes work on Evolutionary Computation and Forecasting. Current research includes work in robotics and reinforcement learning, and swarm intelligence.

www.icgst.com

Self Tuning Adaptive Pole-Shift STATCOM Control for Single and Multi Machine Power Systems

A.H.M.A.Rahim[1] and M. Baber Abbas[2]
(1) Department of Electrical Engineering, King Fahd University of Petroleum & Minerals, Dhahran, Saudi Arabia
http://www.kfupm.edu.sa, ahrahim@kfupm.edu.sa
(2) Transmission Asset Planning Department, Saudi Electricity Company, Dammam, Saudi Arabia.
http://www.se.com.sa, mbabbas@se.com.sa

ABSTRACT
Synchronous static compensator (STATCOM) can be used to improve the dynamic performance of a power system. This article presents an online adaptive pole-shift method for stabilization of a single machine system which is then extended to a multi-machine system. An adaptive linear plant parameter model is used to derive the pole-shift control strategy. The controller performance has been tested for various disturbances. Responses for the single machine system were also compared with optimized PI control and robustness of the proposed adaptive algorithms was tested. From a number of simulation studies on the single machine as well as the multi-machine power system it was observed that the adaptive algorithm converges very quickly and also provides robust damping profiles to the under damped power system.

Keywords
Power system stabilizing control, STATCOM, on-line identification, adaptive control, pole - shifting control

NOMENCLATURE

δ	Generator rotor angle
ω	Rotor speed
ω_o	Base (synchronous) speed
P_m	Mechanical power input
P_e	Electrical power output
M	Inertia constant
D	Damping coefficient of generator
e_q'	Quadrature (q) axis internal voltage
T_{do}'	Open circuit field time constant
E_{fd}	Field voltage
x_d, x_d'	Synchronous, transient direct (d) axis reactance
I_d	d-component of armature current
K_A, T_A	Exciter gain, time constant
V_t	Generator terminal voltage
V_L	STATCOM bus voltage
V_b	Network bus voltage
E_{fdo}, V_{to}	Nominal field, terminal voltage
V_{dc},I_{dc}	dc capacitor voltage, current of STATCOM
C_{dc}	Capacitance of dc capacitor
I_{Lo}	Steady ac STATCOM current
m, ψ	Modulation index, phase of STATCOM voltage
θ	Parameter vector
φ	Measurement Vector
λ	Forgetting Factor Bus admittance matrix of system excluding generator and STATCOM

1. Introduction

The static synchronous compensator (STATCOM) is a power electronic based synchronous voltage generator that generates a three-phase voltage from a DC capacitor. By controlling the magnitude of the STATCOM voltage, the reactive power exchange between the STATCOM and the transmission line and hence the amount of shunt compensation in the power system can be controlled [1]. In addition to reactive power exchange, properly controlled STATCOM can also provide damping to a power system [2, 3].
The modeling, operation and control fundamentals of the STATCOM have been extensively discussed in the literature [1, 4-7]. While most of the control designs are carried out with linearized models, nonlinear control strategies for STATCOM have also been reported recently [8]. STATCOM controls for stabilization have been attempted through complex Lyapunov procedures for simple power system models [8]. Applications of fuzzy logic and neural network based controls have also been reported [9, 10]. Stabilizers based on conventional linear control theory with fixed parameters can be very well tuned to an operating condition and provide excellent damping under that condition. But they cannot provide effective control over a wide operating range

for systems that are nonlinear, time varying and subject to uncertainty. In order to yield satisfactory control performance, it is desirable to develop a controller which has the ability to adjust its parameters from on-line determination of system structure or model, according to the environment in which it works. Application of adaptive control methods to power system excitation control systems and static VAR systems has been reported [11, 12]; however, its application to FACTS devices has been very limited.

This article investigates the stability enhancement problem of power systems installed with STATCOM through adaptive online control of converter voltage magnitude. The adaptive control strategy developed has been tested for its robustness over wide ranges of operation for a single machine as well as a multi-machine system.

The organization of the article is as follows: Section 2 gives the model of the power system including STATCOM; the theory of self-tuning adaptive regulator is included in section 3, and section 4 presents the pole-shift control algorithm used in conjunction with adaptive control. Sections 5, 6, and 7 devote on the simulation results for single machine case, while sections 8 and 9 give simulation results on the multi-machine system. At the end the conclusions of the study are presented in section 9.

2. Single Machine System with STATCOM

A single machine infinite bus system with a STATCOM installed at the mid-point of the transmission line is shown in figure 1. The STATCOM consists of a step down transformer, a three phase GTO–based voltage source converter, and a DC capacitor. The STATCOM is modeled as a voltage sourced converter (VSC) behind a step down transformer. The dynamic equations of the generator-excitation system are [13],

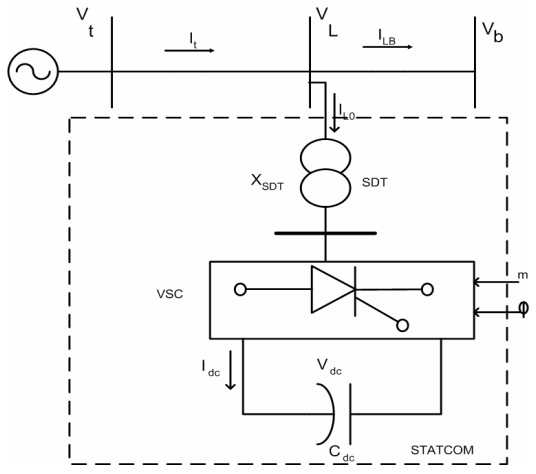

Figure 1 A single machine system with STATCOM

$$\dot{\delta} = \omega_o \Delta\omega$$
$$\dot{\omega} = -\frac{1}{M}[P_m - P_e - D\Delta\omega]$$
$$\dot{e}_q' = \frac{1}{T_{do'}}[E_{fd} - e_q' - (x_d - x_d')I_d] \quad (1)$$
$$\dot{E}_{fd} = -\frac{1}{T_A}(E_{fd} - E_{fdo}) + \frac{K_A}{T_A}(V_{to} - V_t)$$

The state variables [δ ω e_q' E_{fd}] are the generator rotor angle, speed, internal voltage and field voltage respectively. The STATCOM capacitor voltage equation is,

$$\frac{dV_{dc}}{dt} = \frac{I_{dc}}{C_{dc}} = \frac{m}{C_{dc}}\left(I_{Lod}\cos\psi + I_{Loq}\sin\psi\right) \quad (2)$$

Here, m and ψ are the magnitude and phase angle of the STATCOM ac side voltage. Combining (1) and (2), the dynamics of the single machine system is written as a 5th order state model as,

$$\dot{x} = f(x, u) \quad (3)$$

Here, the control is considered to be the vector comprising of m and ψ, respectively.

3. Self-tuning Adaptive Regulator

Self-tuning control is one form of adaptive control which has the ability of self-adjusting its control parameters according to system conditions. Figure 2 shows the structure of an adaptive regulator. The self-tuning strategy is composed of two processes - the system identifier and the controller. The identifier determines the parameters of the mathematical model of the system from input-output measurement of the plant. The parameters of the identifier are updated at each sampling instant so that it can track the changes in the controlled plant. The control for the plant is then calculated based on this recursively updated system model.

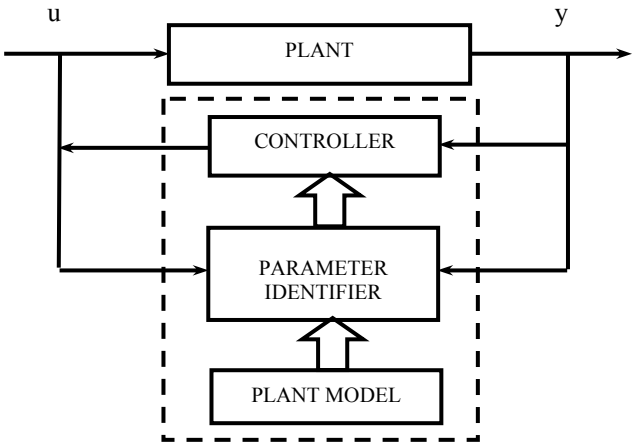

Figure 2 Block diagram of self-tuning controller

The plant model is assumed to be of the form,

$A(z^{-1})y(t)=B(z^{-1})u(t)+e(t)$ (4)

where, y(t),u(t) and e(t) are system output, input and the white noise, respectively; z^{-1} is the delay operator. The polynomial A and B are defined as,

$$A(z^{-1}) = 1+ a_1z^{-1} + a_2z^{-2} + a_3z^{-3} + a_4z^{-4} + ... \quad (5)$$

$$B(z^{-1}) = 1+ b_1z^{-1} + b_2z^{-2} + b_3z^{-3} + b_4z^{-4} + ... \quad (6)$$

The vector of parameters $\theta(t)= [a_1\ a_2\ .....,b_1\ b_2\ .....]^T$ are calculated recursively on-line through the recursive least square [11] technique using,

$$\theta(t+1) = \theta(t) +K(t)\ [y(t) - \theta^T(t)\psi(t)] \quad (7)$$

The measurement vector, modifying gain vector, and the covariance matrix, respectively are,

$\psi(t)= [-y(t-1)\ \ y(t-2).....y(t-n_a)\ \ u(t-1)\ \ u(t-2).....u(t-n_b)]^T$

$$K(t) = \frac{P(t)\psi(t)}{\lambda(t) + \psi^T(t)P(t)\psi(t)} \quad (8)$$

$$P(t+1) = \frac{1}{\lambda(t)}[P(t) - K^T(t)P(t)\psi(t)]$$

$\lambda(t)$ is the forgetting factor; n_a and n_b denote the order of the polynomials A and B, respectively. The identified parameters in (7) can be considered as the weighted sum of the previously identified parameters and those derived from the present signals.

4. The Control Strategy

Using the parameters obtained from the real time parameter identification method, a self-tuning controller based on pole shift is computed on-line and fed to the plant. Under the pole shifting control strategy, the poles of the closed loop system are shifted radially towards the centre of the unit circle in the z-domain by a factor α, which is less than one. The procedure for deriving the pole–shifting algorithm [14] is given below.

Assume that the feedback loop has the form,

$$\frac{u(t)}{y(t)} = -\frac{G(z^{-1})}{F(z^{-1})} \quad (9)$$

where,

$F(z^{-1}) = 1+ f_1z^{-1} + f_2z^{-2} + f_3z^{-3} + f_4z^{-4} + ...+f_{nf}z^{-nf}$

$G(z^{-1}) = g_0+ g_1z^{-1} + f_2z^{-2} + f_3z^{-3} + f_4z^{-4} + ...+f_{ng}z^{-ng}$

$n_f = n_b-1,\ n_g = n_a-1$

From (4) and (9) the characteristic polynomial can be derived as,

$$T(z^{-1})= A(z^{-1})F(z^{-1}) + B(z^{-1})G(z^{-1}) \quad (10)$$

The pole-shifting algorithm makes $T(z^{-1})$ take the form of $A(z^{-1})$ but the pole locations are shifted by a factor α, i.e.

$$A(z^{-1})F(z^{-1}) + B(z^{-1})G(z^{-1}) = A(\alpha z^{-1}) \quad (11)$$

Expanding both sides of (11) and comparing the coefficients give,

$$\begin{bmatrix} 1 & 0 & . & 0 & b_1 & 0 & . & 0 \\ a_1 & 1 & . & 0 & b_2 & b_1 & . & 0 \\ . & a_1 & . & . & . & b_2 & . & 0 \\ a_{n_a} & . & . & 1 & b_{n_b} & . & . & b_b \\ 0 & a_{n_a} & . & a_1 & 0 & b_{n_b} & . & b_2 \\ . & 0 & . & . & . & 0 & . & . \\ . & . & . & . & . & . & . & . \\ 0 & 0 & . & a_{n_a} & 0 & 0 & . & b_{n_b} \end{bmatrix} \begin{bmatrix} f_1 \\ . \\ . \\ f_{nf} \\ g_0 \\ . \\ . \\ g_{ng} \end{bmatrix} = \begin{bmatrix} a_1(\alpha-1) \\ a_2(\alpha^2-1) \\ . \\ . \\ a_{n_a}(\alpha^{n_a}-1) \\ 0 \\ . \\ 0 \end{bmatrix}$$

The above is written in the form,

$$M\ Z(\alpha) = L(\alpha) \quad (12)$$

If parameters $[\{a_i\},\ \{b_i\}]$ are identified at every sampling period and pole-shift factor α is known, the control parameters $Z=[\{f_i\},\{g_i\}]$ solved from (12) when substituted in (7) will give,

$$u(t, \alpha) = X^T(t)Z = X^T(t)M^{-1}L(\alpha) \quad (13)$$

In the above, $X(t)=[-u(t-1)\ -u(t-2).....u(t-n_f)\ -y(t)\ -y(t-1)\ -y(t-2).....y(t-n_g)]$

The controller objective is to force the system output y(t) to follow the reference output $y_r(t)$. The objective function can then be expressed as,

$$J = \min_{\alpha}[y(t) - y_r(t)]^2 \quad (14)$$

In the above, $y(t)=b_1u(t) + X^T\beta$; $\beta=[-b_2\ -b_3\ .....\ a_1\ a_2\ .....]$.

If the variation of J with respect to α can be made smaller than a predetermined error bound ε_1, it can be shown that a minimum of J will occur when,

$$\Delta\alpha = \frac{\varepsilon_1 - f_1f_2}{\varepsilon_2 + \frac{1}{2}[f_1f_3 + 2b_1^2f_2^2]} \quad (15)$$

where, ε_2 is a small number chosen to avoid the singularity. In the above,

$$f_1 = \frac{\partial J}{\partial u};\quad f_2 = \frac{\partial u}{\partial \alpha};\quad f_3 = \frac{\partial^2 u}{\partial \alpha^2}$$

The partial derivatives are evaluated from (13) and (14), and updates of the control is obtained considering first few significant terms of the Taylor series expansion of $u(t,\alpha)$. The algorithm can be


started by selecting an initial value of α and updating it at every sample through the relationship,

$$\alpha(t) = \alpha(t-1) + \Delta\alpha \qquad (16)$$

The control function is limited by the upper and lower limits and the pole shift factor should be such that it should be bounded by the reciprocal of the largest value of characteristic root of A (z^{-1}). The latter requirement is satisfied by constraining the magnitude of α to unity.

5. STATCOM Controller Performance for Single Machine System

For the power system considered in figure 1, the input and output of the plant were considered to be the control of the modulation index (m) in the STATCOM circuit and the generator speed variation (Δω), respectively. In order to excite the plant, a sequence voltage steps and torque pulses in the regulator-exciter and generator shaft, respectively were applied. The diagonal elements of the initial covariance matrix P is assumed be $2x10^5$; the initial pole shift factor 0 and the forgetting factor of 1 were used. The starting values of all the parameters were considered to be 0.001 in all the simulations for consistency. The model order to be estimated was assumed to be 3. For solution of differential equations ode54 function from MATLAB 6.5 was used. The adaptive algorithm was developed by the authors.

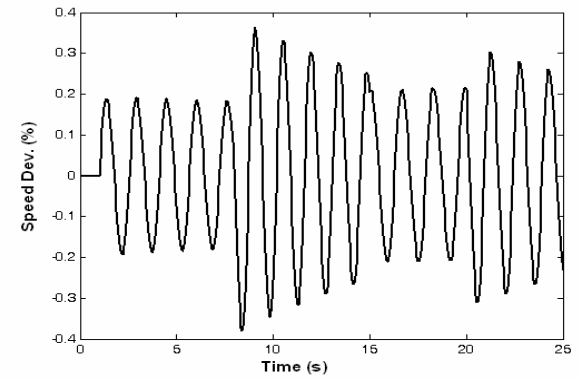

Figure 3. Generator speed deviation when excited with alternate torque steps

Figure 3 shows the generator speed deviation with no control when excited by a sequence of toque steps of +5%, -5%, +5% and -5%. The nominal loading is 0.9 pu at 0.9pf lagging. Figure 4 shows the variation of the generator speed with the pole-shift control applied to the identified process.

From figures 3 and 4, it is apparent that the electromechanical transients are damped very well by the adaptive controller. The plant parameters are unknown at the start of the estimation process giving rise to very large overshoots. However, as the identification process progresses, the plant parameters are estimated more and more accurately to yield better updates of the pole shift factor, and hence providing better damping profiles.

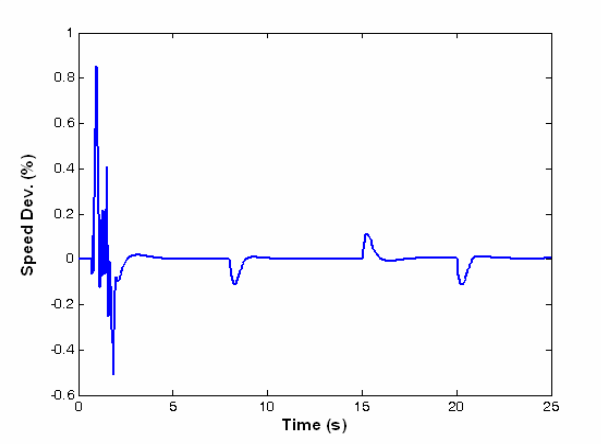

Figure 4 Speed deviation of the generator with adaptive pole-shift control

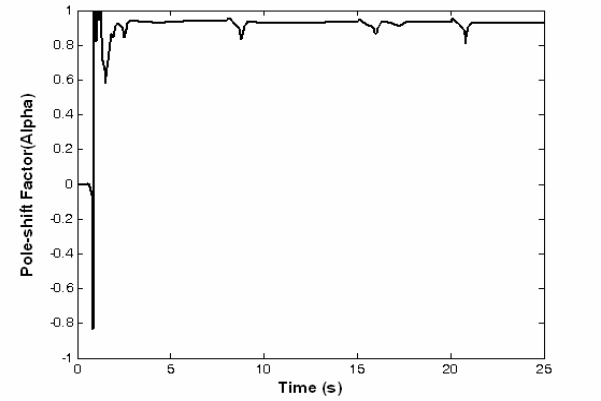

Figure 5 The variation of the pole-shift factor with the progression of the adaptive process

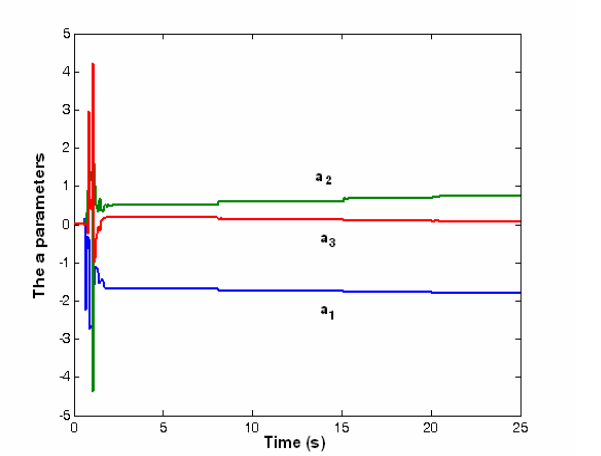

Figure 6 The variation of the a-parameters of the adaptively identified plant function

Figure 5 shows the convergence of the pole shift factor as the estimation process progresses. The convergence of the {a} and {b} parameters of the estimated plant function are shown in figures 6 and 7, respectively. It can be observed that the estimation algorithm converges to the desired values rapidly. The convergence of the algorithm is independent of the initial choice of the pole shift factor α.

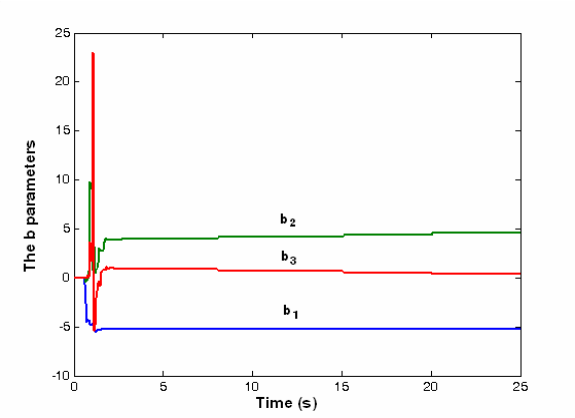

Figure 7 The variation of the b-parameters of the adaptively identified plant function

6. Testing the STATCOM Controller

A number of case studies were performed with the adapted system model and the pole shift parameters arrived at in the previous section. For a 50% input torque pulse on the generator for 0.1s, the rotor angle variations recorded for 3 operating conditions are shown in figure 9. These are for generator outputs of a) 1.2 pu , b) 0.9 pu , and c) 0.5pu. It can be observed that the damping properties are very good for the whole range of operation considered. Figure 10 shows the transient angle variations of the generator with the proposed adaptive control strategy for severe three-phase fault of 0.1s duration for the three loadings. It is to be noted that without control the system is under damped, in general, and unstable in some cases.

7. Evaluation through PI Control

The damping properties of the proposed coordinated robust controller were compared with a conventional PI controller in the STATCOM voltage magnitude control loop. The PI (or PID) controllers are normally installed in the feedback path. An additional washout is included in cascade with the controller to eliminate any unwanted signal in the steady state. The controller function in the feedback loop is written as,

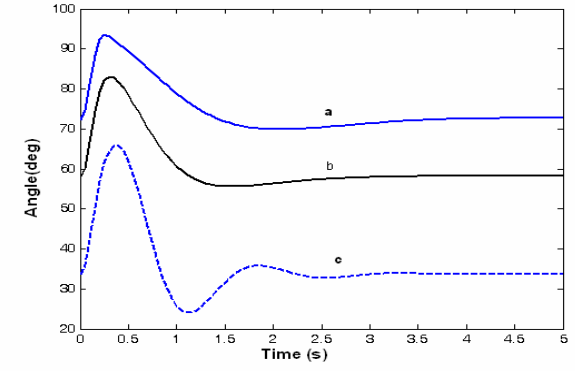

Figure 8 Generator rotor angle variations with the proposed pole-shift control for the loadings of a) 1.2 pu, b) 0.9 pu, and c) 0.5 pu. The disturbance considered is a 50% torque pulse for 0.1s

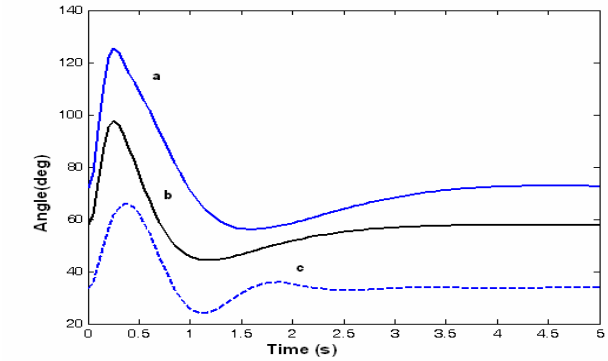

Figure 9 Generator rotor angle variations following a three-phase fault for 0.1s with the proposed pole-shift control. The loadings are: a) 1.2 pu, b) 0.9 pu, and c) 0.5 pu.

A pole–placement technique was used to determine the optimum gain settings (K_P and K_I) of the controller. For a desired location of the dominant closed-loop eigen value λ, the following equation is solved for K_P and K_I,

$$H(\lambda)= [C(\lambda I-A)^{-1}B]^{-1} \qquad (18)$$

H(λ) is obtained from (17) for the desired λ .

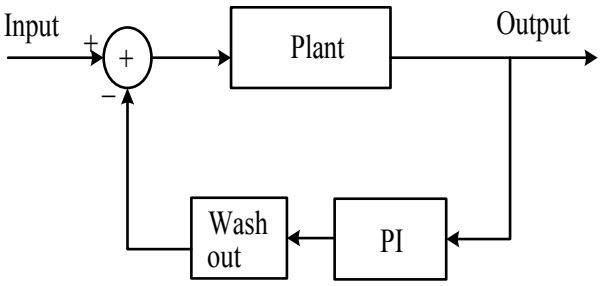

Figure 10 PI controller configuration

$$H(s) = [K_P + \frac{K_I}{s}]\left[\frac{sT_w}{1+sT_w}\right] \qquad (17)$$

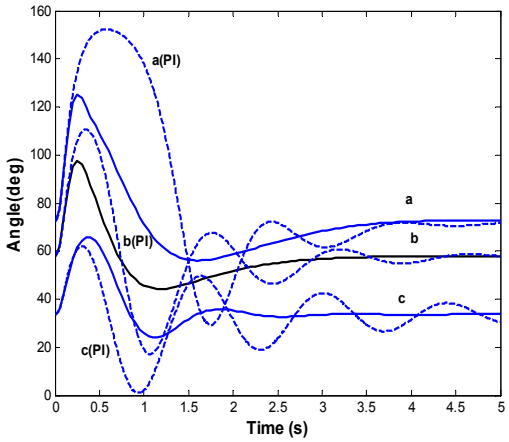

Figure 11 Generator rotor angle characteristics following a three-phase fault for 0.1s

Figure 11 shows the rotor angle variations of the synchronous generator following a three-phase fault with and without PI control for the 3 loading conditions considered in figures 8 and 9. The nominal loading is 1.01 pu. The values of K_P and K_I, respectively are 5.957 and 10.892 for closed-loop system damping ratio of 0.3. The responses with dotted lines are with PI control. The figure shows comparison of the responses of the PI control with the pole-shift adaptive control of STATCOM voltage magnitude. While the PI control provides reasonable response for the nominal operating condition (curve b), for loadings farther away from nominal it is not satisfactory. The pole-shift adaptive control, on the other hand, provides very well damped stable response for all the 3 operating conditions considered.

8. STATCOM Performance on a Multi-machine System

A 4-machine power system with STATCOMs located at the middle of the transmission lines connecting each generator to the rest of the grid is shown in figure 12. The system dynamics involves a set of equations similar to (3) for each generator in addition to the network voltage-current relationships. The network quantities are transformed to individual machine d-q frames and a closed form state model for the multi-machine system is arrived at.

The variable pole-shift adaptive control strategy was tested on the 4-machine power system given in figure 12. The output was considered to be the change in power of generator #2 which is connected to the system through bus 9. The input signal is the modulation index of the STATCOM converter voltage. In order to excite the plant, a sequence of torque pulses was applied on the shaft of generator #2.

Figure 13 shows the relative speed deviations of the generators with no control when excited by a sequence of toque steps of +5%, -5%, +5% and -5%. Figure 15 shows the variation of the generator speed with the adaptive variable pole-shift control applied to the identified process. The initial parameters of the adaptive algorithm were selected as in the single machine case.

From figure 14, it is apparent that the electromechanical transients are damped very well by the adaptive controller. The plant parameters are unknown at the start of the estimation process giving rise to large overshoots. However, as the identification process progresses, the plant parameters are estimated more and more accurately to yield better updates of the pole shift factor, and hence providing better damping profiles.

Figure 15 shows the convergence of the pole shift factor as the estimation process progresses. The convergence of the {a} parameters of the estimated plant function is shown in figures 16. It can be observed that the estimation algorithm converges to the desired values rapidly with minimum subsequent control expenditure. The convergence of the algorithm is independent of the initial choice of the pole shift factor α

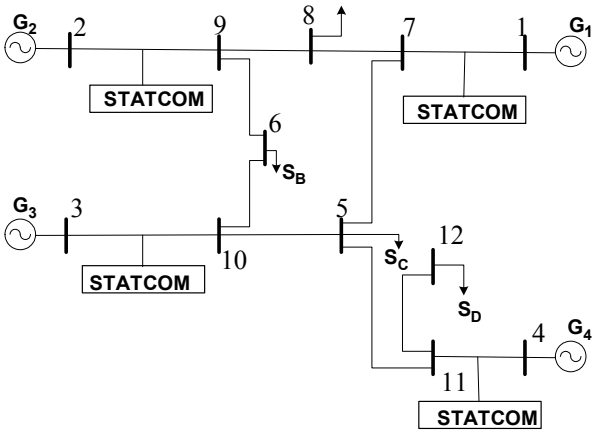

Figure 12 The multi-machine power system configuration

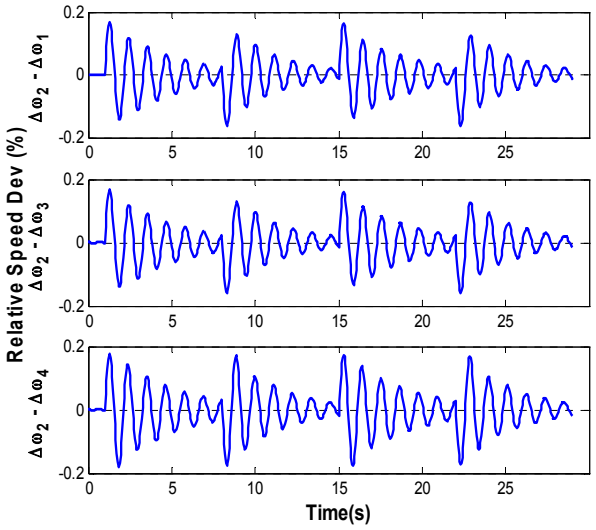

Figure 13 Generator speed deviation when excited with alternate torque steps

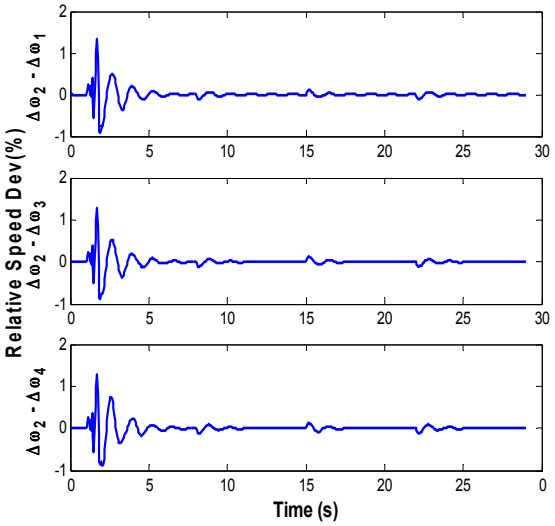

Figure 14 Speed deviation of the generator with adaptive pole-shift control

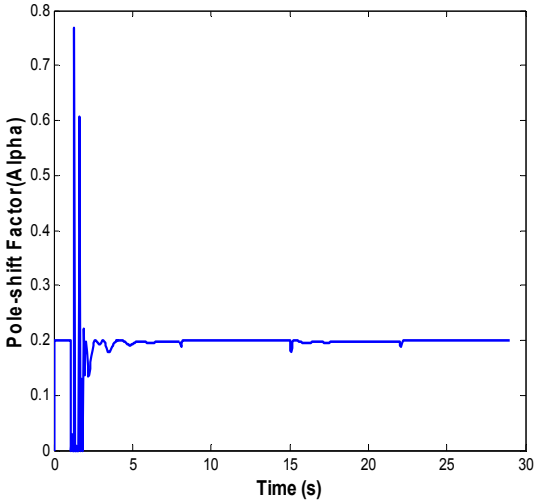

Figure 15 The variation of the pole-shift factor with the progression of the adaptive process

9. Testing the Multi-machine System Adaptive Controller

A number of case studies were performed with the adapted system model and the pole shift parameters arrived at in the previous section. For a 50% input torque pulse on generator #2 for 0.1s, the rotor angle variations recorded for 2 operating conditions are shown in figure 17.The loadings are quite apart from each other. It can be observed that the damping properties are very good for the whole range of operation considered. It is to be noted that without control the system is very much under damped, and for this disturbance is on the verge of instability.

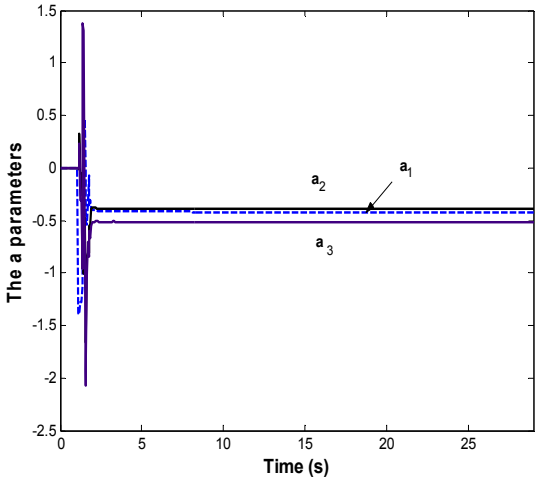

Figure 16 The variation of the a-parameters of the adaptively identified plant function

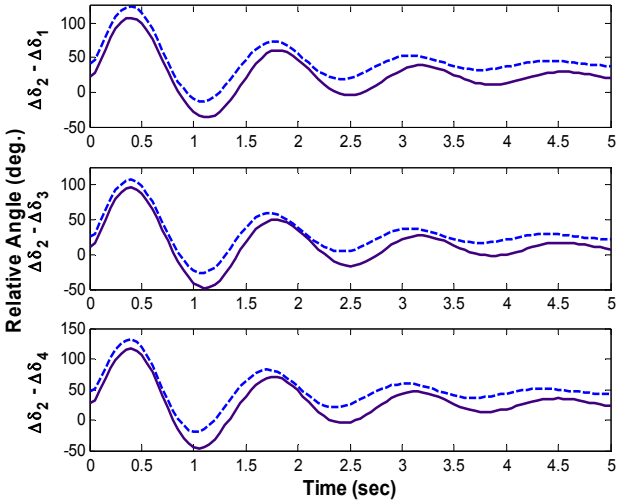

Figure 17 Relative rotor angle variations of the generators with the proposed pole-shift control for two loading conditions. The disturbance considered is a 100% torque pulse for 0.1s on generator 2.

10. Conclusions

An adaptive stabilizing control technique has been used to enhance the dynamic performance of a single machine as well as a multi-machine power system installed with synchronous static compensators. The control employed is the modulation index of one of the converter voltages. The proposed technique generates a stabilizing control on the basis of shifting the poles of the closed loop system towards the center of the unit circle in z-domain, thus providing more damping to the not so stable modes. The algorithm has been shown to converge to estimated parameter model rapidly for both the single machine as well as the multi-machine system. The on-line controller has demonstrated to provide very good damping to the electromechanical modes. The robustness of the control strategy was tested by simulating different types of disturbances including three phase faults covering a number of operating states. The adaptive strategy was also compared with optimized PI control response for a single machine system and was observed to provide much superior performance

Acknowledgement

The authors wish to acknowledge the facilities provided by the King Fahd University of Petroleum and Minerals and the Saudi Electricity Company towards this research.

References

[1] A.H. Noorazi and A.M. Sharaf, "Two control schemes to enhance the dynamic performance of the STATCOM and SSSC," *IEEE Trans. Power Delivery,* vol. 20, no. 1, pp. 435-442, January 2005.

[2] P. Rao, M.L.Crow and Z. Young, "STATCOM control for power system voltage control applications," *IEEE Trans. on Power Delivery,* vol. 15, no. 4, pp. 1311-1317, October 2000.

[3] P.S. Sensarma, K.R. Padiyar and V. Ram-narayanan, "Analysis and performance evaluation of a distribution STATCOM for compensating voltage fluctuation," *IEEE Trans. Power Delivery,* vol. 16, no. 2, pp. 259-264, April 2001.

[4] D.Shen and P.W. Lehn, "Modeling, analysis and control of a current source inverter-based STATCOM," *IEEE Trans. Power Delivery,* vol. 17, no. 1, pp.248-253, January 2002.

[5] Y. Ye, M. Kazerani and V.H. Quintana, "Current source converter based STATCOM: Modeling and control," *IEEE Trans. Power Delivery*, vol. 20, no 2, pp.795-800, April 2005.

[6] L. Cong and Y. Wang, "Coordinated control of generator excitation and STATCOM for rotor angle stability and voltage regulation enhancement of power systems," *IEE Proc- Gener. Transm. Distrib.,* vol. 149, no. 6, pp.659-666, November 2002.

[7] D. Soto and R. Pena, "Nonlinear control strategies for cascaded multilevel STATCOM," *IEEE Trans. Power Delivery,* vol.19, no. 4, pp. 1919-1927, October 2004.

[8] M.H.Haque and P. Kumkratng, "Application of Lyapunov stability criterion to determine the control strategy of a STATCOM," *IEEE Proc. – Gener. Transm. Distib.,* vol.151, no. 3, pp.415 -420, May 2004.

[9] L.O.Mak, Y.X. Ni and C. M. Shen, "STATCOM with fuzzy controllers for interconnected power systems," *Electric Power Systems Research,* Vol. 55, pp.87-95, 2000.

[10] G.W.Kim and K.Y.Lee, "Coordination control of ULTC transformer and STATCOM based on an artificial neural network," *IEEE Trans. Power Systems,* Vol. 20, no. 2, pp.580-586, May 2005.

[11] W.M.Hussein and O.P.Malik, "Study of System Performance with Duplicate Adaptive Power System Stabilizer", *Electric Power Components and Systems*, 31, 2003, pp. 899-912.

[12] P.K.Dash, P.C.Panda, A.M.Sharaf and E.F.Hill, "Adaptive Controller for Static Reactive Power Compensation in Power Systems", Proc. IEE, 134(3), 1987, pp. 256-284.

[13] A.H.M.A.Rahim and M.F.Kandlawala, "Robust STATCOM Voltage Controller Design Using Loop-shaping Technique", Journal of Electric Power Systems Research, 68(1), 2004, pp.61-74.

[14] O.P.Malik, G.P.Chen, G.S. Hope, Q.H.Qin and G.Y.Xu, "Adaptive Self-optimizing Pole Shifting Control Algorithm", IEE Proc.-D, 139(5), 1992, pp. 429-438.

Abu H. M. A. Rahim did his Ph.D. from the University of Alberta, Edmonton, Canada in 1972. Since his Ph.D., he has worked at the University of Alberta, Bangladesh University of Engineering, University of Strathclyde (Glasgow), University of Bahrain, DeVry Institute of Technology, Calgary and at the University of CalgaryDr. Rahim is presently working at the King Fahd University of Petroleum and Minerals, Dhahran where he is a Professor. Dr. Rahim's main fields of interest are power system stability, control and application of artificial intelligence to power systems. Dr. Rahim is a senior member of the IEEE and Fellow of the Institute of Engineers, Bangladesh.

M. Baber Abbas did his B.Tech in Electrical Engineering degree from JNT University, Hyderabad, India in 2001 and M.S. from the King Fahd University of Petroleum and Minerals, Dhahran, Saudi Arabia in 2005. Mr. Abbas is presently working as an Electrical Engineer in Transmission Asset Planning Department, Saudi Electricity Company, Dammam, Saudi Arabia. Mr. Abbas's main fields of interest are power system analysis, FACTS devices & control, optimization.